A Study of the Analytical and Diagnostic Potential of Fibre-Optic Surface Plasmon Resonance-Extraordinary Optical Transmission Biosensors

by

Thai Thao LY, BE(Hons)(ChemPharma)

School of Chemical Engineering and Advanced Materials

The University of Adelaide

A thesis submitted for the examination for the degree of

Doctor of Philosophy

October 2021

STATEMENT OF DECLARATION

I certify that this work contains no material which has been accepted for the award of any other degree or diploma in my name, in any university or other tertiary institution and, to the best of my knowledge and belief, contains no material previously published or written by another person, except where due reference has been made in the text. In addition, I certify that no part of this work will, in the future, be used in a submission in my name, for any other degree or diploma in any university or other tertiary institution without the prior approval of the University of Adelaide and where applicable, any partner institution responsible for the joint-award of this degree.

The author acknowledges that copyright of published works contained within the thesis resides with the copyright holder(s) of those works.

I also give permission for the digital version of my thesis to be made available on the web, via the University's digital research repository, the Library Search and also through web search engines, unless permission has been granted by the University to restrict access for a period of time.

Signature:

Date: 21/02/2022

EXECUTIVE SUMMARY

A fibre-optic surface plasmon resonance-extraordinary optical transmission (SPR-EOT) biosensor is developed based on a conventional SPR biosensor, utilising optical fibres and extraordinary optical transmission to miniaturise the biosensor for point-of-care diagnosis and real-time online analysis. The SPR biosensor is a well-established biosensing platform based on surface plasmon and it has been commercialised to study the binding kinetics of biomolecules. The EOT biosensor is based on enhanced light transmission when it goes through a metallic periodic array of subwavelength nanoholes. A fibre-optic SPR-EOT biosensor is fabricated by transferring a thin gold film with a nanohole matrix to a tip of an optical fibre. The portability and practicability of the EOT biosensor are significantly enhanced thanks to this fabricating technique. In this thesis, I evaluated the performance of fibre-optic SPR-EOT biosensors in detecting different biomolecules including monoclonal antibodies, toxin B and spike proteins by optimising the fabricating procedure and the sensing surface preparation process. Furthermore, regeneration of the sensing surface was also studied to allow multiple use of these sensors.

The fibre-optic SPR-EOT biosensor was evaluated as a process analytical technology tool for detection and measurements of monoclonal antibodies in the bioreactor during the antibody manufacture process. Peaks at 830 nm of light transmission spectra were shifted during the detection. The biosensor detected an antibody concentration as low as 4.4×10^{-4} mg/mL. Due to the robustness of protein A, the protein A-based biosensor was tested for surface regeneration, and the result demonstrated that the biosensor could withstand up to 10 regenerations using 0.1 M glycine hydrochloride (pH=2.8).

The biosensor was also assessed for detection of biomolecules for disease diagnosis at the early phase. It was used to detect toxin B produced from *Clostridium Difficile* with

the limit of detection of 1.4 pg/ml, which was comparable to other novel methods. A procedure of preparing the fabricating materials and the fabrication process were established to ensure a consistent batch-to-batch quality of the biosensor. The potential of using the biosensor for early diagnosis of *Clostridium Difficile* infection was revealed through three batches of toxin B samples.

Finally, the biosensor was tested for rapid detection of the N protein of the SARS-CoV2 virus. The limit of detection was 1.77 μg/mL, which was far above that obtained from other detection methods (ELISA and lateral flow assay for COVID-19 diagnosis) although these methods often take a much longer time than our developed biosensor. The limit of detection could be lowered to 0.046 pg/mL by altering the fabricating method and materials, but the quality of fabricated biosensors would not be consistent.

This thesis accentuates the potential of fibre-optic SPR-EOT biosensors for bioapplications, especially for analytical and diagnostic applications. My PhD study has contributed to preparation of the biosensor components, establishment of fabricating techniques, and development of methods of functionalization, which lay a solid foundation for commercialisation of the fibre-optic SPR-EOT biosensor.

ACKNOWLEDGEMENT

I would like to express my deepest thanks to Professor Hu Zhang from Keck Graduate Institute, my principal supervisor, for his generous support throughout the project. This project would not have been possible without his constant guidance. I would also like to thank my co-supervisor, Dr Yinlan Ruan, from the School of Physical Sciences at the University of Adelaide, for all the invaluable advice. I would also like to acknowledge the help of my other co-supervisor, Associate Professor Jingxiu Bi, from the School of Chemical Engineering and Advanced Materials at the University of Adelaide, for motivating me to pursue the Doctor of Philoshophy degree. I would not have been where I am today without her. I should also appreciate my editor, Dr Alison-Jane Hunter, writing and language tutor from the School of Mechanical Engineering at the University of Adelaide, for always encouraging me and editing the thesis.

I am very grateful for the company and friendship of my research fellows, Bobo Du, Shuang Yin, Rouyan Chen, Nhat Hoang Huynh, Binyang Zhang, Yiran Qu, Yechuan Zhang, Afshin Karami. You made this challenging journey feel rewarding, and your passions motivated me every day.

I would also like to thank all the staff members in the School of Chemical Engineering, School of Physical Sciences, and Australian National Fabrication Facility - South Australian Node, for their support in administration and laboratory services.

I would like to extend my deepest gratitude to my parents, Professor Gareth Myles, sister, and housemates for their love, caretaking, and emotional support. I must also thank the “40 plus cycling club” members for being my academic and life advisers. Finally, I would like to give my special regards to Associate Professor Yung Ngothai

for being my mentor and inspiring me to stay resilient and optimistic despite all the hardship.

TABLE OF CONTENTS

LIST OF FIGURES

LIST OF TABLES

ABBREVIATIONS

3-MPA	3-Mercaptopropionic Acid
AMCA	Aptamer-Mediated Colourimetric Assay
ANOVA	Analysis Of Variance
BSA	Bovine Serum Albumin
CCNA	Cytotoxicity Neutralisation Assay
CCTA	Cell Cytotoxicity Assay
CDI	Clostridioide Difficile Infection
COVID-19	Coronavirus Disease
CPPs/KPPs	Critical/Key Process Parameters
DEP	Dielectrophoresis
EDC	1-ethyl-3-(3-dimethyl aminopropyl) carbodiimide hydrochloride
EIA	Enzyme Immunoassay
ELISA	Enzyme-Linked Immunosorbent Assay
EOT	Extraordinary Optical Transmission
EUA	Emergency Use Authorization
FDTD	Finite-Difference Time-Domain
GHD	Glutamate Dehydrogenase
GMP	Good Manufacturing Practices
HLPC	High-Performance Liquid Chromatography
HPC	Hydroxypropyl Cellulose
HPR	Horseradish Peroxidase
IgG	Immunoglobulin G
LED	Light Emitting Diode
LFA/LFAs	Lateral Flow Assay/Assays
LOD	Limit Of Detection
LSPR	Localised Surface Plasmon Resonance

Mab/Mabs	Monoclonal Antibody/Antibodies
N protein	Nucleocapsid Protein
NAAT	Nucleic Acid Amplification Test
PAT/PATs	Process Analytical Technology/Technologies
PBS	Phosphate-Buffered Saline
PDMS	Polydimethylsiloxane
POC/POCT	Point-Of-Care/Point-Of-Care Testing
QMC	Quarzt Crystal Microbalance
RI	Refractive Index
RIU	Refractive Index Unit
RT-PCR	Reverse Transcriptase-Polymerase Chain Reaction
SAM	Self-Assembled Monolayer
SERS	Surface-Enhanced Raman Scattering
SIMOA	Single Molecular Array
SMC	Single Molecule Counting
SPR	Surface Plasmon Resonance
Sulfo-NHS/NHS	N-Hydroxysulfosuccinimide
TC	Toxigenic Culture

1. Chapter 1

INTRODUCTION

1.1. Background

Biosensors are one of the most attractive research topics in academia and industry (Bhalla et al., 2016). Biosensors are exploited for applications in many fields, including agriculture, environmental control, food safety, clinical diagnosis, the pharmaceutical industry, and security (Damborský et al., 2016).

Biosensors can be classified into several different types, such as electrochemical, piezoelectric, thermometric, magnetic, and optical biosensors. Amongst these biosensors, optical biosensors are the most popular. The optical biosensor advances real-time and label-free biosensing with high sensitivity and specificity. The innovations in relevant technologies have matured the development of highly sensitive, compact, and cost-effective optical biosensors (Jackman et al., 2017).

The most popular optical biosensors are surface plasmon resonance (SPR) biosensors, and many companies have commercialised this biosensor for various applications (Couture et al., 2013). However, a biosensing platform that is highly sensitive, cost-effective, and simple is currently not available for routine point-of-care applications in a non-laboratory environment. In recent years, localised nanoplasmonic biosensors have emerged as the next generation of SPR biosensors (Jackman et al., 2017, Kasani et al., 2019). Nanoplasmonic biosensors are easily fabricated and miniaturised; therefore, they hold great potential for low-cost and high throughput biosensing (Couture et al., 2013). The two main nanoplasmonic sensing strategies are extraordinary optical transmission (EOT) and localised surface plasmon resonance (LSPR). Both EOT and LSPR offer better surface sensitivity and robustness to environmental interference than SPR biosensors; therefore, interest in EOT and LSPR has been increasing, especially for the development of simple and highly sensitive biosensors.

EOT is an SPR-related optical phenomenon that occurs when incident light interacts with an array of nanoholes to generate extraordinary optical transmission. This optical transmission is highly sensitive to binding of biological or chemical substances at the nanohole array interface (Jia and Yang, 2014). Consequently, EOT biosensors have attracted significant attention for novel biosensing development, while they have not yet been commercialised for real-world applications (Jackman et al., 2017).

Several issues hamper the commercialisation of EOT biosensors. The first issue is the design of the biosensors. In the early development phase of the EOT biosensor, this factor was not considered. However, as the EOT biosensor approaches commercialisation, biosensor design arises as a crucial element. Although a few studies have reported on designs of biosensors to comply with the applications, the design of reliable and portable EOT biosensors for economic mass production is rarely studied. Secondly, very few studies have investigated immobilisation and stability of bioreceptors. Bioreceptors can specifically recognise the target analytes. They are usually immobilised on the sensing surface to capture the analyte, and biorecognition signals can be generated for the biosensors. The stability of the bioreceptors is vital to the applicability of a biosensor because biosensing probes with immobilised bioreceptors are often kept in storage before use. The third issue is the lack of a standard fabrication route for nanohole arrays. Currently different fabrication routes have been used, thus, there is variability between and across different EOT biosensing platforms. Additionally, fabrication must allow mass production of the sensing surface with a low cost to promote commercialisation. Other issues related to clinical validation have also hindered the progress of commercialisation of the EOT biosensor. An in-depth study on developing a reliable and cost-effective EOT biosensor with improved practicability is demanded and the feasibility of using EOT biosensors should be demonstrated.

1.2. Research Aim and Objectives

In this dissertation, I focused on developing a fibre-optic SPR-EOT biosensor with a high readiness level for analytical and diagnostic applications. This biosensor was prototyped by Prasad et al. (2019). It implemented a metal nanohole array on the tip of an optical fibre to miniaturise the biosensor and simplify the optical setup. However, the biosensing performance of the prototype was poor.

This study aims to improve the biosensor design, achieve a reliable biosensing platform, and demonstrate the biosensing potential for analytical and diagnostic applications. The objectives of this study are to:

- Use an engineering approach to address the prototype design flaws and implement a standard biosensor fabrication procedure to achieve consistent quality of the sensing probes;
- Employ the biosensor to detect and quantify different biomolecules via investigating the immobilising strategies, confirming the feasibility of regeneration, and determining the impact of fabricating techniques and materials on the sensing performance.

The schematic concept of the biosensor is displayed in **Figure 1-1**. The fibre-optic SPR-EOT biosensing platform has been demonstrated to show great potential for various biosensing applications. My study contributes to the maturation of development of EOT biosensors. Throughout my PhD study, I have had great opportunities to collaborate with multidisciplinary scientists, which has been crucial for developing the EOT biosensors.

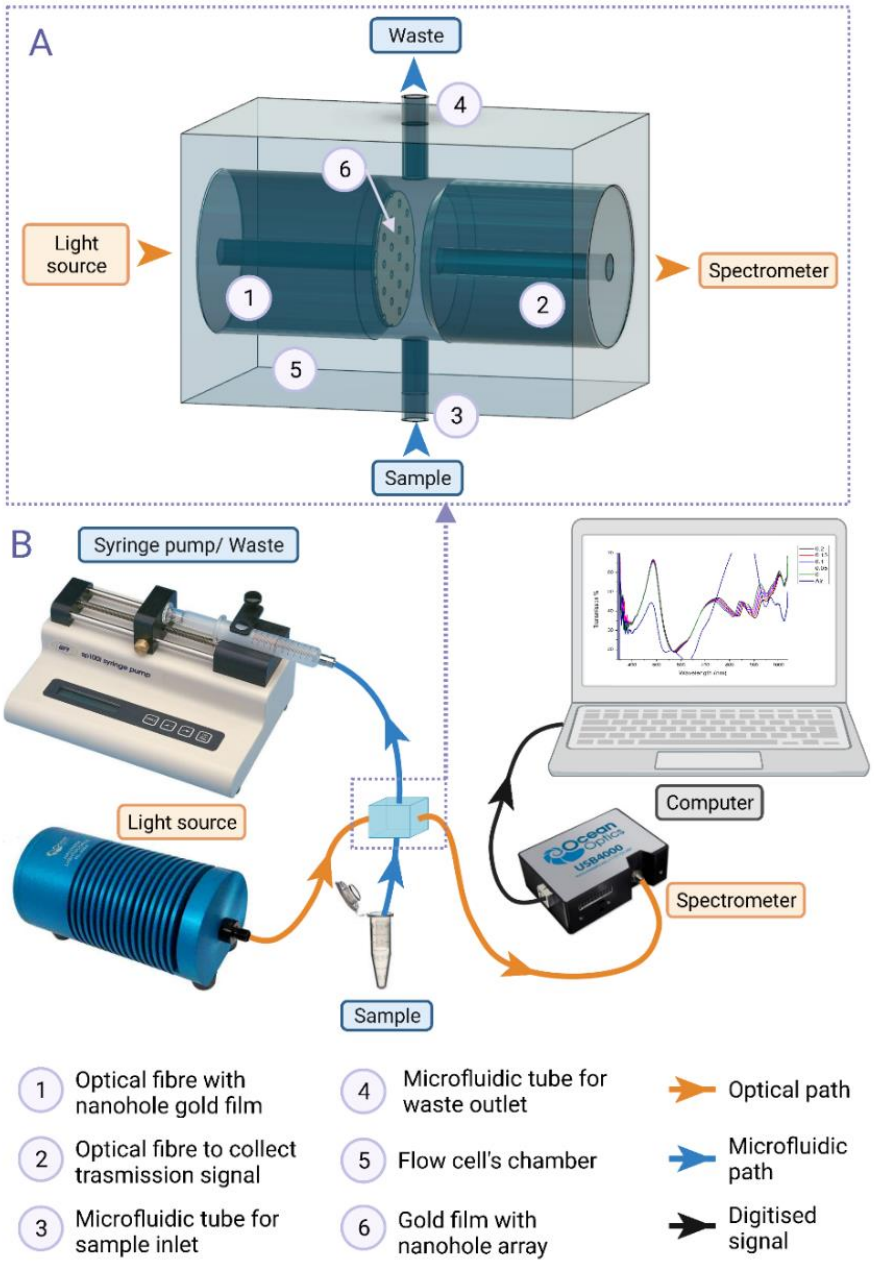

Figure 1-1 Schematic diagram of the setup of a fibre-optic SPR-EOT biosensor and details of the flowcell.

1.3. Thesis Outline

This thesis is compiled in a publications format; the main chapters, including Chapters 3, 4 and 5, are presented in a scientific article format.

Chapter 1 describes the background of biosensors, research aim and objectives, and thesis outline.

Chapter 2 provides a review of the recent development of biosensors, SPR biosensors, EOT biosensors, and fibre-optic SPR-EOT biosensors. The review includes a brief introduction of biosensors, highlights the substantial development of SPR biosensors and details the development of EOT biosensors in recent years. This chapter reveals very few studies on bioapplications of fibre-optic SPR-EOT biosensors and the need for more in-depth studies to allow breakthrough development of these biosensors.

Chapter 3 describes the optimisation of the fibre-optic SPR-EOT biosensor prototype. The fabrication procedure was standardised to achieve consistent sensitivity throughout all the sensing probes. The biosensing probes were immobilised with protein A to detect and quantify monoclonal antibodies. Two different strategies of protein A immobilisation were employed to compare the impacts of immobilisation on the detection performance. Regeneration of protein A was also demonstrated to demonstrate the practicability of using a fibre-optic SPR-EOT biosensor for routine monoclonal antibody titer quantification.

In Chapter 4, the results of using the fibre-optic SPR-EOT biosensor for toxin B detection are presented. Toxin B is a biomarker to diagnose *Clostridioide difficile* infection, which might lead to fatal colonic inflammation. After optimising antibody immobilisation, the biosensor was tested to detect toxin B at the concentration of picogram per millilitre. The results confirm the potential for using a fibre-optic SPR-EOT biosensor as a diagnostic tool for early phase infection.

In Chapter 5, I explore the use of the fibre-optic SPR-EOT biosensor for early detection of COVID-19. The nucleocapsid protein of SARS-CoV-2 was chosen as a biomarker for early diagnosis. The detection result revealed a low sensitivity of the biosensor to the nucleocapsid protein; but another fabricating technique was developed to improve the sensitivity. The sensitivity of the fibre-optic SPR-EOT biosensor can be enhanced by selecting the appropriate fabricating technique and materials and has the potential for sensitive nucleocapsid protein detection.

Chapter 6 concludes the findings from my PhD study and suggests the prospects for future studies on fibre-optic SPR-EOT biosensors.

Supplementary data for each experiment is included at the end of each chapter.

2. Chapter 2

LITERATURE REVIEW

2.1. Overview of Biosensors and their Applications

A biosensor is an analytical device that recognises a biological reaction and converts it into a measurable electrical or optical signal to quantify the concentration of an analyte in the reaction. Biosensors as onsite/online/atline diagnosis systems possess a few advantages, including delivering highly accurate results in a short timeframe, portability, and user-friendliness (Bhardwaj et al., 2017).

An ideal biosensor should have high sensitivity and specificity to the targeted analyte in a rapid assay time. Apart from the requirements for sensitivity and specificity, an ideal biosensor needs to have a high tolerance to external changes (e.g., pH, temperature), good shelf-life stability, and consistent reproducibility. Moreover, user-friendliness and portability would be significant advantages for point-of-care testing. Recently, Bhalla et al. (2020) addressed 11 critical attributes of biosensors that make them excellent candidates for rapid COVID-19 diagnosis: high selectivity, high sensitivity, rapid response time, multiplexing, multimode sensing for on-chip validation, disposable, long shelf life and easy to use, cost-effective, mass manufacturing, autonomy and connectivity to central healthcare systems.

A biosensor consists of four main elements: a bioreceptor, a transducer, a signal processor, and a display, as shown in **Figure 2-1**.

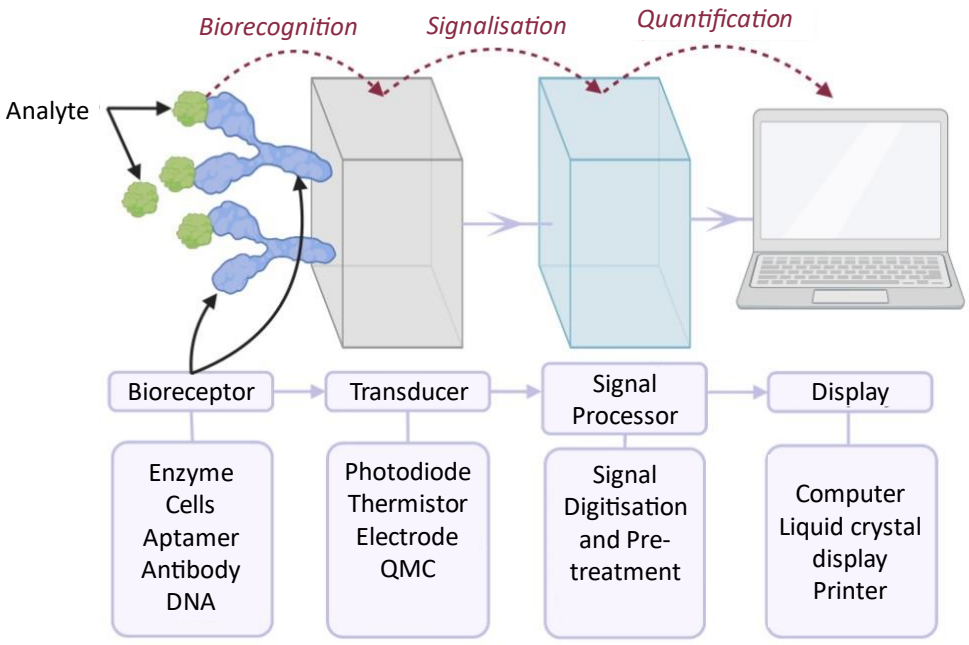

Figure 2-1 Schematic depiction of a biosensor (Adapted with permission of Portland Press, Ltd., from Bhalla et al. (2016); permission conveyed through Copyright Clearance Centre, Inc.).

Two critical elements of a biosensor are the bioreceptor and the transducer. As shown in **Figure 2-2**, there are various bioreceptors and transducers to choose from when designing a biosensor. Bioreceptors are molecules with specific biorecognition of the targeted analyte; they recognise the targeted analyte in the sample and produce a biological response. Transducers convert the biological response into measurable signals, such as optical or electrochemical signals. The signal goes through a signal processor to be amplified and/or prepared for display. The display presents the processed signal in a user-friendly manner, which allows the end-user to conduct further analysis. The display could be a printer, a simple liquid crystal display, or a computer. Choosing an appropriate bioreceptor is critical to the specificity of the biosensor, while the transducer plays an essential role in determining the sensitivity.

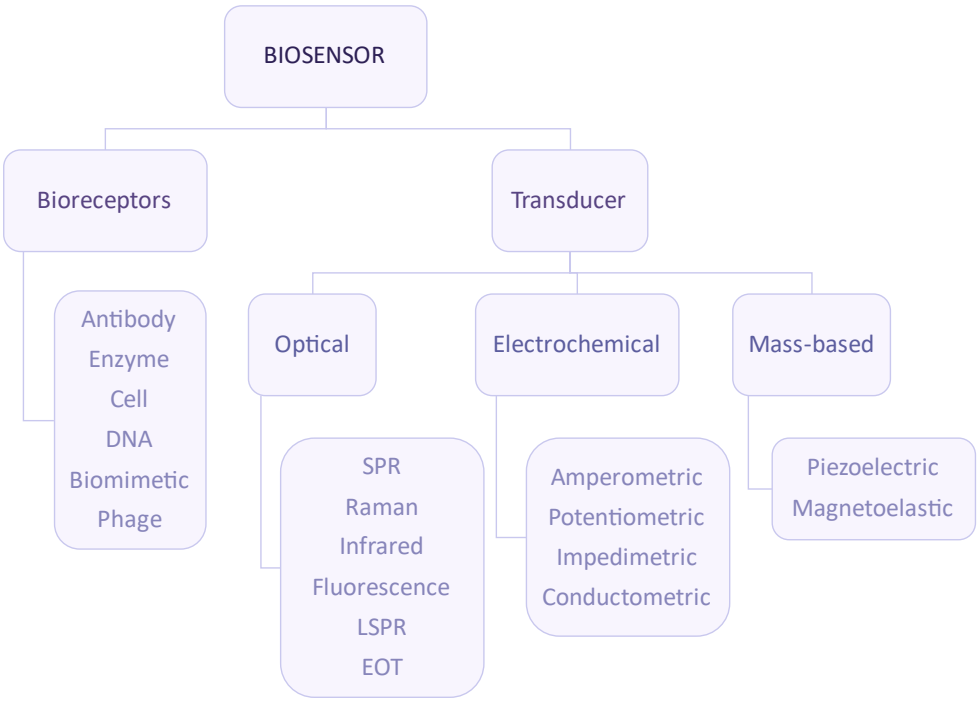

Figure 2-2 Types of bioreceptors and transducers used to construct a biosensor (Adapted from Velusamy et al. (2010), Copyright 2010, with permission from Elsevier).

Biosensors have attracted considerable interest over the last few decades due to their unique properties of being extremely responsive to a biorecognition event occurring on a transducer. Biosensors have been employed for various purposes, such as drug discovery, disease detection, environmental monitoring, food quality monitoring, bioprocess control, and many more (Bhalla et al., 2016). Since the introduction of amperometric biosensors for glucose detection in 1962, biosensor research has seen tremendous development, and numerous studies have exploited biosensors for medical applications (Metkar and Girigoswami, 2019). The most popular biosensors in the market are lateral flow pregnancy tests and electrochemical glucose biosensors (Bhalla et al., 2016). These two popular biosensors are excellent examples of well-designed biosensors that can be implemented for routine use at home.

A biosensor is an innovative tool and becoming ubiquitous due to the broad range of potential applications. With the development of disciplines such as physics, chemistry,

engineering, and biochemistry, biosensors are expected to see exponential evolution in the future. For medical applications, biosensors are anticipated to be potential point-of-care diagnostic tools that can deliver results quickly and accurately and overcome the limitations associated with current methods of diagnosis. The advantages of a biosensor are much needed to support early diagnosis of fatal diseases such as cancer, diabetes, and COVID-19, and to prevent disease progression (Metkar and Girigoswami, 2019).

2.2. Surface Plasmon Resonance Biosensor

There are many popular biosensing platforms, including electrochemical biosensors, optical biosensors, field-effect transistor-based biosensors, piezoelectric biosensors, and lateral flow biosensors (Bhalla et al., 2016). However, optical biosensors have advantages over other forms because they are highly sensitive to biorecognition, whilst being robust to external interference (Chen and Wang, 2020, Leonard et al., 2003). The most popular optical biosensor is the surface plasmon resonance (SPR) biosensor. SPR biosensors have been used for many years. This type of biosensor is one of the earliest developed: it supports effective, rapid, label-free detection of biomolecules with excellent sensitivity.

SPR is an optical phenomenon that occurs when incident light excites the electromagnetic oscillations at the interface between metal and dielectric materials. As shown in **Figure 2-3**, when illuminating a gold film through a prism at a certain angle, the energy of the incoming light is absorbed by the electrons at the interface of the gold film, resulting in a dark band in the reflected light. Since the energy absorption occurs at the interface of a metal surface and a dielectric medium, it is susceptible to changes at the interface. Analytes captured at the interface through biorecognition introduce an immediate shift in the angle of the dark band, as illustrated in **Figure 2-3**.

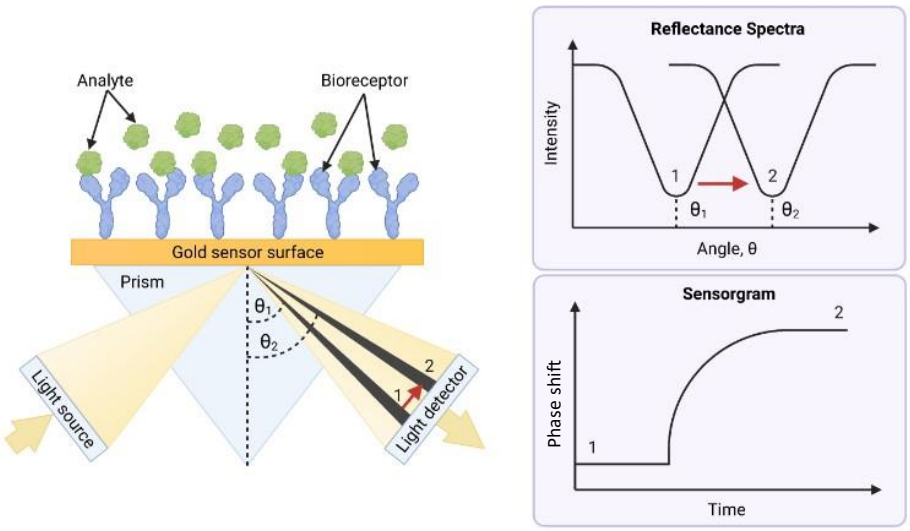

Figure 2-3 An illustration of an SPR biosensor's mechanism in detecting a biological analyte (Adapted with permission of Portland Press, Ltd., from Damborský et al. (2016); permission conveyed through Copyright Clearance Centre, Inc.).

Due to the high sensitivity of SPR to the changes at its interface, the prism configuration of SPR has been widely employed in biosensor applications. SPR sensors have broad applications in medical diagnostics, biotechnology, the pharmaceutical industry, food safety, environmental monitoring, and security (Couture et al., 2013). SPR biosensors have been commercialised under various names such as Biacore (Cytiva, USA), ProteOn XPR36 (Biorad, USA), OneStep SPR Systems (Sartorius, Germany), XanTec's SPR system (XanTec, Germany), Spreeta (Texas Instruments, USA) and many more (Couture et al., 2013).

SPR sensors have been studied extensively and employed for many applications. There have been about 1700 publications about SPR sensors annually since 2014 (Nangare and Patil, 2021). Many excellent review papers have covered this sensor (Couture et al., 2013, Chen and Wang, 2020, Yesudasu et al., 2021). A few current review papers cover the recent developments of SPR sensors in a particular field, such as food analysis (Ravindran et al., 2021), viral diagnostics (Shrivastav et al., 2021), cancer diagnostics (Shrivastav et al., 2021) or in a specific subtopic, such as SPR-based plastic optical fibre sensors (Kadhim et al., 2020), SPR-based crystal optical fibre sensors (Mittal et al., 2021), or graphene-based SPR

biosensors (Nurrohman and Chiu, 2021, Nangare and Patil, 2021). The novel configurations for SPR sensors and employment of nanomaterials such as graphene have been demonstrated to improve the readiness level of SPR biosensors for point-of-care testing.

SPR biosensors have great potential for highly sensitive bioassays due to their high sensitivity, low detection limits, real-time biomolecular detection, high throughput, excellent versatility, and great robustness (Couture et al., 2013, Ravindran et al., 2021). Nonetheless, conventional SPR equipment is only suitable for laboratories and is too bulky and expensive for point-of-care and onsite testing (Ravindran et al., 2021, Chen and Wang, 2020). Developing novel technologies and nanomaterials has enabled the miniaturisation of SPR biosensors for point-of-care testing (Chen and Wang, 2020); however, the readiness level of point-of-care SPR biosensors remains nascent (Couture et al., 2013, Shrivastav et al., 2021). Interdisciplinary collaboration among physicists, engineers, material scientists, medical scientists and clinicians should be promoted to mature the readiness level of point-of-care SPR biosensors for real-world applications (Falkowski et al., 2021). Moreover, SPR sensors should be engineered to have good sensitivity and reproducibility with low manufacturing costs to be ready for commercialisation. Overall, the SPR biosensor is poised to become a user-friendly, inexpensive and effective tool for point-of-care testing against highly contagious and fatal diseases like COVID-19 to assist in disease control (Shrivastav et al., 2021).

2.3. Extraordinary Optical Transmission Biosensors

Extraordinary optical transmission (EOT) is a propagating and localised SPR phenomenon that is exhibited by metallic nanohole arrays. As fabricating techniques of the metallic films have advanced over the last three decades, different geometrical structures of metallic films have been investigated for SPR applications (Ebbesen et al., 1998, Mayer and Hafner, 2011). The nanostructural arrays for EOT sensors have attracted great interests (Mayer and Hafner,

2011, Jackman et al., 2017), with approximately 1000 research articles about EOT biosensors between 2016 to 2021.

To better understand the EOT biosensor, the mechanism of an EOT sensor is briefly described in this section, followed by a review of recent developments in sensor configurations, fabrication methods, and recent studies on their bioapplications. The potential of EOT sensors for medical diagnostics is addressed to highlight their advantages over conventional SPR biosensors.

2.3.1. Mechanism of EOT Sensors

In 1998, Ebbesen et al. (1998) observed and reported a novel nanoplasmonic phenomenon, EOT, when investigating the optical properties of subwavelength hole arrays in metallic films (Jackman et al., 2017, Ebbesen et al., 1998).

EOT occurs when the transmission of incident light is selectively enhanced when illuminating through a metallic subwavelength nanohole array. The enhanced optical transmission arises from the plasmon mediated with a nanohole array (Couture et al., 2013). Before discovering the EOT in 1998 (Ebbesen et al., 1998), it was believed that light could barely transmit through subwavelength apertures (Rodrigo et al., 2016). Besides the unexpected extraordinary light transmittance, the transmitted light exhibits maximas and minimas (informally known as peaks and dips) that are characterised by the dimensions of the nanohole array, such as the hole diameter and periodic configurations of the array.

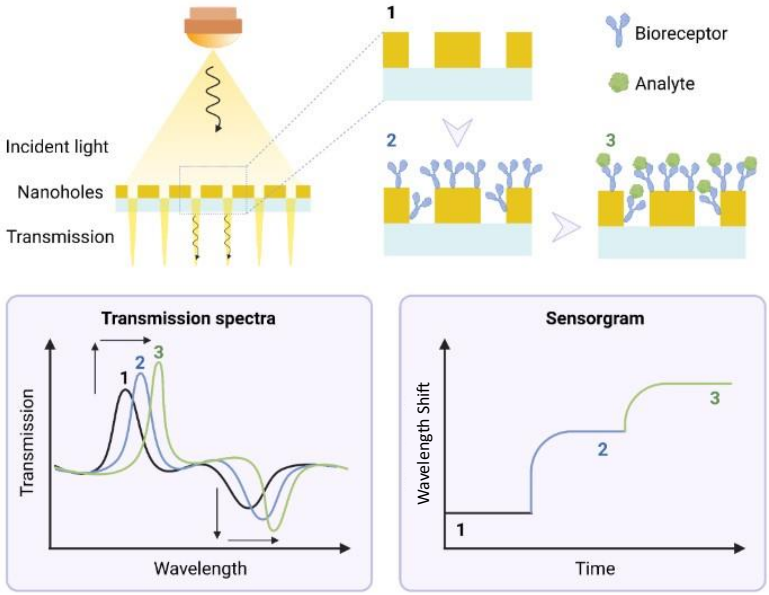

Figure 2-4 Illustration of a typical EOT biosensor and signal changes during and after biorecognition (Adapted with permission of Royal Society of Chemistry, from Jackman et al. (2017); permission conveyed through Copyright Clearance Centre, Inc.).

Figure 2-4 depicts the EOT biosensor and its typical transmission spectra and signal changes during a biorecognition event. As shown in **Figure 2-4,** the transmission spectra obtained from an EOT biosensor has distinct peaks and dips. These peaks and dips shift to longer wavelengths (redshifts), and the transmittance intensity changes when biomolecules bind to the gold film interface. Like the SPR sensor, an EOT sensor is also highly sensitive to any change in the refractive index at the gold and dielectric layer interface. A refractive index indicates the speed of light travelling through solids, liquids, and gases. For instance, when the solute concentration in a solution increases, the solution's refractive index also increases proportionally. The binding of molecules to the gold film interface can induce the refractive index change at the interface of the gold film and the dielectric fluid. The sensitivity of an optical biosensor is determined by the change in the measurement signal over a unit of refractive index. The signal change of an EOT biosensor is commonly indicated by the shift of the peaks and dips in the transmission spectra at different refractive index values, as shown in **Figure 2-4**. The peak redshifts as the refractive index of the dielectric fluid increases. The

position of the peak at different refractive index values is identified, then the redshifts from the original position are used to calculate the sensitivity. The sensitivity unit is the wavelength shift per refractive index unit (nm/RIU), which describes the magnitude of the redshift over the change of a refractive index unit. An optical sensor with a higher value of wavelength/RIU means it has better sensitivity (Monteiro et al., 2016). Sensitivity may also be defined as the change in the transmission intensity per refractive index unit (%/nm) (Briscoe et al., 2015, Hackett et al., 2018, Qian et al., 2019). Other terms that related to sensitivity of biosensors are bulk sensitivity and surface sensitivity. The definition of bulk sensitivity is described earlier in this paragraph, and it represents the biosensor's sensitivity to the surrounding medium. Surface sensitivity decribes the biosensor's sensitivity to mass changes or thickness variation at the sensing surface. Mass changes and thickness variation could be due to the binding of biomolecules on the sensing surface (Abbas et al., 2011). In other studies, change in thickness arose due to shrinkling or swelling of microgel on the sensing surface (Aliberti et al., 2017, Scherino et al., 2018). Bulk sensitivity and surface sensitivity can be measured for both planar and nanostructural sensing surface.

EOT biosensors have several advantages over prism-coupled SPR biosensors that make them more compatible for portable sensors. First, EOT biosensors have higher localised surface sensitivity than SPR biosensors (Mayer and Hafner, 2011, Jackman et al., 2017). Thanks to their excellent surface sensitivity, EOT biosensors only require a small sample volume. Such a small sample volume allows the EOT biosensors to be implemented in a microfluidic system (Mayer and Hafner, 2011, Wei et al., 2010). Second, EOT biosensors are less sensitive to environmental changes than SPR, which means the detecting signal is less likely to suffer interference from environmental factors such as temperature (Mayer and Hafner, 2011, Jackman et al., 2017). Conventional SPR biosensors have variable penetration depths from 100 nm to 1000 nm in the normal direction away from the interface (Jackman et

al., 2017, Mayer and Hafner, 2011), while the penetration depth of EOT biosensors ranges more narrowly from 10 nm to 180 nm (Jackman et al., 2017, Mayer and Hafner, 2011, Kee et al., 2013). Such a short penetration depth of the EOT biosensor facilitates small molecule detection and helps minimise any signal noise from the environmental factors (Jackman et al., 2017). Third, EOT requires simple, common laboratory instruments, while SPR requires complicated and precise optical instruments (Mayer and Hafner, 2011, Jackman et al., 2017). The optical setup of the EOT biosensor is quite simple, with no strict requirements on the angle of the incident light that must be maintained in a conventional SPR configuration; hence, increasing interest is shown in the development of EOT biosensors (Jackman et al., 2017).

The last decade has seen tremendous development in EOT biosensors. Many approaches have been developed to reduce the size of the EOT biosensor and enhance its sensitivity. Novel metal nanostructures, microfluidic flow cells and chips, and fabrication methods have been invented and implemented to gain a more insightful understanding of EOT biosensors, maximise sensitivity and make them more suitable for point-of-care practical applications. The following sections will elaborate further on how these studies improve EOT biosensors.

2.3.2. Nanostructural Arrays of EOT Biosensors

A myriad of new nanostructural arrays has been investigated to acknowledge the effects of the nanostructural configurations on sensing performance. Unconventional nanostructures could be an irregular nanohole shape (Yue et al., 2014, Lei et al., 2020, Cui et al., 2015), a nanoslit (Afsheen et al., 2019), nanowire gratings (Zentgraf et al., 2009, Liang et al., 2018), or a multiperiodicity array (Blanchard-Dionne and Meunier, 2019). In most of the studies about nanostructural arrays, simulations have been used to estimate and optimise the sensitivity of sensors: the arrays are then fabricated and the actual sensing performance is

compared with the simulated results. **Figure 2-5** summarises these exceptional studies on nanostructural arrays for EOT biosensors in recent years and details of these arrays are discussed.

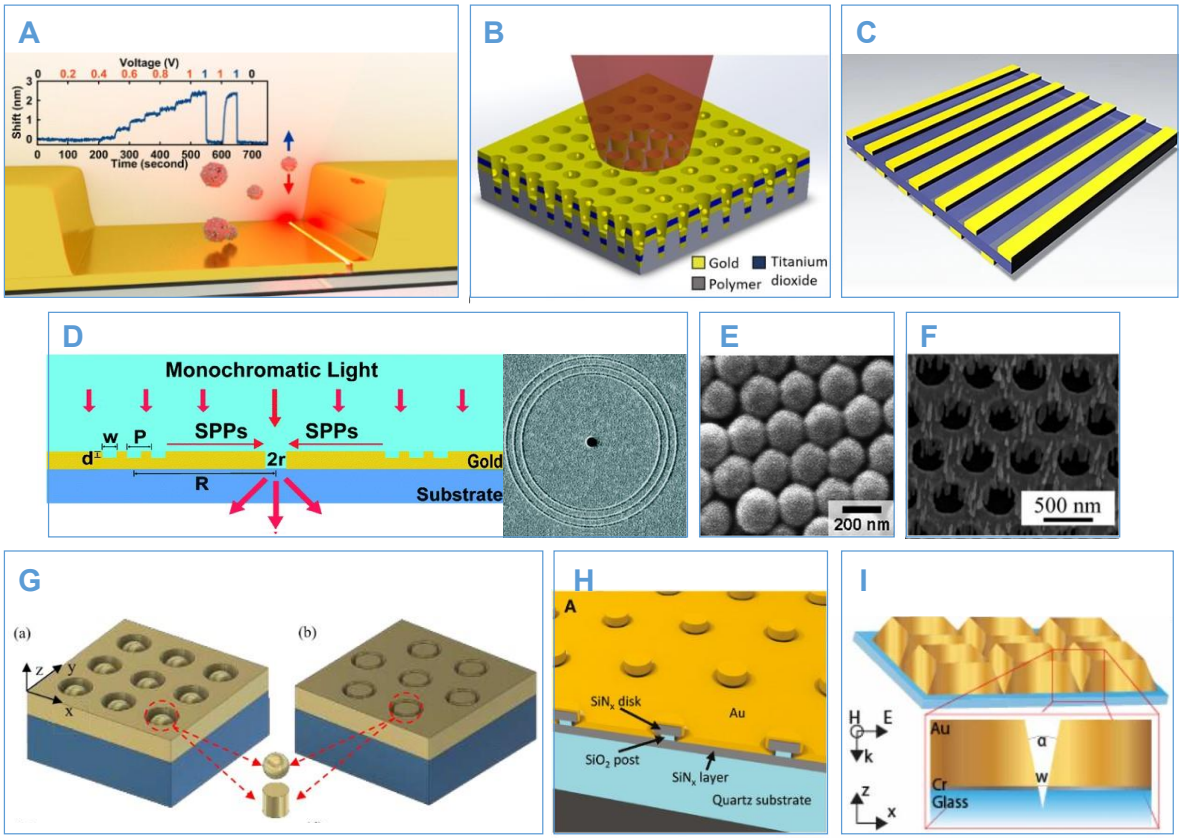

Figure 2-5 Novel nanostructural arrays for EOT sensors. **(A)** Split-trench resonator platform in combination with DEP (Reprinted with permission from Yoo et al. (2021). Copyright 2021 American Chemical Society); **(B)** Metal–Insulator–Metal Nanocup Arrays (Reprinteded with permission from Hackett et al. (2018). Copyright 2018 American Chemical Society); **(C)** Bilayer plasmonic-waveguide structure (Reprinted with permission from Yu et al. (2021). Copyright 2021 PubMed); **(D)** Nanoplasmonic circular interferometric biosensor (Reprinted with permission of Royal Society of Chemistry, from Qian et al. (2019); permission conveyed through Copyright Clearance Centre, Inc.); **(E)** Metal-coated microsphere monolayer (Reprinted with permission from Farcau (2019). Copyright 2019 Scientific Reports); **(F)** Silver nanorod-covered silver nanohole array (Reprinted with permission from Song et al. (2020). Copyright 2020 American Chemical Society); **(G)** Metal nanohole and nanoparticle arrays (Reprinted with permission from Du et al. (2019). Copyright 2019 IOP Publishing); **(H)** Coaxial aperture array (Reprinted with permission from Lee et al. (2020). Copyright 2020 De Gruyter); **(I)** Nanoplatelet array with a sub-20 nm gap (Reprinted with permission from Pisano et al. (2020). Copyright 2022 IOP Publishing).

Yoo et al. (2021) developed a split-trench resonator platform with a 10 nm slit, which serves as a nanoplasmonic resonator and a nanoelectrode for dielectrophoresis (DEP). DEP

was employed to concentrate the analytes at the sensing surface (**Figure 2-5** (**A)**). This novel sensing platform exhibited a sensitivity of 687 nm/RIU, which was comparable with other nanoplasmonic biosensors. Thanks to DEP, bovine serum albumin (BSA) was trapped and concentrated near the slit, resulting in a limit of detection (LOD) of 10 pM after 25 minutes. DEP reduced the detection duration 23 times, enabling rapid and label-free detection of BSA. Bagra et al. (2020) published a similar biosensing concept to detect anti-insulin antibodies at the order of ng/mL; however, this biosensor was not integrated with DEP. The nanoledge served as a nanoplasmonic resonator, a trap for small biomolecules, and a microfluidic dam for the sample. A nanoslit surrounded by a regular array of grooves was modelled and simulated by Daniel and Bawuah (2019) to investigate the optimal arrangement of grooves and slits and potential material to fabricate the sensing surface. The study has shown that a nanoslit could manipulate the output light, and this nanostructural arrangement may be employed for both optical sensors and imaging.

Nanowells and nanocups are also amongst the most studied nanostructures. A metal-insulator-metal nanocup array was invented by Hackett et al. (2018) (**Figure 2-5 (B)**). The EOT biosensor built from this novel nanocup array could be operated in a spectrometer-free manner; thereby providing great potential for point-of-care testing applications. Thanks to the optimal coupling between the cavity and plasmonic resonances, this transmission intensity-based biosensor offered excellent sensitivity of 800 ΔT%/RIU and an LOD of 10 ng/mL for carcinoembryonic antigens, which makes it potentially applicable for point-of-care diagnosis of cancer. Besides the usual circular nanowell, Liu et al. (2019) used a novel fabrication technique to create an elliptical nanowell array. The deep-elliptical-silver-nanowell-array was reported to have a sensitivity of 1,414.1 nm/RIU. This extraordinary sensitivity was acquired after optimising the angle of polarisation, the depth of the nanowell, and the ratio between the major and minor axis lengths of the elliptical hole. Interestingly, it was claimed that the

elliptical nanowell enhanced the sensing performance by over 50% compared with the normal circular nanowell. An EOT sensor with an elliptical nanohole array was also reported by (Robinson et al., 2019). Instead of the nanohole dimension, sensing performance was investigated under different incident light polarisations. The sensitivity was reported to be 414 nm/RIU under optimised conditions.

Nanowire grating also attracts attention for EOT biosensors (Rodrigo et al., 2016). **Figure 2-5 (C)** demonstrates a nanostructure of bilayer nanowire gratings with a lateral shift between the two grating layers (Yu et al., 2021). Although two gratings with perfect lateral alignment have been reported previously (Liang et al., 2018), the study from Yu et al. revealed that the lateral displacement could tune the coupling mode of the nanowire pairs. The weak coupling mode resulted in an exceptionally narrow transmission peak with a high signal-to-noise ratio and ultrasensitivity. The simulation predicted that this nanostructure could provide a refractive index sensitivity up to 1195 nm/RIU, which was much higher than that in previous studies (Yu et al., 2021, Liang et al., 2018).

An EOT biosensor with a sensing surface consisting of an array of hole-ring interferometers was reported to have great sensitivity when these interferometers were compacted in a small sensing area of $9.8 \times 9.8\ \mu m^2$ (Qian et al., 2019) (**Figure 2-5 (D)**). The biosensor was used to monitor the concentration of matrixin secretion from human cells and had an LOD of approximately 18 ng/mL. This novel nanoplasmonic interferometric sensor has great potential in studying cell secretions in a real-time and label-free manner. It was also reported that EOT could be observed from metal-coated microsphere monolayers (**Figure 2-5 (E)**). The use of microspheres smaller than 210 nm in a monolayer propagates the secondary EOT maxima with a better sensing efficiency than previous studies (Farcau, 2019).

Song et al. (2020) covered the silver nanohole array with silver nanorods to fabricate a dual-mode biosensor, as shown in **Figure 2-5 (F)**. The biosensor could detect the analytes through both surface-enhanced Raman scattering (SERS) and SPR signals. This study reported that the sensitivity of the biosensor was 400 nm/RIU. It detected DNA in the human serum at a concentration as low as 0.77 fM and 0.51 pM in the SERS and SPR mode, respectively. The dual-sensing mode provided detecting information from both modes; hence, it enhanced the overall reliability of the biosensor and potentially reduced the rate of false diagnostic results.

Another novel nanostructural array that has been studied for EOT biosensors is a combination of a nanohole array and nanoparticles, as shown in **Figure 2-5 (G)**. The effects of the array period, hole diameter, nanoparticles, and illumination angle on the light transmission were investigated thoroughly through a three-dimensional finite-difference time-domain (FDTD) simulation (Du et al., 2019). The simulated results showed that the addition of nanoparticles could enhance the sensitivity by over 100% due to the Fabry-Perot effect.

Other nanostructural arrays such as a sub-10 nm coaxial aperture (Lee et al., 2020) and a nanoplatelet array with a sub-20 nm gap (Pisano et al., 2020) were explored to identify the distinct feature of each nanostructural array. As shown in **Figure 2-5 (H)**, the coaxial aperture demonstrated a highly tunable EOT platform, in which EOT maximas could be tuned by more than several hundred nanometers (Lee et al., 2020). On the other hand, the nanoplatelet array at a sub-20 nm gap (**Figure 2-5 (I)**) had good sensitivity, and it could be implemented in spectrometer-free optical biosensors (Pisano et al., 2020).

Regardless of the shape or structure of the nanosize array, the goal of these studies is to develop highly sensitive EOT biosensors that could be used in a clinical setting. Innovative fabricating techniques and simulation programs have allowed the exploration of more novel

nanostructural arrays for EOT biosensors and improved the readiness level of the EOT biosensors for point-of-care testing.

2.3.3. Fabrication of an EOT Sensor

The conventional fabricating procedure for a metallic nanohole array includes two main stages: creating a metal film and patterning the nanohole array. A metal film can be fabricated by metal sputtering (Zhang et al., 2015b, Kee et al., 2013) or metal evaporation (Aliberti et al., 2017, Cetin et al., 2015). In the second stage, the nanohole array can be patterned by several methods, including focus ion beam milling (Monteiro et al., 2016, Briscoe et al., 2015, Bdour et al., 2020), E-beam lithography (Cetin et al., 2015, Lee et al., 2018b), and deep ultraviolet lithography (Kee et al., 2013, Soler et al., 2017). Although these methods can create a nanohole array with high quality and resolution, they require a long fabricating time, along with complicated and expensive equipment (Ding et al., 2015, Jia et al., 2013, Im et al., 2011, Valsecchi et al., 2019). These drawbacks may hamper the mass production of nanohole arrays.

Novel patterning techniques have been developed to overcome the limitations of conventional methods, including nanoimprinting lithography (Ding et al., 2015, Jackman et al., 2016, Couture et al., 2016), deep UV lithography (Li et al., 2018, Kee et al., 2013, Soler et al., 2017, Kilic et al., 2018), soft lithography, and nanosphere lithography (Liang et al., 2019, Nan et al., 2020). Details about these methods, resolutions, and throughputs were recently reviewed by Kasani et al. (2019). These novel methods can fabricate the nanohole array in a large surface area more rapidly and cost-effectively (Ding et al., 2015, Jia et al., 2013); however, their resolutions are not as good as those from conventional methods (Im et al., 2011, Kasani et al., 2019). Template stripping is a novel method that can produce a large nanostructural array in a short time, with high resolution and minimal roughness (Im et al., 2011). Briefly, a nanohole array is coated with gold, and the template is slightly pressed

against a substrate with a thin adhesive layer. Because of poor adhesion between gold and templates, the gold film can be stripped and transferred to the substrate with the adhesive layer. Template stripping is relatively simple (Im et al., 2011, Jia et al., 2013) and economical since the template can be reused multiple times (Jackman et al., 2017). Overall, these approaches for fabricating nanostructural sensing surfaces have achieved high quality in a uniform, inexpensive manner, paving the way for mass production.

In recent years, novel nanostructural fabrication methods based on established fabricating techniques have been reported with great innovations, technical modifications, or new materials to achieve enhanced quality and throughput. Novel techniques allow rapid and precise fabrication of nanostructural arrays, such as stretchable imprinting (Liu et al., 2019), interference lithography (Valsecchi et al., 2019), and dual nanotransfer printing (Shin et al., 2019). Stretch imprinting is a derivation of soft lithography, in which the negative template of nanowell arrays is made from polydimethylsiloxane (PDMS), a stretchable material. PDMS enables the fabrication of an elliptical nanostructure in a large area with better control than conventional approaches (Liu et al., 2019). Interference lithography or pure laser interference lithography is a relatively new method that can produce a nanostructural array with high quality and resolution on large areas.

Shin et al. (2019) developed dual nanotransfer printing, a derivation of the template stripping method, to fabricate a nanohole and nanodisk array from one template master. A silicon master with a nanohole array (depth of 100 nm) was deposited with a thin layer of gold (20 nm). A thin adhesive layer was spin-coated onto a glass slide, partially cured, then joined to the master under mild pressure. They were then exposed under UV to cure the adhesive completely, and the gold film with a nanohole array was transferred to the glass slide. Another transfer was conducted with the same master using a thick layer of resin on a glass slide. The resin was pressed against the master with a light pressure to fill up the

nanoholes on the master. After the resin was cured, an array of nanodisks was transferred to the glass slide. This method offered low-cost fabrication because it fabricated a nanohole and nanodisk array on large areas simultaneously; therefore, it has the potential for mass production of sensing surfaces for EOT and localised surface plasmon resonance (LSPR) sensors. An ultrafast femtosecond-laser patterning was reported by Pavlov et al. (2021) for fabricating a doughnut-shaped nanohole array at a rate of 10^6 elements per second. This method allowed fabrication of tunable hole arrays in a high-throughput manner; however, it was only applicable for hole arrays at a micrometre-scale.

Alongside developing high throughput and reliable fabricating techniques, novel materials for the EOT biosensor have been extensively investigated to enhance the sensor's sensitivity. Choosing a suitable substrate to support the metallic film of the nanohole array is crucial because it determines the mode of resonance coupling and impacts the sensing efficiency. Silicon nitride, a high refractive index material, was used as the substrate to manufacture a gold nanohole array in several studies, and it could improve the sensitivity of EOT biosensors (Kee et al., 2013, Soler et al., 2017, Cetin et al., 2015). A thin layer of silicon nitride between a gold and glass substrate could eliminate the EOT mode of the gold and glass layer. The transmission spectra only consist of the plasmonic resonance of the gold/dielectric medium mode. Consequently, the wavelength shift becomes easier to monitor (Cetin et al., 2015). To fabricate a nanostructural gold film on quartz, magnesium oxide could be used as an adhesion layer because it is adequately stable to support the gold film during e-beam lithography. Ultimately, magnesium oxide exhibits no adverse effect on the plasmonic resonance of the gold film, while use of standard adhesives like tantalum, titanium, and chromium leads to considerable optical transmission loss (Sadri-Moshkenani et al., 2020).

For the template stripping method, the adhesives also act as a substrate; therefore, the choice of an adhesive might become vital to both the fabrication process and the sensitivity of sensors. Dore et al. (2020) employed hydroxypropyl cellulose (HPC) membranes as sacrificial water-soluble adhesives for template stripping. Gold films with different nanostructural arrays were successfully transferred to different substrates simply by dissolving HPC in water. Additionally, HPC was adequately rigid to support the crack-free transfer of the gold film, whilst this adhesive allowed high throughput fabrication of the sensing surfaces. HPC-based template stripping was demonstrated to be a practical and straightforward fabrication method with excellent versatility. Vala et al. (2019) explored template stripping with a Cytop film, a water-index-matched polymer, to create a symmetric plasmonic sensor. The sensing platform consisted of a nanostructural gold film and a Cytop-optical adhesive-glass substrate in a backside reflection mode. Theoretically, the symmetrical refractive index environment created a hybrid plasmonic mode that was highly sensitive to changes in the refractive index. However, the reported bulk sensitivity was only 168 nm/RIU in a symmetrical mode and 183 nm/RIU in an antisymmetrical mode, which is below that of other EOT biosensors. To minimise the impact of the substrate and the adhesive layer on the plasmonic resonance, Liu et al. (2020) introduced an innovative, simple method to fabricate a free-standing gold film with a 1.5 μm hole array. A nickel grid supported the gold film with a mesh size of 100 μm, thereby providing a sensing area of approximately 7800 μm^2 for the suspended gold film. Furthermore, the incident angle and the period of the array were tuned to acquire an EOT mode through the entire mid-infrared wavelength range. Free-standing gold film has attracted increasing attention in recent years because it is an ultimate solution to minimize the adverse effect of the substrate on plasmonic resonance (Liu et al., 2020, Du et al., 2020b).

Fabricating methods have also been explored to create nanostructural arrays on large areas with high resolution. A large sensing area enables engineering of a multichannel sensing chip or achieving multiplex sensing. Additionally, the roughness of the gold film contributes to the sensing performance (Nagpal et al., 2009, Zhang et al., 2015a). The supporting substrate of the sensing platform is absolutely crucial to the sensitivity of biosensors. Many substrate materials have been investigated to optimise the optical signal transmission/reflection (Vala et al., 2019, Cetin et al., 2015), simplify the fabrication process (Dore et al., 2020), reduce the interference of the substrate on the plasmonic resonance mode, and enhance the stability of the sensing surface (Sadri-Moshkenani et al., 2020). Current research interest is shifting from identifying the optimal substrate material to diminishing the needs of the supporting substrate or eliminating its adverse effects on the plasmonic resonance mode. Although fabrication does not impact biosensors' sensitivity, it does determine the throughput, manufacturing cost, and productivity of biosensors. Consequently, developing suitable fabrication methods with proper materials plays an important role in commercialising EOT biosensors for point-of-care testing.

2.3.4. Configurations of EOT Biosensors

The configuration of an EOT biosensor also enhances the biosensors' sensitivity, alongside developing novel nanostructural arrays and fabrication techniques. To determine the configuration of the EOT biosensors, the design, engineering, and setup of the sensing platform need to be considered in order to meet the requirements of end-users. An elegant design for the EOT biosensor could improve the portability of sensors, reduce manufacturing and delivery costs, enhance ease of use, and sustain both stability and robustness of the sensor. For instance, DEP was integrated into a sensing platform with a nanometre-scale slit to concentrate the analytes on the sensing surface and amplify the sensitivity whilst reducing

the detecting time significantly (Yoo et al., 2021). **Figure 2-6** outlines several EOT configurations from recent studies.

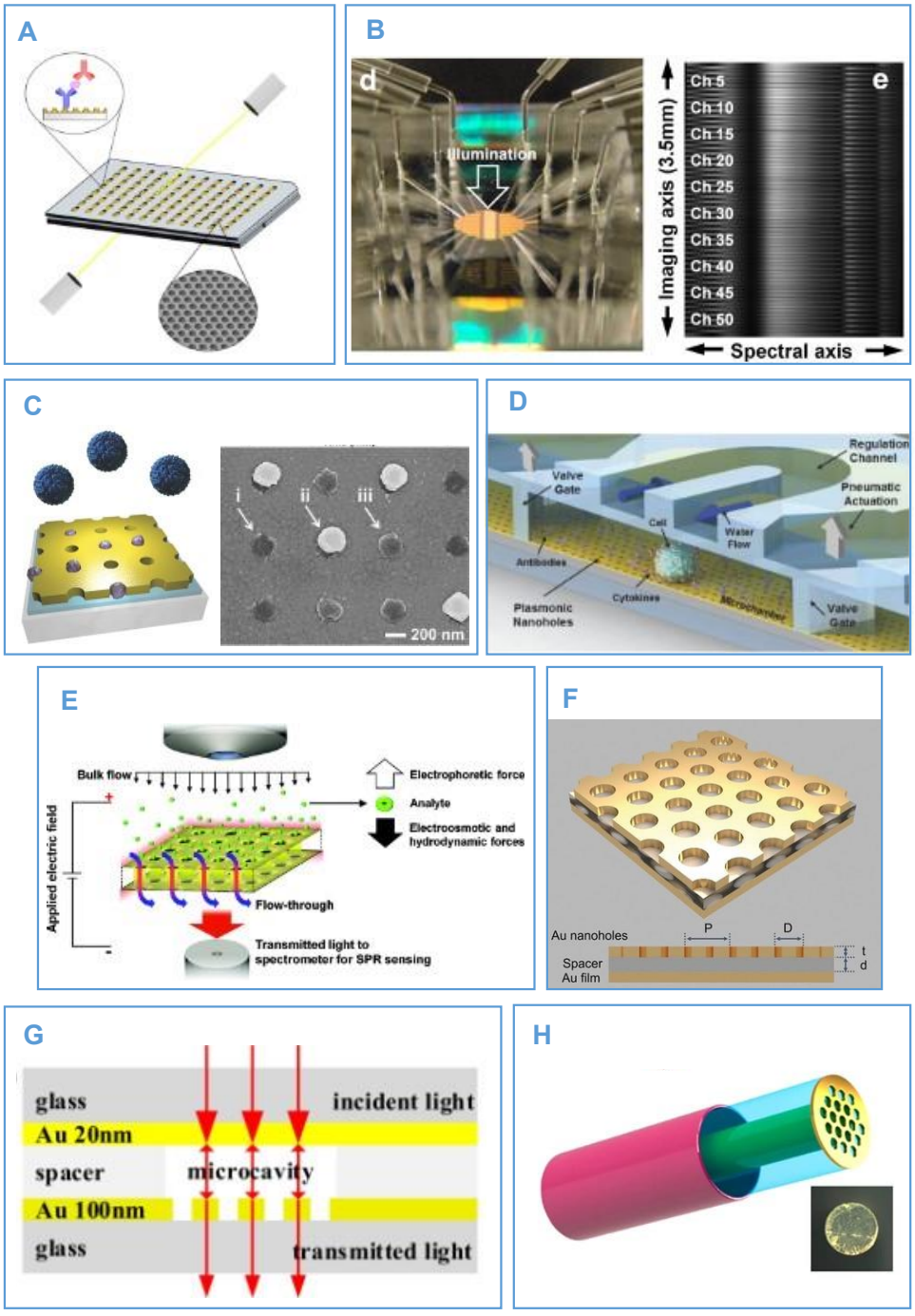

Figure 2-6 Different configurations of EOT biosensors: **(A)** 96-well plasmonic sensing with nanohole arrays (Reprinted with permission from Couture et al. (2016). Copyright 2016 American Chemical Society); **(B)** EOT biosensor with 50 microfluidic channels (Reprinted with permission of Royal Society of Chemistry, from Lee et al. (2012); permission conveyed through Copyright Clearance Centre, Inc.); **(C)** Plasmonic nanohole sensor for capturing single virus-like particles (Reprinted with permission from Jackman et al. (2016). Copyright

2016 Wiley-VCH); **(D)** Optofluidic nanoplasmonic biosensor for single-cell cytokine secretion analysis (Reprinted with permission from Li et al. (2018). Copyright 2018 Wiley-VCH); **(E)** EOT optofluidic concentration (Reprinted with permission from Escobedo et al. (2012). Copyright 2012 American Chemical Society); **(F)** Sandwiched plasmon ruler (Reprinted with permission from Nan et al. (2020). Copyright 2020 Wiley-VCH); **(G)** Micromachined Fabry-Perot interferometer (Reprinted from Tu et al. (2019), Copyright 2019, with permission from Elsevier); **(H)** Fiber-optic SPR-EOT biosensor (Reprinted with permission from Liang et al. (2019). Copyright 2019 Scientific Reports).

During the early phase of EOT biosensor development, most studies focused on improving EOT biosensors' throughput to advance the sensing efficiency. The EOT biosensors were integrated into a 96-well plate system (Couture et al., 2016) (**Figure 2-6 (A)**) or a multichannel microfluidic chip (Soler et al., 2017, Lee et al., 2012) (**Figure 2-6 (B)**) to achieve higher throughput. These high-throughput EOT systems were demonstrated to process multiple samples simultaneously with high accuracy in a short time, and they could even be customised for multiplex sensing. However, in recent years, attention has shifted to improving the sensitivity through novel biosensor designs or built-in preconcentration systems.

The configuration of the EOT biosensor can be engineered and modified to optimise the sensing performance for a specific biosensing application. Jackman et al. (2016) developed an EOT-based biosensor to detect virus-like particles by passively trapping the targeted particles in the nanoholes of the gold film, as shown in **Figure 2-6 (C)**. Based on the size distribution of the targeted virus-like particles, the gold nanohole array was designed and chemically modified to trap the virus-like particles within the nanoholes. The results showed that the biosensor could effectively trap the virus-like particles inside the nanoholes, and the virucidal drug could be evaluated using this EOT biosensor. Another innovative design of an EOT biosensor was proposed by Li et al. (2018) to monitor the cytokine secretion of a single cell accurately and stably in a real-time and label-free manner for several hours (**Figure 2-6 (D)**). The novel biosensor design enhanced the sensing performance in two aspects. First, it allowed cytokine detection at a minimal chamber volume (180 nL); the cytokine

concentration was elevated inside the chamber, thus improving the sensitivity. Second, an additional hydraulic regulation channel helped establish a reliable condition for cell culture across an extended time. Since cell cultures needed to be maintained at 37 °C at a stable oxygen level, the hydraulic channel reduced water evaporation due to the operating temperature and regulated the oxygen level. Both studies have demonstrated that intelligent biosensor design can upgrade the biosensor's readiness for real-world applications.

Optofluidic EOT biosensors have also attracted considerable attention over the last decade. Escobedo et al. (2012) developed a flow-through optofluidic biosensor combined with an electric field gradient to concentrate the analytes at the sensing surface rapidly. The biosensor reduced the testing time to only 1 minute, lowered the LOD by two orders of magnitude, and enhanced protein enrichment by 100 times (see **Figure 2-6 (E)**). Another flow-through optofluidic EOT biosensor was developed and employed as optical chromatography to separate bioparticles by their sizes (Zhu et al., 2019). Reliable separation of nano-bioparticles has been successfully achieved by thoroughly analysing the forces applied on bioparticles during the sensing process. This optofluidic EOT chromatography could replace current optical chromatography techniques because it is simple, inexpensive, tunable, and reliable (Zhu et al., 2019). One challenge of this optofluidic EOT chromatography is the occurrence of deflection of the nanohole sensing surface due to the fluidic flow-through pressure. Bdour et al. (2020) investigated this issue using theoretical, modelling, and experimental approaches. The theoretical models and experimental results suggested that the nanostructural array could withstand less than a trans-membrane pressure of 20 psi. The result helped to determine an operable pressure margin for the application of EOT optofluidic sensors to maintain the geometrical configuration of sensors during the sensing process.

A sandwiched plasmon ruler configuration of an EOT biosensor (**Figure 2-6 (F)**) was found to enhance the sensitivity remarkably. **Figure 2-6 (F)** shows the sensing platform consisting of a planar gold film at the bottom, an artificial polystyrene spacer as the middle layer, and a gold film with a nanohole array on the top. The sandwiched plasmon ruler was reported to be extremely sensitive to the thickness of the polystyrene spacer. A thickness sensitivity of 61 nm/nm resulted in a refractive index sensitivity of up to 1198.6 nm/RIU (Nan et al., 2020). The thickness sensitivity specifies that the transmission dip shifts by 61 nm when the thickness of the polystyrene spacer layer increased by 1 nm. After the analytes were captured on the polystyrene layer, the nanostructural gold film was deposited on the top for detection. This biosensor provided an LOD 18 times lower than ELISA when detecting the inflammatory markers in the blood serum. Tu et al. (2019) investigated an interesting EOT biosensing platform, a micromachined Fabry-Perot interferometer (**Figure 2-6 (G)**) that is similar to a sandwiched plasmon ruler. However, the spacer was modified to be a microcavity to create a microfluidic chip. Moreover, two gold layers were utilised as DEP electrodes to concentrate the analyte on the sensing surface. The experimental results showed that DEP enhanced the sensing sensitivity by six times. The sensitivity of this EOT biosensor was 593 nm/RIU, and it detected down to 1 pM of BSA (equivalent to 66.4 pg/mL) in only 78 seconds. Although the sensitivity of the micromachined Fabry-Perot interferometer (593 nm/RIU) is lower than the sandwich plasmon ruler (1198.6 nm/RIU), their biosensing performance is quite comparable. Nan et al. (2020) reported an LOD of 1.81 ng/mL for procalcitonin (MW = 14.5 kDa) from the sandwich plasmon ruler, while Tu et al. (2019) claimed an LOD of 66.5 pg/mL for BSA (MW = 66.5 kDa) from the micromachined Fabry-Perot interferometer. Both studies have demonstrated that an EOT biosensor with two layers of gold film is promising for ultrasensitive biosensing; however, fabrication issues need to be addressed and optimised to enhance the biosensor applicability (Tu et al., 2019).

A few novel approaches have been reported to simplify the optical setup of EOT biosensors to allow them to be used for point-of-care testing. For instance, spectrometer-free EOT biosensors were developed to reduce instrumentation costs and pave the way for smartphone-based EOT biosensors (Lertvachirapaiboon et al., 2018, Hackett et al., 2018, Belushkin et al., 2020). A fibre-optic SPR-EOT biosensor is a novel configuration of an EOT biosensor (**Figure 2-6 (H)**) with the nanohole array fabricated on the tip of an optical biosensor. A fibre-optic SPR-EOT biosensor allows miniaturisation of the sensing system and simplifies the optical alignment (Liang et al., 2019, Aliberti et al., 2017, Jia and Yang, 2014, Dhawan and Muth, 2008, Polley et al., 2019, Arghir et al., 2015).

These novel configurations of EOT biosensors have been designed to improve the sensing sensitivity and throughput, as well as endow them with great flexibility and portability for clinical and industrial applications. Among them, a sandwich plasmon ruler, flow-through optofluidic, and integration of DEP have been outstanding in enhancing the sensing sensitivity.

2.4. Fibre-optic SPR-EOT Biosensors

2.4.1. Overview about fibre-optic biosensors

Biosensors based on the tip of optical fibres have emerged as a new type of optical biosensor in the last few years. Optical fibres improve mobility and reduce the overall size of optical biosensors; while ensuring optimal optical signal transmission (Lee et al., 2021). Most of the fibre-optic biosensors were developed based on LSPR biosensors. Only a few EOT-based fibre-optic biosensors were studied. **Figure 2-7** exhibits some fibre-optic LSPR biosensors to provide examples for developing fibre-optic biosensors. Many fibre-optic LSPR biosensors generate LSPR signals through an array of nanoparticles. The nanoparticles could be fabricated directly onto the optical fibre facet through lithography (Lin et al., 2011) or immobilised using chemical or physical absorption (Jeong et al., 2013, Lee et al., 2018a, Kim

et al., 2019). The nanoparticles could come in many shapes such as dot (Lin et al., 2011), sphere (Jeong et al., 2013), rod (Lee et al., 2018a), or mushroom shape (Roether et al., 2019), as seen in **Figure 2-7 (A)**, **(B)**, **(C)**, and **(E)**. Regarding the nanoparticle array, a study concluded that a 3D nanostructural array could improve the biosensor's sensitivity by 400% compared to a 2D array (Kim et al., 2019) (**Figure 2-7 (D)**). Furthermore, Roether et al. (2019) reported that the nanostructural array could be fabricated onto a microfluidic chip's surface instead of an optical fibre's facet. However, the sensitivity of this fibre-optic LSPR biosensor is relatively low, only 54 ± 6 nm/RIU. More recent studies on fibre-optic biosensors can be found in the two exhaustive reviews by Lee et al. (2021) and Ricciardi et al. (2015).

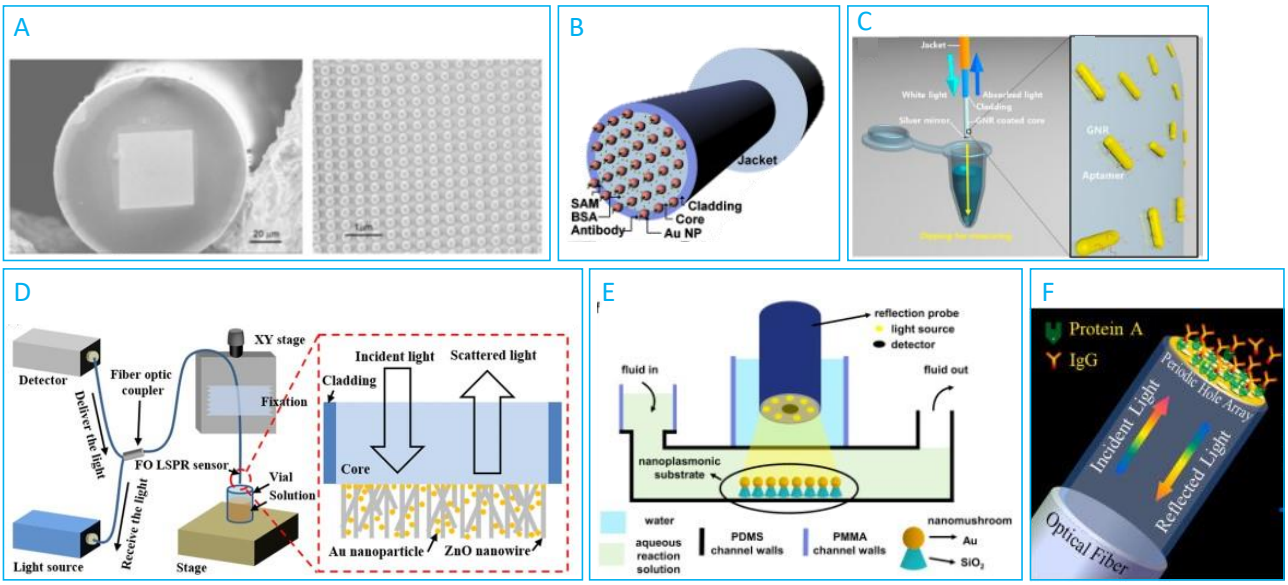

Figure 2-7 (A) Fibre-optic LSPR sensing probe with an array of gold nanodots fabricated by electron beam lithography (Reprinted with permission from Lin et al. (2011). Copyright 2011 Scientific Reports); **(B)** Illustration of an LSPR biosensor created by immobilising Au nanoparticles onto the core of optical fibre through SAM (Reprinted from Jeong et al. (2013), Copyright 2013, with permission from Elsevier); **(C)** Set up of a reflection-based fibre-optic LSPR biosensor and a zoom-in figure of the optical fibre's tip. The gold nanorods (GNR) were immobilised onto the end of optical fibre through thiol and gold physisorption (Reprinted from Lee et al. (2018a), Copyright 2018, with permission from Elsevier); **(D)** Set-up of a reflection-based fibre-optic LSPR biosensor with 3D nanostructure consists of ZnO nanowire and Au nanoparticles (Reprinted with permission from Kim et al. (2019). Copyright 2019 Scientific Reports); **(E)** Depiction of a fibre-optic LSPR biosensor's microfluidic chip. The nanomushroom, which consists of silicon dioxide base and Au nanoparticle tip, were embedded inside the microfluidic channel and not on the tip of the optical fibre (Reprinted from Roether et al. (2019), Copyright 2019, with permission from Elsevier); **(F)** Illustration of a reflection-based fibre-optic EOT biosensor used for IgG detection (Reprinted from Polley et al. (2019), Copyright 2019, with permission from Elsevier).

Although fibre-optic EOT biosensors do not receive as much attention as fibre-optic LSPR biosensors, they were studied and used for several different purposes, such as gas sensing, glucose quantification, and protein detection. The following section further reviews the development of fibre-optic EOT biosensors and their applications.

2.4.2. Fibre-optic SPR-EOT biosensor

Fibre-optic SPR-EOT biosensors or fibre-optic EOT biosensors have been studied for different bioapplications. A fibre-optic EOT biosensor is a novel configuration of an EOT

biosensor. Integrating a metallic nanohole array with an optical fibre makes an EOT-based biosensor more portable, and the setup, significantly, is also simple (Jackman et al., 2017).

An optical fibre effectively guides the light travelling direction; meanwhile, it is lightweight and compact, allowing miniaturisation of the EOT-based biosensor. Unlike the regular setup of an EOT-based biosensor (**Figure 2-4**), the metallic nanohole array is fabricated directly onto the tip of the optical fibre to simplify the optical setup. Although the fibre-optic EOT biosensor holds great promise in point-of-care applications, the fabrication process still hampers the development of fibre-optic EOT biosensors. Table 2-1 outlines the fibre-optic EOT biosensors reported over the last decade. A fibre-optic EOT-based sensing probe was first introduced by Dhawan and Muth (2008). The bottleneck for developing the fibre-optic EOT biosensor is the fabrication of a gold nanohole array on the tip of the optical fibre. Most of the fibre-optic EOT biosensors have been fabricated using focused ion beams (FIB). This method provides high resolution for the nanohole array; however, it is time-consuming to fabricate a large sensing area, and the roughness of sensing gold film is not well controlled (Nagpal et al., 2009). Jia and Yang (2014) used a template stripping/template transfer method to fabricate a gold nanohole array onto the tip of an optical fibre with optical epoxy as an adhesive and supporting substrate. This fibre-optic EOT biosensor offered excellent bulk sensitivity compared with other studies (see Table 2-1). A few novel fabrication methods for fibre-optic EOT biosensors have been established. Liang et al. (2019) used nanosphere lithography to fabricate a gold nanohole array on an optical fibre tip. Polley et al. (2019) employed template stripping; however, the gold film was not mechanically supported by epoxy but was directly fixed onto the tip of an optical fibre through chemical bonds. Du et al. (2020c) reported a novel method to fabricate a free-standing gold film on the tip of an optical fibre using template transfer and wet etching; however, the gold film was attached to the optical fibre solely through physical adsorption. A free-standing gold film is

preferable because it minimises the adverse effects of the supporting substrate on the nanoplasmonic resonance (Liu et al., 2020).

Although a fibre-optic SPR-EOT biosensor is an excellent promising candidate as a point-of-care testing device thanks to its excellent sensitivity and compact size, its application is still very scarce, as shown in **Table 2-1**. Many fabrication challenges remain to be addressed, such as advancing the fabrication of free-standing gold films onto the fibre tips and maturing the flow cell system. The sensitivity of fibre-optic SPR-EOT biosensors could be improved by integrating them with novel EOT biosensor configurations. The micromachined Fabry-Perot interferometer reported by Tu et al. (2019) (see **Figure 2-6 (G)**) could be implemented into a fibre-optic SPR-EOT biosensing platform to achieve better sensing sensitivity. The thin planar gold film can be fabricated on the tip of the incident light optical fibre, and the nanohole array gold film can be assembled on another optical fibre tip to make an EOT sensing probe. The two optical fibres can be aligned face-to-face with extremely small proximity (less than 100 μm) to follow the original configuration design (Tu et al., 2019) and wired together to integrate DEP into a fibre-optic SPR-EOT biosensor. The use of DEP can improve sensitivity, reduce response time, and enhance the overall sensing performance (Yoo et al., 2021).

Table 2-1 Summary of fibre-optic SPR-EOT biosensors.

Targeted analyte	LOD	Detection time	Sensitivity	Fabrication method	Novelty	Potential application	Reference
N/A	N/A	N/A	573 nm/RIU	Focused Ion Beam	A gold nanohole array was successfully fabricated and implemented on the tip of a standard single-mode optical fibre	A compact EOT probe for chemical and biological sensing	(Lan et al., 2014)
BSA	N/A	30 min	595 nm/RIU	Template transfer using adhesives	A simple fabrication method was developed for the nanohole array with high resolution		(Jia and Yang, 2014)
N/A	N/A	N/A	220 nm/RIU	Focused Ion Beam	Peak shifts due to temperature variations were investigated to determine temperature sensitivity	A compact EOT biosensor that can be used for refractive index and temperature sensing simultaneously	(Zhang et al., 2015b)
Glucose	Dependent on microgels concentration	Dependent on microgels concentration	N/A	Focused Ion Beam	Microgels were used to enhance the sensitivity of a temperature-sensitive EOT biosensor with tunable LODs	Glucose detection and quantification	(Aliberti et al., 2017)

IgG from rabbit	N/A	Less than 30 min	420 ± 83 nm/RIU	Template transfer using covalent chemical bonds	A simple method was developed to fabricate a free-standing gold film	A potential device for studying interactions between biomolecules, such as protein A and different types of IgG	(Polley et al., 2019)
Concanavalin A	8.1 µg/mL	Less than 20 minutes	Bulk sensitivity: 432 nm/RIU Surface sensitivity: 389 nm/RIU	Self-assembly nanosphere lithography	The fabrication method was simplified	Characterisation of glycoproteins on the surface of cells	(Liang et al., 2019)
Methanol	2 % volume in gas	N/A	N/A	Template transfer	Epoxy, a nanohole array, and molybdenum disulphide were combined to enhance the sensitivity	Stable sensors for methanol detection at room temperature	(Du et al., 2020a)
Relative humidity (RH)	11 %RH	Milliseconds	279 pm/%RH	Template transfer and wet etching	A free-standing gold film was fabricated using a wet etching method	Compact and rapid detection of humidity in human breath	(Du et al., 2020c)

2.4.3. Interim conclusion

Considering the micrometre-scaled size of the optical fibre, a flow cell with dimensions less than 1 mm needs to be built to enhance the portability and throughput of the fibre-optic SPR-EOT biosensor. The reported fibre-optic SPR-EOT biosensors consist of only one sensing probe. The micrometre flow cells could be connected using microfluidic tubes to produce a multiplexed sensing platform. Alternatively, the flow cells can be installed in parallel to mimic multichannel microfluidic chips. The signal collecting fibres can be connected to a multichannel CCD spectrometer to simultaneously obtain the transmission/reflectance spectra from the flow cells. A biosensing system consisting of multiple individual flow cells allows easy customisation of the biosensor scale. The flow cells could be added or removed to build a sensing system to meet the demand of end users. Additionally, a Light Emitting Diode (LED) can be used as the light source instead of the currently used white light source (Polley et al., 2019, Jia and Yang, 2014) to reduce the biosensor cost and promote its portability. The period of the nanohole array can be tuned to match the transmission/reflectance peaks with the LED wavelength (Qian et al., 2019), thus allowing LED integration into fibre-optic SPR-EOT biosensors.

The fibre-optic SPR-EOT biosensor is not as mature as the EOT biosensor; however, it can inherit the technologies and configurations established for the EOT biosensor to acquire better sensitivity. More studies are needed to develop a commercial fibre-optic SPR-EOT biosensor in the future.

2.5. Applications of EOT Biosensors

Since the discovery of the EOT phenomena (Ebbesen et al., 1998), many EOT-based biosensors have been developed for detection and analysis of various biomolecules (Jackman et al., 2017) due to good sensitivity and simplicity. Applications of EOT have expanded beyond optical biosensors (Rodrigo et al., 2016, Baburin et al., 2019, Prakash et al., 2019); however, only those studies on the bioapplications of EOT biosensors are included. **Table 2-2** lists recent studies on their bioapplications in chronological order. The novelty of each study is also described to provide an insightful perspective on the development of EOT biosensors over recent years.

At an early stage of the development of EOT biosensors, most studies focused on exploring their real-time and label-free sensing ability. They demonstrated the feasibility of using EOT biosensors for different applications. In recent years, novel nanostructural arrays, fabrication techniques, detection strategies and sensor configurations were implemented to boost the sensitivity of EOT biosensors. These studies have addressed technical challenges and paved the way forward for their clinical and industrial applications. Common bioapplications of EOT biosensors include immunoassay, clinical diagnosis, cell analysis, and drug screening and evaluation. EOT biosensors are popular for immunoassay because they are capable of real-time and label-free detection of biomolecules using antibodies on the gold film. The bioapplications in immunoassay are summarized in **Table 2-2**.

Table 2-2 Summary of the studies that used EOT biosensor for bioapplications.

Targeted analyte	LOD	Detection time	Sensitivity	Novelty	Potential application	Reference
E. coli	10^2 cells	2 h	Bulk sensitivity: 406.4 nm/RIU; Surface mass sensitivity: 1.802 ng/mm^2	Capturing bacteria and providing a temperature-controlled environment to monitor the growth of bacteria	Rapid bacterial detection; Rapid antibiotic susceptibility test	(Kee et al., 2013)
Immunoglobin G	0.7 ng/mL	N/a	671 nm/RIU	Impact of a hybrid substrate (silicon nitride + glass) on plasmonic resonance; A spectral integration method to monitor wavelength shifts	Rapid, label-free, and sensitive immunoassay	(Cetin et al., 2015)
Microcystin-LR	10 ng/L	Less than 15 min	946.1%/RIU (Transmission intensity per RIU)	Layer-by-layer polyelectrolyte adsorption to immobilise the bioreceptor	Real-time monitor of quality of drinking water	(Briscoe et al., 2015)
Cardiac biomarker-tropnin I	0.55 ng/mL	30 min	345 nm/RIU	Nanoimprinting lithography to produce nanohole arrays with a low variance between batches	Diagnosis of acute myocardial infarction	(Ding et al., 2015)
Human epidermal receptor protein-2 (HER2) antigen	30 ng/mL	3h	304.5 nm/RIU	Secondary antibody for sandwich capturing of antigens and enhancing the sensitivity	Breast cancer/ tumour diagnosis	(Monteiro et al., 2016)
Virus-like particle	N/a	Less than 20 min	Au/epoxy mode: 307 nm/RIU Au/water mode: 220 nm/RIU	Engineering the nanohole parameters and functionalising the sensing surface to trap the virus-like particles inside the nanoholes	Detection of viruses or viral particles	(Jackman et al., 2016)

Immunoglobin G	Direct detection: 5nM (≈ 800 ng/mL) Sandwich detection: 0.4 nM (≈ 64 ng/mL)	Less than 90 min	900 nm/RIU	Nanohole arrays combined with a 96-well plate to create a 96-well plasmonic plate reader	Multiplex detection of various biomolecules	(Couture et al., 2016)
Prostate-specific antigen (PSA)	Sandwich detection: 0.1 nM (≈ 3.2 ng/mL)					
Methotrexate (MTX) small-molecule drug	10 nM (≈ 4.5 ng/mL)					
C. trachomatis *N. gonorrhoeae*	For *C. trachomatis*: 300 CFU/mL For *N. gonorrhoeae*: 1500 CFU/mL	N/a	600 nm/RIU	Multiplexed microfluidic chips by employing microarray spotting for surface functionalisation	Rapid, label-free, and multiplexed detection of sexually transmitted infections from urine	(Soler et al., 2017)
Albumin	10^7 ng/mL	N/a	460 nm/RIU	Simple detection of biomolecules in complex fluids	Detect hypoalbuminemia for liver damage diagnosis	(Lee et al., 2018b)
Carcinoembryonic antigen (CEA)	10 ng/mL	N/a	800 ΔT%/RIU (Transmission intensity per RIU)	A metal-insulator-metal plasmonic nanocup array for sensing surface combined with image-based detection to replace the spectrometer	Spectrometer-free CEA detection for label-free and rapid cancer diagnosis	(Hackett et al., 2018)
Cytokine of lymphoma cell	0.039 ng/mL		630 nm/RIU	A sub-microliter cell chamber with humidity regulation channels to facilitate stable optical measurements of cytokine secretion	Monitor cytokine secretion of a single cell in a label-free and real-time manner	(Li et al., 2018)

Antipsychotic drug: Buspirone	N/a	1 h	N/a	Conjugating with gold nanoparticles to enhance signal detection for competitive inhibition assays	A rapid, label-free, inexpensive method for drug screening in the early stages of drug development	(Kilic et al., 2018)
BSA	N/a	6 min	Bulk sensitivity: 168 nm/RIU Surface sensitivity: 10.62 nm/RIU	A layer with an equivalent refractive index as water underneath the gold film to create a refractive-index-symmetric environment and enhance the sensitivity	Sensitive and rapid detection of various biomolecules	(Vala et al., 2019)
Anti-human IgG	N/a	30 min	1414 nm/RIU	Deep-elliptical-silver-nanowell-arrays to achieve 50% enhancement compared with circular nanowells	Ultrasensitive EOT sensing of various biomolecules	(Liu et al., 2019)
Matrix metalloproteinase 9	1.78 ng/mL	90 min	2.05×10^3 %/RIU (Transmission intensity per RIU)	Nanoplasmonic interferometer sensor	Real-time and label-free analysis of cell responses	(Qian et al., 2019)
Exosomes	N/A	N/A	N/A	Optofluidic PlasmonIC (OPtIC) microlens at a thickness of subwavelength to support objective-free focusing and a nanohole array with an enlarged central aperture for nanofluidic integration	Optical chromatography to sort exosomes by size	(Zhu et al., 2019)
DNA in human serum	SPR: 0.51 pM (≈ 0.0038 ng/mL)	6 h	400 nm/RIU	A silver nanorod-covered silver nanohole array as the sensing surface to achieve	Ultrasensitive detection of disease-related DNA biomarkers in the serum	(Song et al., 2020)

	SERS: 0.77 fM ($\approx 5.74 \times 10^{-6}$ ng/mL)			dual biosensing mode: SERS and SPR; Tetrahedral DNA probes as the bioreceptor and DNA to form a sandwich configuration to enhance the sensitivity		
Anti-insulin antibodies of type 1 diabetes	0.1 ng/mL	Few minutes	N/a	A nanoledge array fabricated by lithography and focused ion beam	Diagnosis and prediction of the development of type 1 diabetes	(Bagra et al., 2020)
Procalcitonin (PCT) and C-reactive protein (CRP)	PCT: 0.0213 ng/mL CRP: 0.036 ng/mL	15 min	N/a	Au-NP for signal enhancement; microarray spotting for surface functionalisation; Spectrometer-free EOT biosensor	Rapid diagnosis of sepsis and other infections at point-of-care	(Belushkin et al., 2020)
Procalcitonin (PCT) and C-reactive protein (CRP)	CRP: 1.81 ng/mL PCT: 1.24 ng/mL	Less than 90 min	Bulk: 1198 nm/RIU Surface sensitivity: 61 nm/nm	A sandwiched plasmon ruler with a tunable LOD to match the desired detection range	Assists diagnosis of infections	(Nan et al., 2020)

Clinical diagnosis using EOT biosensors includes the detection of microorganisms or biomarkers for specific diseases. EOT biosensors have been developed for the detection of *E. coli* (Kee et al., 2013), sexually transmitted bacteria (Soler et al., 2017), and virus-like particles (Jackman et al., 2016). The most significant advantage of the EOT biosensor for bacterial detection is its detection time. It is less time-consuming than conventional methods. *E.coli* can be cultured on the sensing surface and detected within 3 hours using the EOT biosensor, whilst conventional cell culture requires 24 to 36 hours, or even longer (Fronczek and Yoon, 2016). Sexually transmitted bacteria, including *C. trachomatis* and *N. gonorrhoeae* in urine, can be detected simultaneously and accurately within 15 minutes in a multiplexed microfluidic chip. Two recent studies on using EOT biosensors for infection diagnosis clearly demonstrated that the obtained measurement results from EOT biosensors agreed well with those from current clinical methods (Belushkin et al., 2020, Nan et al., 2020). However, different strategies of signal amplification (sandwiched plasmon rulers and gold nanoparticles) were employed for the EOT sensors in two studies. Belushkin et al. (2020) acquired accurate clinical results within 15 minutes using simple test equipment, while Nan et al. (2020) achieved an LOD that was 18 times lower than that from ELISA, but the EOT biosensor was quite complicated. Moreover, EOT biosensors can assist in rapid susceptibility tests for bacteria or viruses (Kee et al., 2013, Jackman et al., 2016), as well as antibiotic or drug screening. The biomarkers for acute myocardial infarction (Ding et al., 2015), breast cancer (Monteiro et al., 2016), prostate cancer (Couture et al., 2016), various types of cancer (Hackett et al., 2018), liver damage (Lee et al., 2018b), type 1 diabetes (Bagra et al., 2020), and infections (Belushkin et al., 2020, Nan et al., 2020) have been detected with EOT biosensors. A few studies have demonstrated that an EOT biosensor could replace current clinical methods like ELISA and chemiluminescence (Ding et al., 2015, Bagra et al., 2020, Nan et al., 2020). The LOD for detecting biomarkers in the human serum or blood

could be significantly reduced by the EOT biosensor to match the standard level (Lee et al., 2018b, Couture et al., 2016, Monteiro et al., 2016). Some of the studies did not achieve the desired LOD; however, they still provided novel fabrication techniques of nanostructural arrays or improving the sensitivity of the EOT biosensors (Ding et al., 2015, Hackett et al., 2018). Besides detecting microorganisms and biomarkers, detection of DNA is often executed for clinical diagosis. The ultrasensitive EOT and SERS biosensor developed by Song et al. (2020) was shown to assist in detection of disease-related DNA in human serum. In this study, the ultrasensitivity of the biosensor was attributable to a novel nanostructural array and the use of tetrahedral DNA probes as bioreceptors and DNA supersandwiches. This study also demonstrated that the success of detecting various biomolecules entails collaboration between physicists and biomedical scientists.

Cellular analysis has been explored using EOT biosensors because they can detect cellular secretions in a real-time manner with high sensitivity. Monitoring cell secretions is crucial because it helps expand the knowledge of cell behaviour under different circumstances, predict pathological and physiological processes, and assist in developing novel therapies for incurable diseases. Qian et al. (2019) successfully monitored matrix metalloproteinase 9 (MMP 9) from human monocytic cells in a real-time and label-free manner. The cells were cultured separately, and the supernatant was collected every hour to monitor the concentration of MMP 9. The biosensor obtained highly accurate detection results, but the operation was relatively laborious for cell analysis. A better EOT biosensor configuration for cell analysis was developed by Li et al. (2018), and it could capture and culture a single cell on the sensing surface stably over a long time with minimal labour requirement (see **Figure 2-6 (D)**).

A few studies have confirmed the potential of using the EOT biosensor for drug screening and evaluation. For example, EOT biosensors have been used to evaluate antibiotic

and virucidal drug candidates (Kee et al., 2013, Jackman et al., 2016). A susceptibility test of *E. coli* to two antibiotics: tetracycline and ampicillin, was conducted in only two hours. The growth of *E. coli* in the presence of two antibiotics was monitored using an EOT biosensor. It was concluded that *E. coli* was resistant to ampicillin. Kilic et al. (2018) investigated the use of an EOT biosensor for antipsychotic drug screening. A competitive inhibition assay was developed to screen drugs that could bind to dopamine at different drug concentrations. The EOT biosensor helped determine the drug candidate's half-maximal inhibitory concentration, which is a crucial parameter for drug evaluation. An EOT biosensor offers a simple, reliable, label-free, and rapid method for analysing drug candidates, especially during drug development. EOT biosensors have also been used as a platform for environmental analysis (Briscoe et al., 2015) or rapid optical chromatography (Zhu et al., 2019).

EOT biosensors have been explored for clinical tests of real samples for diagnosis of diseases; however, the development of a highly sensitive, reliable and user-friendly EOT biosensor for clinical use requires close collaboration of experts from many disciplines, such as physics, biomolecular science, material engineering, product engineering, and software engineering. One of the very effective methods to improve the sensitivity of the EOT biosensor is to amplify the signal of EOT biosensors, such as employing secondary antibodies (Couture et al., 2016) and gold nanoparticles conjugated with secondary antibodies (Belushkin et al., 2020), or developing novel biosensor configurations (Nan et al., 2020, Tu et al., 2019). Material engineers provide novel materials that meet the demands of fabricating an EOT biosensor. Product and software engineers ensure that the final product of the EOT biosensor and the digital interface are suitable for the targeted end-users. More in-depth studies have been reported involving complicated optimisation of the nanostructural arrays, novel fabricating techniques and combined detection strategies. Physical scientists have simulated and investigated novel nanohole arrays and materials; biomolecular scientists have

identified various bioreceptors and developed detection strategies to achieve the best sensitivity and improve the feasibility of using EOT biosensors for bioapplications. These studies have provided a solid proof-of-concept of using EOT biosensors for point-of-care analysis and diagnostics; however, more clinical tests with clinical samples are still required to demonstrate the robustness and reproducibility of the EOT biosensing platform for point-of-care tests.

2.6. Chapter Summary and Conclusions

Biosensors are one of the most popular research hotspots. Especially during the current pandemic, biosensors are playing a critical role in rapid diagnosis of infected patients. The SPR biosensor is one of the most well-established biosensing platforms, and it has been implemented in many commercialised biosensing devices. Along with the evolution of novel fabrication technologies, EOT biosensors have emerged as potential point-of-care replacements for SPR biosensors.

EOT biosensors are expected to have equivalent sensitivity to SPR biosensors but offer a simpler optical alignment. They have a great potential for point-of-care testing. Previous studies have explored the biosensing capability of EOT biosensors. Many novel nanostructural arrays have been designed, such as nanowire, nanoslit, and nanosphere arrays, to optimise the sensitivity of EOT biosensors for bioapplications. Novel fabrication techniques of the nanostructural array have been developed to demonstrate high-throughput, inexpensive, and effective fabrication methods. The configuration for EOT biosensors has also been studied extensively to increase the readiness level of EOT biosensors for commercialised bioapplications. These configurations optimise the usability of EOT biosensors by improving the biosensing throughput, creating a stable sensing environment, and enhancing sensitivity. Although a highly sensitive, label-free, and real-time biosensing platform using EOT biosensors is still being sought, a high sensitivity, over 1000 nm/RIU,

has been achieved (Nan et al., 2020, Liu et al., 2019, Valsecchi et al., 2019). A fibre-optic SPR-EOT biosensor is a derivative of an EOT biosensor to simplify the optical alignment further and allows miniaturisation of the biosensor. This biosensor is still in its infancy. More in-depth studies are needed to optimise its designs, improve the fabrication methods, and validate the accuracy, sensitivity, reproducibility, and robustness using real samples in industrial or clinical settings.

3. Chapter 3

FIBRE-OPTIC SURFACE PLASMON RESONANCE BIOSENSOR FOR MONOCLONAL ANTIBODY TITER QUANTIFICATION

3.1. Statement of Authorship

Title of paper	Fibre-Optic Surface Plasmon Resonance Biosensor for Monoclonal Antibody Titer Quantification
Publication Status	Published
Publication Details	Ly, Thai T., Yinlan Ruan, Bobo Du, Peipei Jia, and Hu Zhang. 2021. "Fibre-Optic Surface Plasmon Resonance Biosensor for Monoclonal Antibody Titer Quantification" Biosensors 11, no. 10: 383. https://doi.org/10.3390/bios11100383

Principal Author

Name of Principal Author (Candiate)	Thai Thao Ly		
Contribution to the Paper	Designed the conceptualisation and methodology; conducted the experiments, compiled program for data analysis; performed data analysis, investigation, and validation; wrote the original draft.		
Overall percentage	80%		
Certification	This paper reports on original research I conducted during the period of my Higher Degree by Research candidature and is not subject to any obligations or contractual agreements with a third party that would constrain its inclusion in this thesis. I am the primary author of this paper.		
Signature		Date	19/10/2021

Co-author Contributions

By signing the Statement of Authorship, each author certifies that:

i. the candidate's stated contribution to the publication is accurate (as detailed above);
ii. permission is granted for the candidate in include the publication in the thesis; and
iii. the sum of all co-author contributions is equal to 100% less the candidate's stated contribution.

Name or Co-Author	Yinlan Ruan		
Contribution to the Paper	Designed conceptualisation and methodology; performed data validation; provided resources; supervised the project; edited the manuscript; and acted as corresponding author.		
Signature		Date	20 Oct 2021

Name or Co-Author	Bobo Du		
Contribution to the Paper	Designed simulation and performed data analysis.		
Signature		Date	20/10/2021

Name or Co-Author	Peipei Jia		
Contribution to the Paper	Provided resources and prototype		
Signature		Date	Oct 21, 2021

Name or Co-Author	Hu Zhang		
Contribution to the Paper	Supervised the project, provided resources, edited the manuscript, and acted as corresponding author		
Signature		Date	Oct 17,2021

3.2. Publication

3.2.1. Abstract

An extraordinary optical transmission fibre-optic surface plasmon resonance biosensing platform was engineered to improve its portability and sensitivity, and was applied to monitor the concentrations of monoclonal antibodies (Mabs). By refining the fabricating procedure and changing the material of the flow cell and the components of the optical fibre, the biosensor is portable and robust to external interference. After the implementation of an effective template cleaning procedure and precise control during the fabrication process, a consistent sensitivity of 509 ± 5 nm per refractive index unit (nm/RIU) was achieved. Protein A, which can specifically capture Mab, was immobilised on the sensing surface to act as a pair of receptors and ligands. The biosensor can detect the Mab with a limit of detection (LOD) of 0.44 μg/mL. The results show that the biosensor is a potential tool for the rapid quantification of Mab titers. The biosensor can be regenerated at least 10 times with 10 mM glycine (pH = 2.5), and consistent signal changes were obtained after regeneration. Moreover, the employment of a spacer arm $SM(PEG)_2$, used for immobilising protein A onto the gold film, was demonstrated to be unable to improve the detecting sensitivity; thus, a simple procedure without the spacer arm could be used to prepare the protein A-based biosensor. Our results demonstrate that the fibre-optic surface plasmon resonance biosensor is competent for the real-time and on-line monitoring of antibody titers in the future as a process analytical technologies (PATs) tool for bioprocess developments and the manufacture of therapeutic antibodies.

3.2.2. Introduction

The growth in continuous processes for therapeutic Mab production demands innovative/disruptive technologies to monitor the Mab concentration. However, there are few reliable PATs that can be used to measure the Mab titer. The rapid at/in/on-line determination

of a Mab titer is important because it provides real-time information to monitor the product yield for immediate decision-making during production (Gody et al., 2019). In addition, it reflects the impacts of critical/key process parameters (CPPs/KPPs) on the process efficiency. Ideal titer measurement methods should provide Mab titers in a timely manner, with acceptable measuring frequency, accuracy, and precision. Moreover, they need to have sufficient reproducibility and comply with the Good Manufacturing Practices (GMP) requirements and pharmaceutical regulations. An appropriate in/at/on-line titer method should present low-to-no risk of contaminating the process in a GMP production environment (Jenzsch et al., 2018). Portability and ease of maintenance are also crucial factors that influence the choice of titer detection method. The production site usually has limited space; therefore, only compact analytical equipment can be coupled with bioreactors or downstream equipment in/at/on-line. Moreover, in case of failure, the instrument should be able to be repaired or replaced quickly to avoid delays (Gody et al., 2019). Many available Mab titer measurement methods such as Patrol ultraperformance liquid chromatography and Idex Tridex protein analyser satisfy some of these crucial factors; however, they have distinct drawbacks such as high capital and maintenance costs, a substantially spacious dimension, poor accuracy, and low reliability (Gody et al., 2019).

Fibre-optic surface plasmon resonance (SPR) biosensors could emerge as a potential PATs tool to measure Mabs titers. They can rapidly and selectively measure the Mab concentrations through the binding of specific biological factors with outstanding robustness and decent sensitivity. Furthermore, fibre-optic SPR biosensors are very portable and could readily be implemented on-line in a GMP environment. The small size of the biosensors means that a backup biosensor can be accommodated on-site in case of instrumental failure.

SPR biosensors employ a metal film as their sensing surface. The metal surface has free electrons that form collective oscillations when excited by an incident light source. Collective

oscillations of free electrons are also known as SPR, a principal mechanism behind many optical sensors (Jackman et al., 2017). The excitation of electron oscillations at a metal surface creates an electromagnetic field that is highly sensitive to a subtle change in the refractive index at the metal–dielectric interface (Jackman et al., 2017). Therefore, SPR biosensors have excellent sensitivity.

SPR has been well-developed and commercialised for products such as Biacore by Cytiva Life Sciences. Biacore is used to analyse the interaction between biomolecules with excellent sensitivity. However, it is based on a continuous gold film and requires the incident optical beam to illuminate the sample at a specific angle relative to the film to excite the SPR, which leads to a complicated optical setup. Additionally, it is only applicable in a laboratory environment because of its bulky size and high cost. Extraordinary optical transmission (EOT) biosensors are a family member of SPR biosensors, which were developed based on an optical phenomenon observed by Ebbesen et al. (1998). EOT occurs when light incidents a metal film with a sub-wavelength nanohole array at a normal angle (Ebbesen et al., 1998) or a bevelled angle (Zhao et al., 2017). Compared to the SPR biosensors based on the continuous gold film, EOT biosensors based on localised SPR do not require a bulky and fragile prism, and their SPR modes are excited by the beam illuminating the nanohole film with a very flexible angle. This makes them much simpler than SPR biosensors. Furthermore, the nanohole array provides a larger surface area for binding the analytes and facilitates the detection of analytes at a more comprehensive detection area (Du et al., 2020a). Consequently, EOT biosensors have attracted interest as a portable alternative to conventional SPR biosensors.

The development of EOT biosensors becomes more attractive as the technique for surface fabrication with nanohole arrays evolves. A gold film with nanohole array for EOT sensors is usually fabricated by a focused ion beam (FIB) (Aliberti et al., 2017, Briscoe et al.,

2015, Dhawan and Muth, 2008, Escobedo et al., 2011, Escobedo et al., 2012, Ferreira et al., 2009, Im et al., 2009, Im et al., 2010, Lan et al., 2014, Li et al., 2015, Monteiro et al., 2016, Thio et al., 2000, Zhang et al., 2015b) or lithography (Couture et al., 2012, Junesch et al., 2015, Xiong et al., 2016, Dahlin et al., 2014, Couture et al., 2016, Cetin et al., 2015, Ding et al., 2015, Kee et al., 2013). These methods are very costly and time-consuming (Im et al., 2011, Kee et al., 2013), as they require a dedicated instrument to fabricate the surface. Moreover, they cannot fabricate long-order patterns with good precision (Im et al., 2011) and the sensing surface usually has considerable roughness, which may impact the sensing sensitivity (Nagpal et al., 2009). In recent years, template-stripping (also known as template transfer) has been extensively as an alternative method for fabricating the gold film with nanohole arrays to gradually replace the FIB method or lithography (Im et al., 2011, Im et al., 2012, Jackman et al., 2016, Jia et al., 2013, Jia and Yang, 2013, Jia et al., 2016, Lee et al., 2012, Yang et al., 2008, Zhao et al., 2017). Template-stripping was first introduced by Hegner et al. (1993) to generate an ultra-flat gold surface. Nagpal et al. (2009) employed this technique to create an ultra-smooth metal surface with patterns. This method is cost effective since the silicon template can be reused multiple times. It also allows for mass production of the metal film with a smooth surface (Im et al., 2011, Nagpal et al., 2009, Jackman et al., 2016).

The fibre-optic SPR-EOT technique is derived from recently established EOT biosensors and conventional SPR biosensors (Jackman et al., 2017). In most EOT-based biosensors, a nanopatterned gold film is fabricated onto a glass slide, and a polydimethylsiloxane (PDMS) microfluidic chip is attached to the glass slide to form a microfluidic chip. The microfluidic chip could have multiple channels to simultaneously measure many samples (Im et al., 2012, Lee et al., 2012). However, such a setup with microfluidic chips is not adequately portable. The microfluidic chip must be fixed to align

with the focused region of a microscope and the imaging sensor. The biosensor becomes portable, cheap, and robust through the implementation of a gold film on the tip of optical fibres instead of glass slides. Fibre-optic SPR-EOT biosensors have been developed and applied in biomolecular detection by several research groups (Aliberti et al., 2017, Dhawan and Muth, 2008, Lan et al., 2014, Thio et al., 2000, Zhang et al., 2015b, Jia et al., 2016). Herein, template-stripping was used to fabricate a smooth gold-sensing surface with a nanohole array on the tip of an optical fibre for our fibre-optic SOR-EOT biosensors. Our EOT biosensing platform was derived from the platform developed by Jia and Yang (2013).

Our subsequent works have demonstrated that this platform is robust and reliable for practical measurements of large biomolecules. We first improved the reliability and portability of the fibre-optic SPR-EOT biosensor, minimised the external interference via design modifications of the biosensing platform, and elaborated its potential as a PAT tool for detecting Mab titers in a bioreactor. Engineering modifications were made to improve the stability of the biosensor during operation, thus enhancing the overall reproducibility and reliability. After obtaining a biosensing platform with stable operating conditions and excellent reproducibility, the biosensor was applied to detect Mabs at a wide range of concentrations (10^{-5} to 10^{-2} mg/mL). A consistent detection limit of 0.44 µg/mL across three individual sensing probes confirmed the reliability and reproducibility of the biosensor. The results show that our fibre-optic SPR-EOT biosensor can detect a Mab with decent reproducibility and has excellent potential to become a portable at-line PAT device.

3.2.3. Materials and Methods

3.2.3.1. Fabricating the Gold Sensing Surface

The template was a nanopatterned silicon stamp from Lightsmyth (S2D-18D3-0808-350-P, USA) with a hexagonal lattice with a period of 700 nm and a hole diameter of 200 nm. The templates were first cleaned in a Piranha solution for 30 min to remove the residual of the

epoxy glue, then in an Aqua Regia solution for 30 min to remove the residual of gold, and finally in a Piranha solution for 30 min to remove organic contaminants on the template surface. All cleaning steps were carried out in a sonicating bath to maximise the cleaning efficiency. The template quality after each cleaning step was examined under an optical microscope.

After cleaning, the gold film with 100 nm thickness was deposited on the template using a thermal evaporator (Quorum Technology-K975X Turbo-Pumped Thermal Evaporator, UK). The gold nanostructure on the template was then transferred onto the end facet of an optical fibre using epoxy glue.

3.2.3.2. Fabricating and Assembling the Flow Cell

A chamber of the flow cell designed with dimensions of 10 × 6 × 6 mm was printed from a photopolymer resin (Formlabs, USA) by a 3D printer (Form 2, Formlabs, USA), as shown in Figure S1 (Supplementary document). Each complete flow cell consisted of one optical fibre attached with a sensing gold film as the input end, one bare optical fibre to collect the transmission signal from the gold film on the input fibre, two stainless steel microfluidic tubes for the solutions flowing in and out, and a 3D-printed chamber. Finally, all these components were assembled, and all joints were sealed with superglue to ensure that no bubbles were produced in solution samples.

3.2.3.3. Data Interpretation

The optical transmission signal was collected by an optical spectrometer (USB4000, Ocean Insights, Orlando, Florida, USA) with a resolution of 0.1 nm. The data were manually recorded before and after every experiment step and then analysed at the end of the experiment. SpectraSuite exported the automatically recorded data every 5 seconds during the

experiments, which communicated with Matlab (Mathworks, Natick, Massachusetts, USA) to immediately visualize the real-time responses of the sensors during an experiment.

3.2.3.4. Sensitivity Test

The flow cell was alternately injected with water, 5% NaCl, 10% NaCl, and 20% NaCl solutions to investigate the transmission signal change when the refractive index of the NaCl solution increased.

3.2.3.5. Protein A Immobilisation Using Spacer Arm and Zero-length Crosslinker

The gold film was first functionalised with 20 mM of cystamine in Mili-Q water for 1 h. The sensing surface and the flow cell were rinsed with 100 µL of Mili-Q water, and a phosphate-buffered saline (PBS) buffer (pH = 7.4) was used as flow medium for the following steps. A mixture solution of 0.005 M SM(PEG)2 (Sigma Aldrich #22102) and 0.01 M EDTA in PBS (pH = 7.4) was pumped into the flow cell to attach the SM(PEG)2 spacer arm to the amine functional group of cystamine via NHS ester reaction. The flow cell was rinsed with 100 µL of PBS buffer to remove SM(PEG)2 and EDTA residues upon completion of the reaction. The protein A solution (Sigma Aldrich) at 1 mg/mL that was reduced in 0.02 M tris(2-carboxyethyl) phosphine (TCEP) (Sigma-Aldrich) in PBS (pH = 7.4) for 2 h was injected into the flow cell to attach protein A to the SM(PEG)2 molecules. After 70 min of protein A immobilisation, the excess of protein A was rinsed with 100 µL of PBS buffer. Unspecific binding sites on the gold film after protein A immobilisation were blocked with 1% of bovine serum albumin (BSA) in PBS buffer (pH = 7.4) for 30 min.

In another experiment, protein A was immobilised on the sensing surface using a zero-length crosslinker to study the contribution of the spacer arm to the biosensor's detecting sensitivity. Protein A was immobilised to a 3-Mercaptopropionic acid (3-MPA) self-assembled monolayer (SAM) on the gold film via carbodiimide crosslinking reaction. The

gold sensing surface was first functionalized with 20 mM of 3-MPA in Mili-Q water for 1 h. A total of 200 µL of a mixture solution of 0.2 M 1-ethyl-3-(3-dimethyl aminopropyl) carbodiimide hydrochloride (EDC) and 0.05 M N-hydroxysulfosuccinimide (Sulfo-NHS) was injected into the flow cell to create a SAM monolayer. The surface was quickly rinsed with PBS buffer for 1 min. A total of 1.5 mL of 1 mg/mL of protein A was pumped through the surface for 70 min to allow for the immobilisation of protein A on the SAM on the surface. The immobilising reaction was quenched using 300 µL of 0.1M ethanolamine. Unspecific binding sites were blocked with 1% of bovine serum albumin (BSA) in PBS buffer (pH = 7.4) for 30 min.

3.2.3.6. Monoclonal Antibody Detection

The anti-β-amyloid monoclonal antibody (Mab) produced in mouse (Sigma Aldrich A8354) (Molecular Weight = 110 kDa) was used to evaluate this sensing platform. The Mab solutions were prepared at a concentration ranging from 10^{-5} mg/mL to 10^{-1} mg/mL. A total of 200 µL of the Mab solution was pumped into the flow cell at an ascending concentration. After each measurement, the gold film was rinsed with 100 µL of PBS buffer. The flow rate was kept at 20 µL/min throughout the experiment.

For the experiments investigating monoclonal antibody detection with and without a spacer arm, the antibody samples were injected into the flow cell in the order of ascending concentrations ranging from 10^{-5} mg/mL to 10^{-2} mg/mL. Each sample was injected for 10 min to measure the wavelength shift. The surface was rinsed with PBS buffer for 5 min to remove any excess antibody on the sensing surface and become ready for the following sample.

3.2.3.7. Protein A Regneration

The regeneration of Protein A was carried out in two attempts, and the same sensing gold film was used in both attempts. In the first regeneration attempt, after 200 µL of antibody solution was applied at a 0.01 mg/mL concentration for measurements, the flow cell was rinsed with 100 µL of PBS buffer and 50 µL of 0.1 M glycine hydrochloride (pH = 2.8) as a stripping solution. The flow cell was equilibrated with 100 µL of PBS buffer. The above process was repeated five times for the first regeneration attempt. After the first regeneration attempt, the immobilised protein A on the sensor surface was stored at 4 °C in PBS buffer with 0.01M EDTA for one week before the second regeneration attempt. In the second regeneration attempt, the sensing gold film was treated with 6 M guanidine hydrochloride in Mili-Q water for 5 min to remove residual proteins or antibodies on the sensing surface. Five regenerating tests were carried out, similarly to the first attempt.

3.2.4. Results

3.2.4.1. Fabrication of Fibre-optic EOT biosensor- Incoporated Mab Detection Device

One of the most remarkable features of the EOT biosensors compared to the traditional SPR biosensors is that it offers a more straightforward optical setup, facilitating miniaturisation of the sensor platform. To further improve the portability of fibre-optic EOT biosensors and address the engineering issues in the previous design by Jia and Yang (2014), modifications were made to the biosensor design on the original prototype. In the original prototype, polydimethylsiloxane (PDMS) was used to fabricate a flow cell; optical fibres and microfluidic tubes were attached to the flow cell by press fits. There were three engineering issues associated with this biosensor prototype. First, the flow cell made from PDMS was quite fragile and not applicable to long-term usage. Second, the optical fibres used in the prototype had sleeves and connectors. These optical fibres could not provide a completely

confined and airtight seal for the flow cell due to gaps between the sleeves and connectors of optical fibres. Consequently, there was a risk of air bubbles in the flow cell during measurements, and air bubbles would interfere with the detection of signals. Third, the optical fibre for the prototype had multiple structural components, but these components were not essential for the biosensor. These structural components accounted for an extra cost, and led to a heavy sensor and complex instrument.

Modifications were made to address the above issues and improve the portability and overall performance of the fibre-optic EOT biosensor for Mab measurements. Redesigning flow cells and selecting suitable materials significantly improved the airtightness and sturdiness of the fibre-optic EOT biosensor. **Figure 3-1** illustrates the 3D simulation of the flow cell and the actual flow cell fabricated by a 3D printer. The chamber of the flow cell. was designed using 3D CAD sketching software to ensure it could be tightly connected to the optical fibres and microfluidic tubes. It was fabricated by a 3D printer using a photopolymer resin, since this material is more durable than PDMS and can be reused multiple times. Second, only the core of optical fibres and a stainless-steel ferrule were used to fabricate the fibre-optic EOT biosensor to reduce the cost and weight of the biosensor. They were assembled with epoxy glue to prevent air-leaking gaps between the optical fibre and the stainless-steel ferrule. Finally, all individual components, including the flow cell’s chamber, two optical fibres, and two microfluidic tubes, were assembled by a superglue to complete the flow cell.

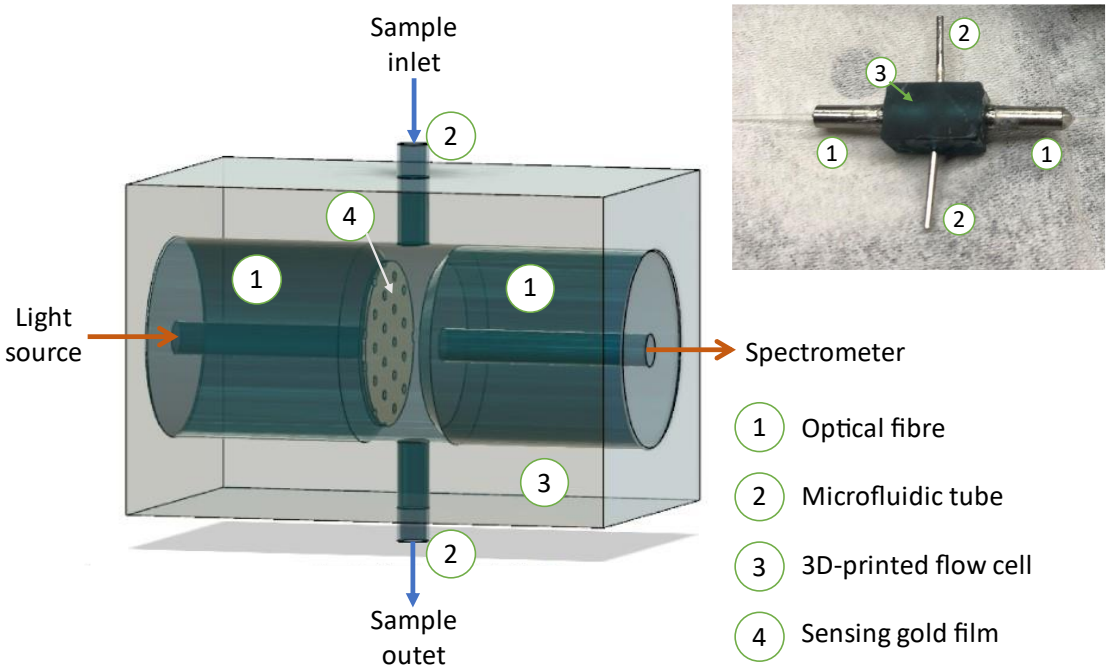

Figure 3-1 3D sketch simulates the flow cell after assembling with optical fibres and microfluidic tubes, and a photo of an actual flow cell after assembly

The weight of the flow cell is approximately 5 g with a dimension of 6 × 6 × 10 mm, which offers good portability and great potential for on-line or point-of-care applications.

3.2.4.2. Sensitivity of the Fibre-Optic EOT Biosensor

Three sensing probes were prepared for Mab detections. Before applying these probes to Mab detections, their sensitivity was determined. NaCl solutions at 0%, 5%, 10%, 15%, and 20%, corresponding to a refractive index (RI) of 1.3330, 1.3418, 1.3505, 1.3594, and 1.3684, respectively, were pumped into the flow cell and the optical transmission spectra were recorded (**Figure 3-2 (a)**). A redshift was observed in the optical transmission wavelengths when the NaCl concentration increased. A higher NaCl concentration at a higher RI is correlated with a larger redshift in the optical transmission spectra.

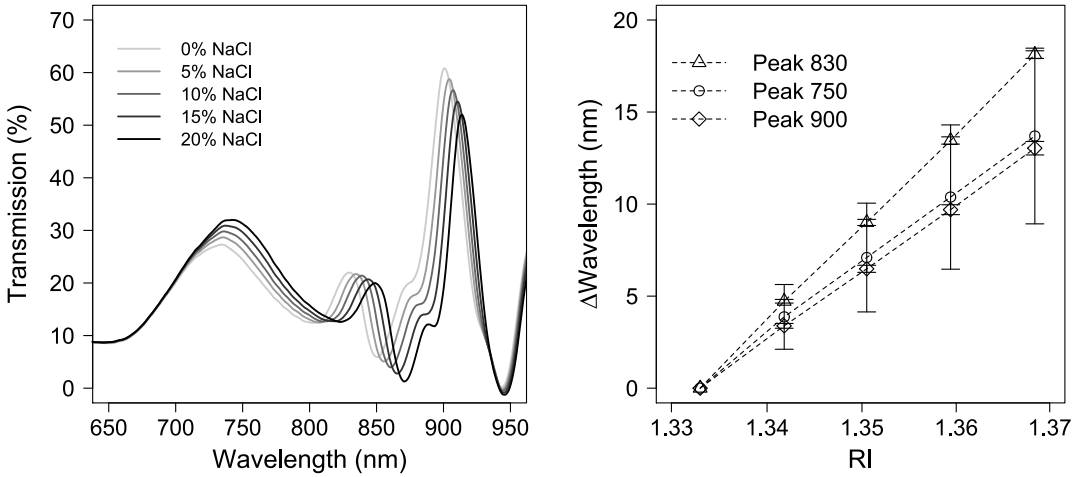

(a) **(b)**

Figure 3-2 (a) Wavelength shifts in optical transmission at different NaCl concentrations for sensitivity tests; **(b)** Average wavelength shifts in optical transmission peaks at different NaCl concentrations from three sensing probes

The wavelength shifts in the optical transmission peaks of three probes were evaluated at different reflective indexes, as shown in the scatter graphs of **Figure 3-2 (b)**. Overall, the wavelength shift has an excellent linear correlation with the refractive index. Prominent peaks were chosen at 750 nm, 830 nm and 900 nm, because these were present in all optical transmission spectra, are highly distinguishable from other peaks and shoulders, and have decent symmetry. These prominent peaks also allow for feasible curve-fitting for data analysis. In **Figure 3-2 (b)**, the peak at 830 nm has the most significant redshifts in the optical transmission spectra, with very consistent sensitivity among the three probes (509 ± 5 nm/RIU) in comparison with the peaks at 750 nm (383 ± 130 nm/RIU) and 900 nm (366 ± 10 nm/RIU). The sensitivity of the peak at 900 nm has a good consistency for the three probes; however, the peak at 900 nm is less sensitive than the peak at 830 nm at different RI values. Although the redshifts of the peak at 750 nm are distinct as the RI value increases, they are less consistent than those at 900 and 830 nm, which might be due to the spectral error resulting from the imperfection and roughness of the gold film. According to finite-difference time-domain (FDTD) simulations, the peak at 750 nm can be attributed to the local surface

plasmon resonance inside the nanoholes when the peak at 830 nm and 900 nm may originate from the top edge of the nanohole and the bottom surface of the gold film. The simulation result agrees well with the sensitivity test result because peaks at 750 nm, 830 nm, and 900 nm shift significantly to the RI change of the NaCl solution. Details of the simulated result are included in the Supplementary document. ANOVA on the sensitivity of peaks at 750 nm, 830 nm, and 900 nm across three sensing probes reveals that the mean values for the sensitivity from three sensing probes at three peaks are not significantly different ($p = 0.12$). Additionally, t-test analysis suggested that the sensitivity of the peak at 830 nm is significantly different from that at 900 nm ($p = 0.002$), while there is no statistical difference for the sensitivity between 750 nm and 830 nm ($p = 0.123$). Since there is a large deviation in the sensitivity of the peak at 750 nm across three sensing probes, the peak at 830 nm is chosen for data analysis in the final analysis due to its excellent sensitivity and consistency.

The minimal variations in the sensitivity of the peak at 830 nm among three probes indicate the excellent reproducibility of the template transfer procedure in the probe preparation process. It is critical to ensure that the template is placed vertically against the optical fibre during the template transfer process. It was reported that the sensitivity of an EOT biosensor could be tuned by changing the light incident angle (Zhao et al., 2017), which indicates that, despite their sharing the same nanohole array, with the same pattern and the same silicon template, the sensitivity could vary due to the different angles between the template and the optical fibre during the template transfer process. We used a microscope camera to monitor the template transfer process and ensure that the template was vertical to the optical fibre.

Minor variations in the sensitivity in **Figure 3-2 (b)** could be further mitigated by a well-controlled template transfer process using robotic arms. It is impossible to examine the consistency of the sensitivity in previous studies, especially those based on multi-channel

microfluidic chips, because these experimental results were presented from a single transfer (Im et al., 2011, Jackman et al., 2016, Jia et al., 2013, Yang et al., 2008, Hegner et al., 1993). Maintaining consistency in the sensitivity during the template transfer is vital because it dramatically impacts the feasibility of commercialising fibre-optic EOT biosensors for application in Mab titer measurements. Our fabrication process is demonstrated to have excellent reproducibility in terms of sensitivity from three template transfers when the process is well-controlled.

3.2.4.3. Monoclonal Antibody Detection

The fibre-optic SPR-EOT biosensor was tested to quantify Mab concentrations in a real-time and label-free manner. The experiments were designed to demonstrate that (1) the measured antibody concentration results could be reproducible; (2) the protein A immobilisation process could be simplified without spacer arms; (3) the sensor could be reused after regeneration.

To detect and quantify the Mab concentrations, protein A was immobilised onto the gold film, since it has a high affinity for the antibody. A murine monoclonal anti-β-amyloid antibody IgGa2 was chosen as a target protein because of its strong interaction with protein A (GE Healthcare 2016). The antibody concentration in the experiment tests ranged from 10−5 mg/mL to 0.1 mg/mL. The experiment was carried out in triplicate to obtain an average standard curve, as shown in **Figure 3-3 (a)**.

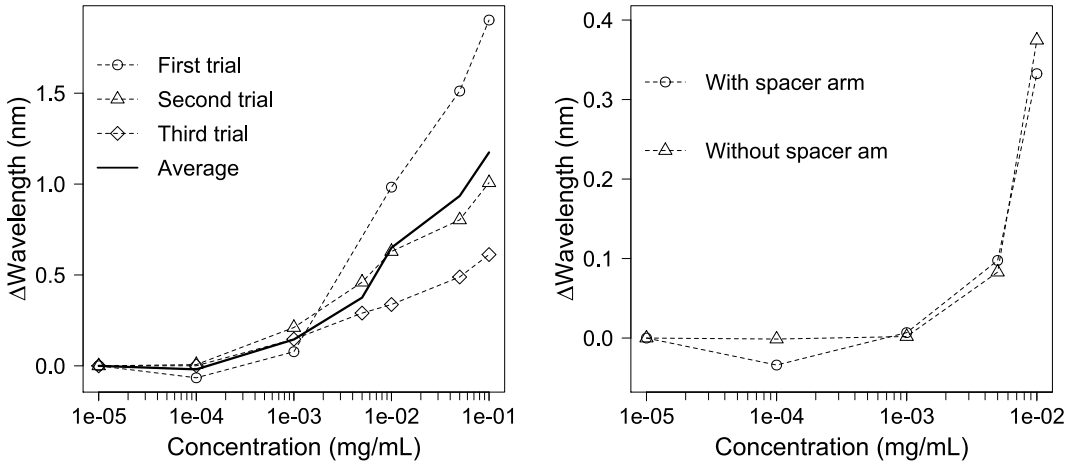

(a) **(b)**

Figure 3-3 (a) Antibody detection using protein A-based fibre-optic SPR-EOT biosensors in triplicate with spacer arm; an average of three replicates is shown as a solid line; **(b)** Impact of spacer arms for immobilising protein A on the detected results

The signal starts to noticeably shift when the Mab concentration is beyond 10−3 mg/mL. As the concentration increases, the wavelength is significantly shifted. From the three trials, a similar limit of detection (LOD) is found for the Mab. The average LOD is calculated as 0.44 µg/mL. Large deviations are observed among the three tests at a high antibody concentration. The deviations could be ascribed to the manual fabrication process for the optic EOT-based biosensor. It is worth mentioning that these measurements were carried out for Mab samples prepared from different batches. An automatic fabrication process for the biosensor for the same batch Mab samples could significantly reduce the variations at a high protein concentration.

3.2.4.4. Monoclonal Antibody Detection Using a Zero-Length Crosslinker

The effect of the spacer arm between immobilised protein A and the gold film on Mab detection was investigated, and the results are depicted in **Figure 3-3 (b)**. Spacer arms were demonstrated to improve the detection sensitivity, reduce non-specific binding and assist in oriented protein immobilisation (Zhang et al., 2016a). However, the employment of a spacer arm in an immobilising process contributes to an additional cost for the materials and a long

preparation time. Hence, we compared the detection sensitivity of Mab titers with and without a spacer arm. Protein A was immobilised either with a spacer arm $SM(PEG)_2$ or directly onto the gold sensing surface using zero-length carbodiimide crosslinking without this spacer arm. The results suggest that the spacer arm does not significantly boost the detecting sensitivity, since the shift is 0.333 nm with a spacer arm at an antibody concentration of 0.01 mg/mL, and 0.375 nm without a spacer arm (as **Figure 3-3 (b)**) Our results do not align with the conclusion from a previous study, in which SMPEG, when used for oriented protein immobilization, could lower the LOD and significantly reduce non-specific binding (Zhang et al., 2016a). The unexpected difference in these experimental results could be due to the difference in antibody–antigen and protein A–IgG binding interactions. The orientation of an antibody is crucial for antibody–antigen interactions because antigens can only bind to the fragment antigen-binding (Fab) region. When the Fab region is affected by the immobilisation process, the detection ability of the biosensor could be severely impaired. For Protein A, each protein A could accommodate up to two IgGs, because the binding ratio between protein A and IgG is 1:2 (Yang et al., 2003). When one binding site of protein A is hidden during the immobilisation process, IgG molecules could bind to another binding site of protein A for detection by the sensor. In our case, the spacer arm could help to enhance the flexibility of the immobilised protein A, but could not oriente protein A molecules during immobilisation. However, due to the considerable size difference between protein A (42 kDa) and IgG (110 kDa) (Yang et al., 2003), the hindrance effect could occur when IgG binds to a layer of protein A that is immobilised onto a 2D surface; thus, the contribution of the spacer arm in improving the protein flexibility could become negligible.

3.2.4.5. Protein A Regeneration

Finally, we investigated the feasibility of using the fibre-optic SPR-EOT biosensor as a PAT tool to continuously monitor the Mab titer in a bioreactor for a fed-batch operation. Two different regeneration attempts were conducted for protein A, using the same sensing probe, immobilised with protein A. In the first regeneration attempt, the sensor was tested with five sample injections (0.01 mg/mL antibody). After each measurement, 0.1 M glycine hydrochloride (pH = 2.8) was applied to strip IgG molecules, and protein A was regenerated after equilibration with the PBS buffer. After five regenerations in the first attempt, the sensor was stored for a week. The sensing surface was then cleaned with 6 M guanidine hydrochloride in Milli Q water for 5 min to dissolve the residue of the sample Mab before a new sample was charged (Esmonde-White et al., 2017). Another five samples were processed in a similar procedure to the first attempt. The sensorgrams of both trials are shown in **Figure 3-4**. Two graphs start from a baseline, where the medium is PBS buffer (pH = 7.4), and no Mab is bound to the immobilised protein A. The signal starts to increase after the injection of 0.01 mg/mL Mab (pH = 7.4) in 10 min. The signal change is maintained even after the sensing surface is rinsed with a PBS buffer (pH = 7.4) for 5 min. The sensing surface is then regenerated by a quick flush with 0.1 M glycine hydrochloride (pH = 2.8), and a sharp and defined peak appears in the sensorgrams. After regeneration, the flow cell is rinsed with PBS buffer (pH = 7.4), and the transmission signal returns to the baseline before the next regeneration experiment. According to the sensorgram of the first attempt (**Figure *3-4* (a)**), the signal does not return to the baseline after the first regeneration; however, the wavelength shifts due to Mab injection after each regeneration are very consistent. An average wavelength shift of 0.126 ± 0.003 nm at an antibody concentration of 0.01 mg/mL is obtained for five regenerations after stripping the sensing surface with a strong acid. The signal shift cannot return to the initial baseline after the first regeneration, indicating that there are

sample residues on the sensing gold film. Although 0.1 M glycine hydrochloride (pH = 2.8) is often used in a protein A column to remove Mab residues before equilibration, Mab samples may be more strongly bound to protein A on the 2D sensing platform than in a protein A column.

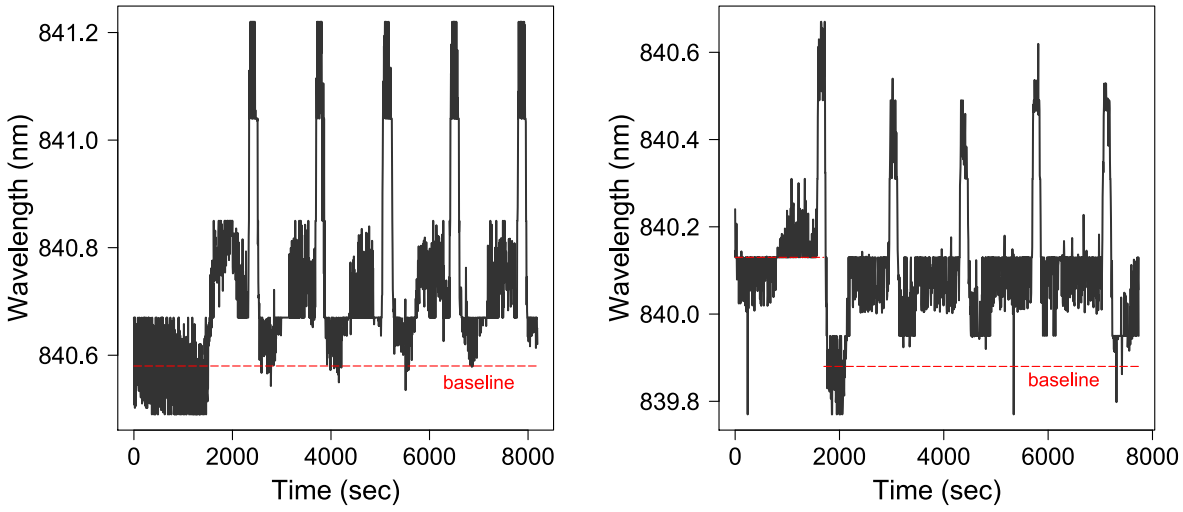

(a) **(b)**

Figure 3-4 Sensor grams of two protein A regeneration attempts. **(a)** First attempt with five runs of protein A regeneration: **(b)** Second attempt on seven days after the first one with five protein A regenerations

In the second regeneration attempt (**Figure 3-4 (b)**), guanidine hydrochloride was used to strip the Mab residues after Mab was injected into the flow cell. According to the sensorgram, the signal drops below the initial baseline after the first regeneration in the second attempt. It is possible that the combination of guanidine hydrochloride then 0.1 M glycine hydrochloride (pH = 2.8) might have stripped more residual Mab than guanidine hydrochloride alone. After the first regeneration attempt, the average signal shift in antibody detection increases to 0.167 ± 0.002 nm, indicating that the sensing surface has fewer Mab residues, while protein A still maintains its bioactivity. The sensing surface is coated with protein A, a very robust protein, as a detecting ligand, so that the signal could be specific to Mab molecules; the sensing surface could be reused many times by regenerating the protein

A surface after each use. Therefore, the sensor could have an excellent potential for the continuous monitoring of Mab samples in a bioreactor.

3.2.5. Discussion

In recent years, optical biosensors have received great attention due to their advantages over other types of sensors. The most distinctive advantages include their excellent sensitivity and specificity, compact size, and label-free detection, making optical biosensors a perfect candidate for point-of-care or at/in/on-line monitoring applications (Chen et al., 2020). They have been extensively studied for their various biological applications such as medical diagnosis, pharmaceutical/food process control, or the detection of chemical residues in the environment/food/water (Chen and Wang, 2020). Despite an increasing number of studies on optical biosensors, few of them have been applied to routine and commercial use (Prasad et al., 2019, Chen and Wang, 2020). Factors that hinder the commercialisation of these optical sensors include the poor stability of the immobilised protein, high cost of the fabrication of sensors, low throughput without miniaturised optical biosensors, and insufficient validity (Prasad et al., 2019). In this study, the regeneration experiment demonstrated that the immobilised protein A could become stable, with similar bioactivity, after one week at 4 °C. Protein A can be immobilised via a zero-length crosslinker to simplify the fabrication procedure.

Additionally, the cost of fabricating a sensing flow cell is around 15 Australian dollars at a laboratory scale, and the flow cell parts are sterilisable and reusable. Compared to other PATs for measuring Mab titers, the cost of fabricating fibre-optic SPR-EOT biosensors is low; the production cost could be even lower at a larger manufacturing scale. The flow cell is compact and portable, with great potential for implementation in a GMP environment. Throughput could be improved by implementing parallel flow cells into the biosensor.

Ultimately, the proof-of-concept using of the fibre-optic SPR-EOT biosensor to quantify Mab samples as an at-line/on-line PAT tool has been demonstrated. Our antibody detection result is comparable to the results from a previous study (Couture et al., 2016). A 96-well EOT biosensor had a sensitivity of 900 nm/RIU and the LOD of 5 nM for IgG detection (equivalent to 0.75 μg/mL, assuming that the MW of IgG is 150 kDa). The overall peak shift was 1.8 nm at the IgG concentration ranging from 1.5×10^{-5} to 1.5×10^{-1} mg/mL. This overall shift is greater than ours, which is less than 1.5 nm over the concentration range from 10^{-5} to 10^{-1} mg/mL. The difference in overall shifts is due to the sensitivity of the two different systems (900 nm/RIU for 96-well EOT biosensor vs. 509 nm/RIU for our biosensors).

Considering the increasing development of therapeutic proteins toward a continuous and automated operation, fibre-optic SPR-EOT biosensors could be applied to the real-time monitoring of Mab titers in an automated feedback control system (Gody et al., 2019). Comparing the methods used to measure Mab samples using HPLC or derive the Mab titer by monitoring the biomass/metabolites concentration, the fire-optic SPR-EOT biosensor is cheap, portable, and rapid in the detection of Mab molecules in the sample, and it is also easy to operate and implement. HPLC with automated sampling is the most accurate chromatographic method for at-line detection of Mab titers; however, it is resource-intensive, laborious, and requires a considerable amount of space (Gody et al., 2019). On the other hand, Raman spectrometry is the most attractive in-line optical method for quantifying titers (Gody et al., 2019). However, the Raman signal is often very weak. The interpretation of the Raman spectra for a Mab sample includes many impurities, including host cell proteins, DNA/RNA, metabolites and Mab variants, which can be very challenging (Esmonde-White et al., 2017). Our fibre-optic SPR-EOT biosensor is a potential PAT for the continuous monitoring of Mab samples in a bioreactor. It can rapidly quantify the Mab concentration at-

line, similar to other optical methods (e.g., pH, O2, and temperature sensors), while providing a similar accuracy to HPLC.

Despite efforts into developing novel technologies for real-time acquisition of Mab titer data in a bioreactor, very few of these technologies are applied for routine use in the biopharmaceutic industry because of strict regulations. Robustness, reproducibility and accuracy of new PATs have to be addressed to meet the requirements from regulatory agencies (Jenzsch et al., 2018); therefore, it is crucial to comply with the guidelines during the device development to optimise the opportunities of commercialisation. Our fibre-optic SPR-EOT biosensor is made from sterilisable materials with a compact size, so it could be easy for implementation, maintenance, and replacement in a GMP environment as an at-line tool to measure Mab titers. Besides, it can be readily adaptable to previously developed automatic sampling systems to make the measurement process completely automated.

3.2.6. Conclusion

We have demonstrated a portable and sensitive fibre-optic SPR-EOT biosensor for the rapid detection of biomolecules, especially for monitoring the product concentration during bioprocesses. After improving the flow cell design, the biosensor can be operated with minimal interference of air bubbles and other external factors. A consistent sensitivity between template transfers is achieved with precise control during the fabrication procedure for three sensing probes. A similar detection limit from three antibody detection tests confirms the repeatability of this biosensor. The biosensor could detect antibodies at a concentration of as low as 0.44 µg/mL. The redshifts in the optical transmission spectra correlate with the Mab concentration, although significant variations were observed at a higher Mab concentration. Additionally, the spacer arms for immobilising protein A onto the gold film does not improve the detecting sensitivity; therefore, protein A could be immobilised with a zero-length crosslinker to save operating time and material cost. The

biosensor could be regenerated for the measurements of Mab concentrations up to ten times. From this proof-of-concept using the fibre-optic SPR-EOT biosensor for the rapid detection of Mabs, it can be concluded that this biosensor is potentially beneficial for at-line measurements of product concentration in the manufacturing process of Mabs, because of its acceptable repeatability, portability, and user-friendliness.

3.3. Supplementary Materials

3.3.1. Flow Cell Design

Figure 3-5 depicts the 3D design of a new flow cell chamber for the fibre-optic SPR-EOT biosensor. The inserts are designed with an appropriate clearance to accommodate optical fibres of Ø = 2.5 mm and microfluidic tubes of Ø = 0.8 mm. All these inserts are designed with fillets to assist in flow cell assembly. The distance between two optical fibres is controlled to be 100 µm or less using a microscope camera.

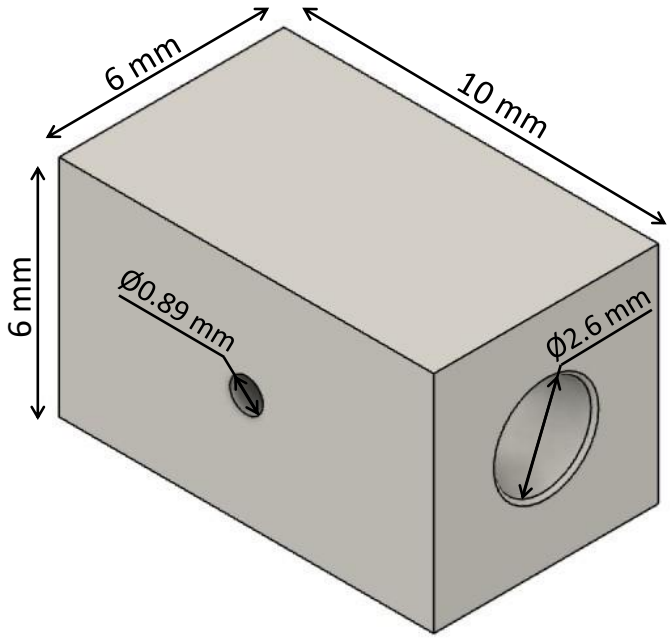

Figure 3-5 Flow cell's chamber design with details about dimensions.

3.3.2. Template Transfer Procedure

The fabrication procedure is depicted in **Scheme 3-1**, with the details of each step in the caption. The procedure is divided into three major tasks: cleaning the template and depositing a gold film; cleaning the optical fibre; template transfer using epoxy glue. Large variations may occur during the template transfer process in Step (E) in the fabrication of different sensors; therefore, a microscope camera is used to ensure the optical fibre is vertical to the template to mitigate variations.

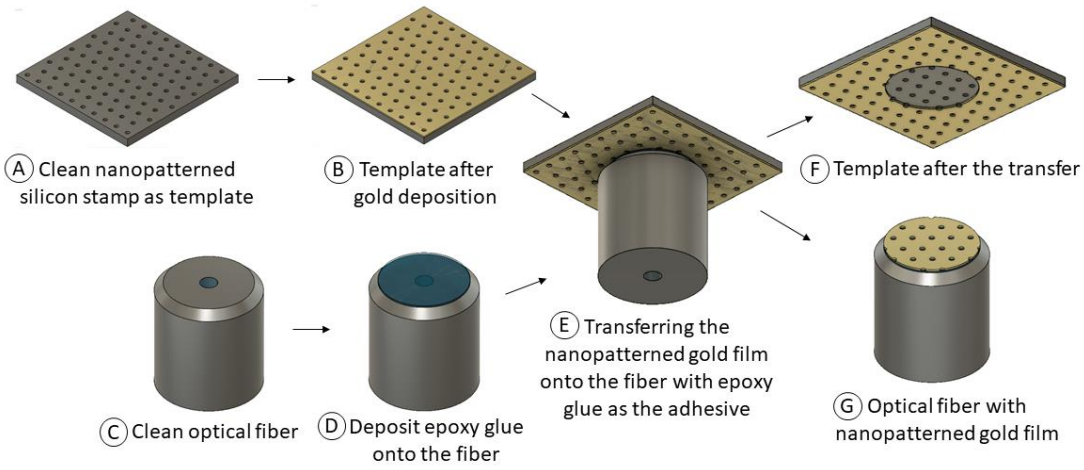

Scheme 3-1 Step-by-step diagram of fabricating the gold-sensing surface with a periodic nanohole matrix using a nanopatterned silicon template and an epoxy glue. **(A)** Thoroughly cleaning the nanopatterned silicon template; **(B)** Coating 100 nm of gold nanoparticles onto the silicon template; **(C)** Cleaning an optical fibre; **(D)** Depositing an epoxy glue layer onto the fibre; **(E)** Attaching the optical fibre with an epoxy glue to the nanopatterned gold film; **(F + G)** Transferring the nanopatterned gold film onto the tip of optical fibre.

3.3.3. Simulation Results

Figure 3-6 shows the transmission spectra in different NaCL concentrations, obtained from the experiment and simulation. The peak at around 500 nm is characteristic of gold and present in both experimental and simulated spectra. The measured peak at 750 nm can be related to the simulated peak at 683 nm. This peak can be attributed to the coupling between the local surface plasmon resonance at the top and bottom corners of the nanoholes. The measured peaks at 830 nm and 900 nm can be related to the simulated peak at 882 nm, which

originates from the water/Au mode. The multiple peaks in the experiments could result from the imperfection and roughness of the gold film. The measured peak at 980 nm can be related to the simulated peak at 991 nm, which originates from the epoxy/Au mode.

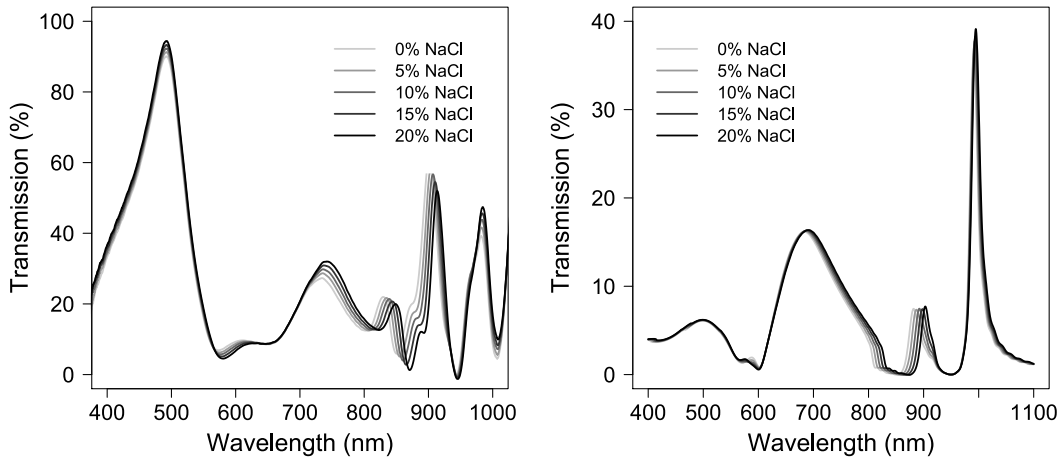

(a) **(b)**

Figure 3-6 Transmission spectra in different NaCl concentrations obtained from **(a)** experiment and **(b)** simulation.

The resonance peaks can be demonstrated and confirmed by the corresponding electric field distributions, as shown in Figure S3. In **Figure 3-7**, the refractive index sensing in experiments and simulations is summarized. For water/Au mode, the sensitivity of peak 880 nm from the simulation is comparable to the sensitivity of peak 830 nm in experiments (509 ± 5 nm/RIU and 593 nm/RIU, respectively). For the epoxy/Au mode, the measured peak at 980 nm has an average sensitivity of 141 ± 70 nm/RIU, which is approximately the simulated sensitivity of 107 nm/RIU of peak 991 nm. However, the peaks at 683 nm in simulations and 750 nm in experiments show a large divergence (193 nm/RIU and 383 ± 130 nm/RIU, respectively), which might be due to the spectral error resulting from the from the imperfection and roughness of the gold film.

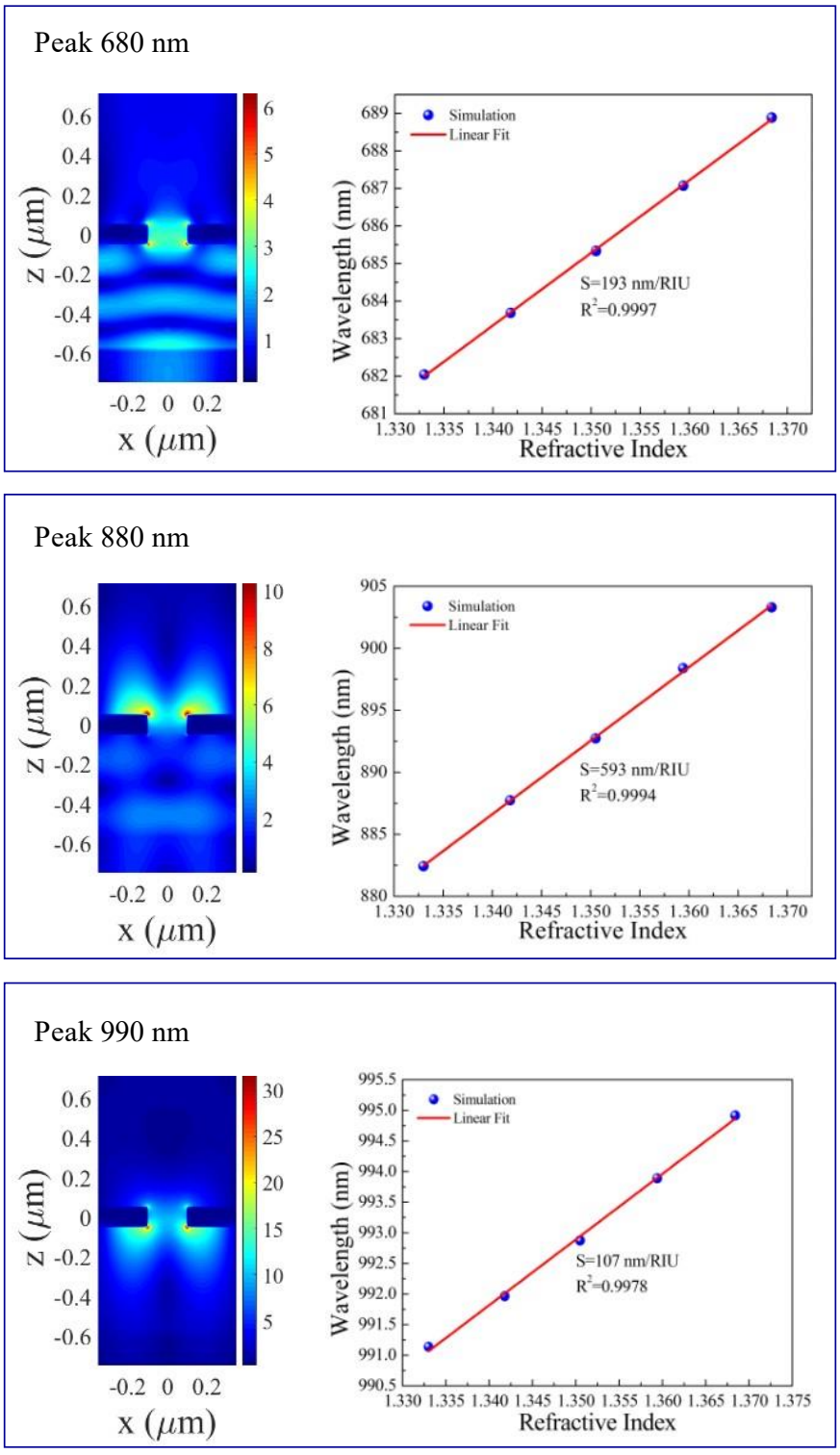

Figure 3-7 Electrical field distribution of the simulated resonance peaks in water and simulated sensitivity results

3.3.4. Protein A Immobilisation

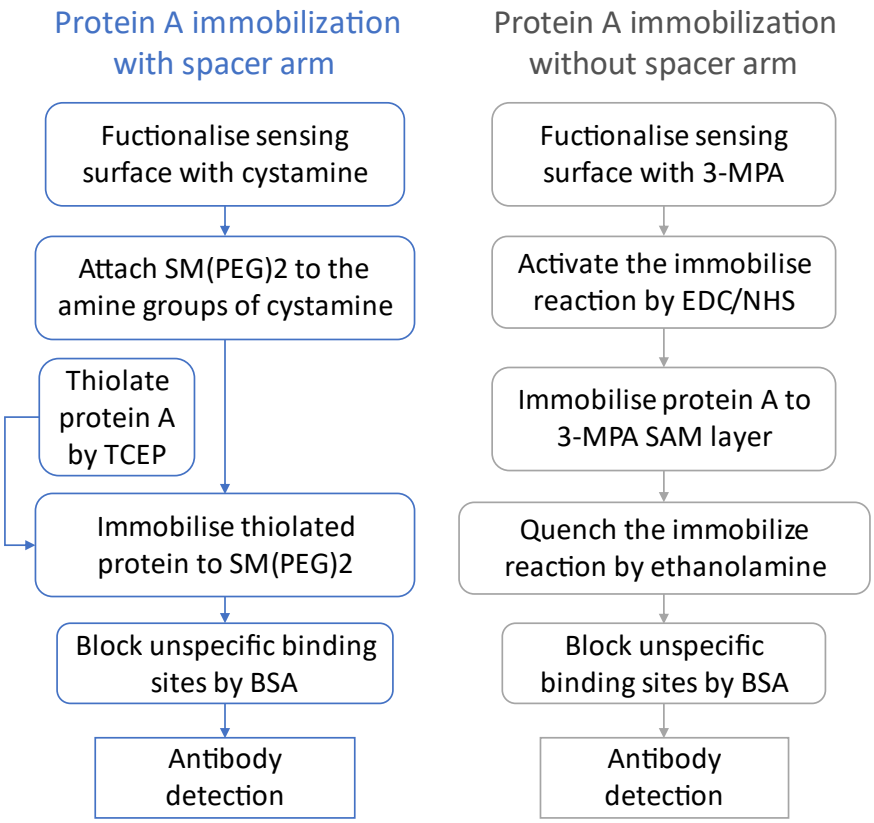

Figure 3-8 Step-by-step diagram of protein A immobilisation with and without spacer arm.

Figure 3-8 outlines the steps in protein immobilisation with and without a spacer arm. The diagram is included to provide a better visualisation of the complicated procedure.

3.3.5. Protein A Regeneration

A diagram explaining the two attempts at a regeneration experiment is provided in **Figure 3-9**.

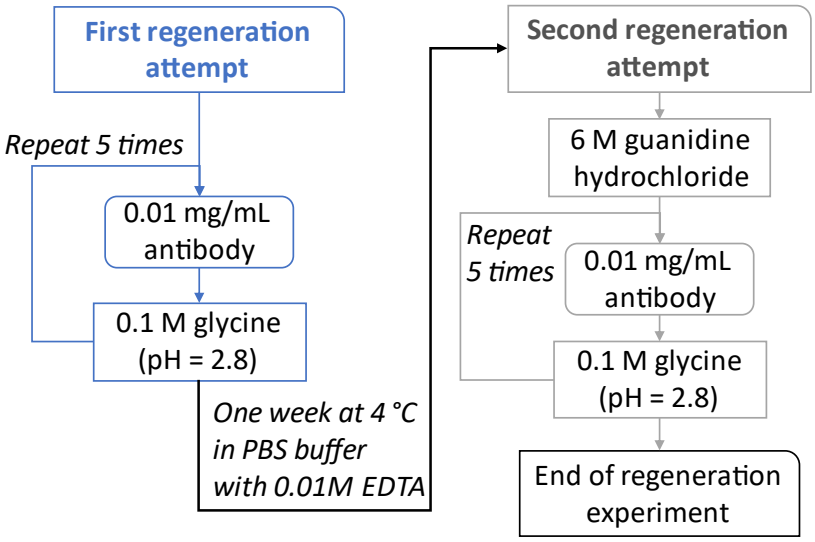

Figure 3-9 Schematic diagram explaining the regeneration experiment procedure.

The detected results of the two attempts at the regeneration experiment are shown in **Figure 3-10**. The detected wavelength shifts are pretty consistent for each trial. The peak shift obtained from the sixth regeneration, which is the first regeneration of the second trial, is not included in the figure because it was not consistent with other values obtained in both attempts. The sixth regeneration was conducted after treating the sensing surface with 6 M guanidine hydrochloride and returned a peak shift of 0.095 nm after detecting 0.01 mg/mL Mab. This peak shift result is remarkably lower than all the peak shifts acquired during the regeneration experiment. It may be that there were still denatured Mab residues on the sensing surface after treatment with 6 M guanidine hydrochloride, which hindered the binding of the Mab, and all these residual Mabs were stripped by 0.1 M glycine hydrochloride (pH = 2.8) during the sixth regeneration. After that, the peak shift dropped below the initial baseline of the second trial and the detected signals were consistent from the seventh regeneration onward (as shown in Figure S6).

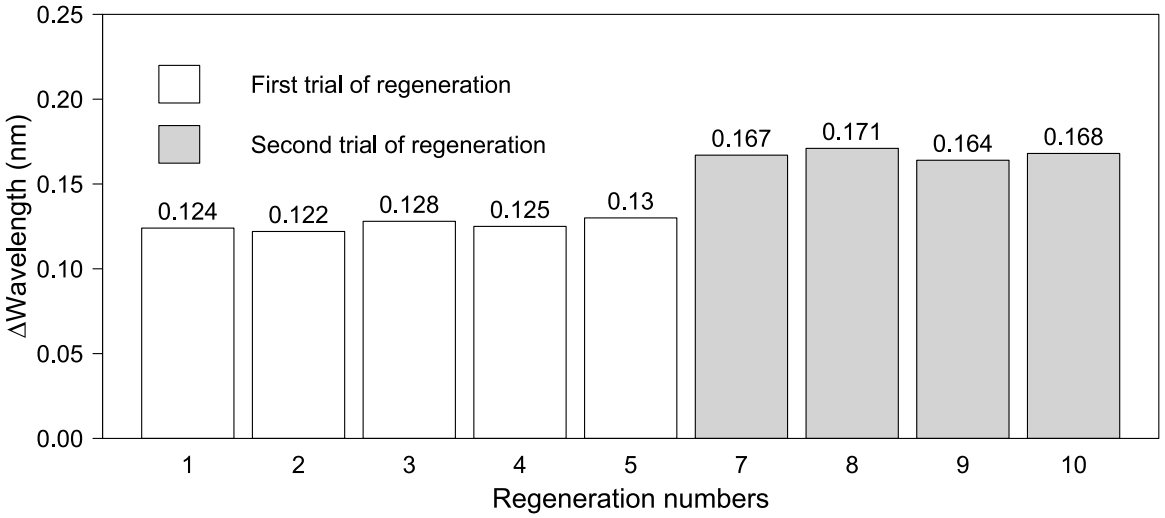

Figure 3-10 Detected results after two regeneration trials. The sensing surface with protein A was cleaned with 6 M guanidine hydrochloride before the second trial.

4. Chapter 4

ULTRASENSITIVE *C. DIFFICILE* TOXIN B DETECTION THROUGH A FIBRE-OPTIC SPR-EOT BIOSENSOR

4.1. Statement of Authorship

Title of paper	Ultrasensitive C. Difficile Toxin B Detection Through a Fibre-optic SPR-EOT Biosensor
Publication Status	Unpublished
Publication Details	

Principal Author

Name of Principal Author (Candiate)	Thai Thao Ly		
Contribution to the Paper	Designed the methodology; conducted the experiments, collected the experimental data, carried out data analysis, compiled the original draft		
Overall percentage	80%		
Certification	This paper reports on original research I conducted during the period of my Higher Degree by Research candidature and is not subject to any obligations or contractual agreements with a third party that would constrain its inclusion in this thesis. I am the primary author of this paper.		
Signature		Date	19/10/2021

Co-author Contributions

By signing the Statement of Authorship, each author certifies that:

i. the candidate's stated contribution to the publication is accurate (as detailed above);
ii. permission is granted for the candidate in include the publication in the thesis; and
iii. the sum of all co-author contributions is equal to 100% less the candidate's stated contribution.

Name or Co-Author	Yinlan Ruan		
Contribution to the Paper	Designed conceptualisation and methodology; provided resources; validated the data, administrated the project; edited the manuscript.		
Signature		Date	20 Oct 2021

Name or Co-Author	Hannah Wardill		
Contribution to the Paper	Designed conceptualisation; provided the resources; validated the materials; edited the manuscript		
Signature		Date	21/10/21

Name or Co-Author	Joanne Bowen		
Contribution to the Paper	Designed conceptualisation; provided the resources; edited the manuscript		
Signature		Date	21/10/2021

Name or Co-Author	Steven Polyak		
Contribution to the Paper	Designed conceptualisation; provided the resources, validated the materials		
Signature		Date	21/10/21

Name or Co-Author	Shuai Ruan		
Contribution to the Paper	Initiated the project		
Signature		Date	Oct. 20, 2021

Name or Co-Author	Hu Zhang		
Contribution to the Paper	Supervised the project, provided resources, edited the manuscript.		
Signature		Date	Oct 17,2021

4.2. Publication

4.2.1. Abstract

Clostridioide difficile infection (CDI) is the leading cause of healthcare-associated diarrhea and places a significant burden on the healthcare system. Rapid, sensitive, and accurate CDI diagnosis could control the spread of infection and mitigate the burden; therefore, many ultrasensitive CDI diagnosis methods have been developed. Unfortunately, they have not been included in the current CDI testing algorithm. In this study, a fibre-optic surface plasmon resonance (SPR)- extraordinary optical transmission (EOT) biosensor was employed to detect *C. difficile* toxin B. When toxin B is injected into the biosensor and bound to the sensing surface, a redshift is seen in the optical transmission spectra. The redshift is linearly correlated with the toxin B concentration when the concentration increases. The biosensor is highly sensitive, and it can detect toxin B at low concentrations, down to 4.8 pg/mL, within 15 mins. This detection limit is comparable with other ultrasensitive methods for toxin B detection. A significant advantage of this method is that the biosensor does not need complicated instrumentation or sample pretreatment with fluorescence labels. The study has demonstrated that the fibre-optic SPR-EOT biosensor could assist in ultrasensitive toxin B detection for rapid CDI diagnosis.

4.2.2. Introduction

Globally, *Clostridioide difficile* infection (CDI) is the most common healthcare-associated gastrointestinal infection (Davies et al., 2014, Australian Commission on Safety and Quality in Health Care, 2018, Balsells et al., 2019, Krishna and Chopra, 2020). CDI may be asymptomatic or symptomatic with mild symptoms such as diarrhea and fever. In severe cases of CDI, it may progress to fatal colonic inflammation. In 2017, the US had a mortality rate of 5% for healthcare-associated CDI (Guh et al., 2020). Between 2011 - 2017, Australia reported a death rate of 0.7% for healthcare-associated CDI (Australian Commission on

Safety and Quality in Health Care, 2018). CDI is an urgent threat to public health, recognised by the Centre for Disease Control (CDC), and it has the highest transmission risks for patients in hospitals and older adults in nursing homes. CDI cases in the healthcare-associated environment also have a higher relapse rate than those occurring in the community. It is forecasted that there will be an increase in CDI cases in nursing homes due to the aging of the tranche of the population born during the baby boom (1946 to 1964) (Krishna and Chopra, 2020). Between 2012 - 2015, Australia recorded three severe cases of CDI caused by an unusual *C. difficile* strain, PCR ribotype 251 (Wehrhahn et al., 2019). Consequently, CDI causes a tremendous economic burden for the healthcare system (Lübbert et al., 2014). From 2010 - 2015, the annual CDI-attributable cost was approximately 6.3 billion US dollars (Zhang et al., 2016b). The economic burden of CDI stems from extended hospitalisation, the costs of treatment and risks of relapse (Zhang et al., 2016b, Australian Commission on Safety and Quality in Health Care, 2018). Timely and accurate diagnosis could mitigate the burden in the long run by enhancing CDI management and reducing undiagnosed and misdiagnosed cases (Davies et al., 2014, Lübbert et al., 2014).

Currently, diagnosis of CDI requires a multi-stage algorithm (Bollam et al., 2020, Davies et al., 2014). The first stage of screening is to detect genes encoding for glutamate dehydrogenase (GDH) or the GDH protein in stool samples using rapid enzyme immunoassay (EIA) (Davies et al., 2014, Lübbert et al., 2014). GDH is a protein that can be found in every strain of *C. difficile*. This test is highly sensitive (94.5%); however, it has low specificity because it cannot distinguish between non-toxigenic and toxigenic *C. difficile (Bollam et al., 2020)*. The second stage employs an EIA test to confirm the presence of toxins, specifically endotoxins A and B of *C. difficile,* to identify toxigenic strains (Lübbert et al., 2014). This test has high specificity (94-100%); however, its sensitivity can vary from 69% to 99% (Bollam et al., 2020). The third stage is optional and usually emerges when the

results of the first two stages are intermediate (that is, GDH-positive and toxin-negative or GDH-negative and toxin-positive) (Davies et al., 2014). The tests used for the third stage are highly specific, including the nucleic acid amplification test (NAAT), cell cytotoxicity assay (CCTA) or cytotoxicity neutralisation assay (CCNA), and toxigenic culture (TC) (Lübbert et al., 2014, Davies et al., 2014). NAAT can confirm the presence of toxigenic strains, yet it cannot determine active production of the toxin A/B protein and may diagnose asymptomatic carriers as CDI. Consequently, despite a quick turnaround time (less than 4 hours) and excellent specificity (94-100%), NAAT must be used in conjunction with other CDI diagnostic tests (Lübbert et al., 2014, Bollam et al., 2020). CCNA is the standard test to confirm the presence of toxins in stool samples; however, it requires technical expertise and has a long turnaround time (up to 24 hours) (Lübbert et al., 2014). Toxigenic culture is the gold standard for CDI diagnosis; however, it is not practical for acute diagnosis due to its very long turnaround time (over three days) and strict utility requirements (Lübbert et al., 2014). The current optimal rapid CDI diagnostic algorithm consists of GDH EIA as a screening test and toxins EIA as a confirmation test (Lübbert et al., 2014). The key to CDI diagnosis is to find confirmation of toxigenic *C. difficile* in stool samples. The most straightforward way is to detect toxins A and B using EIA. Nonetheless, EIA for toxins detection has limited sensitivity; thus, EIA alone is not recommended for CDI diagnosis (Bollam et al., 2020).

This study developed a fibre-optic SPR-EOT biosensor as a sensitive, novel platform for rapid *C. difficile* toxins immunoassay. The EOT biosensor is a variant of the optical nanoplasmonic biosensors developed based on the discovery of EOT. Compared with conventional SPR biosensors, EOT biosensors are highly surface-sensitive, more robust to external fluctuations, and have less complicated instrumentation (Jackman et al., 2017). EOT occurs when incident light transmits through a thin gold film with a subwavelength nanohole

array. The electrons at the metal interface are excited by incident light to oscillate and propagate surface plasmon. This surface plasmon couples with a nanohole array to generate an unusual light transmission with distinct peaks (Jackman et al., 2017). The EOT transmission is highly sensitive to changes in the refractive index at the interface; therefore, EOT has attracted considerable research attention. It has been studied for various biosensing applications, such as antibody screening (Couture et al., 2016, Cetin et al., 2015, Polley et al., 2019), evaluation of virucidal drugs (Jackman et al., 2016), detection of an algal toxin in freshwater (Briscoe et al., 2015), screening of cardiac biomarkers (Patra et al., 2017, Ding et al., 2015), breast cancer diagnosis (Monteiro et al., 2016), and rapid diagnosis of sexually transmitted infections in urine samples (Soler et al., 2017). The limit of detection (LOD) for the EOT biosensor reported from the abovementioned studies is in the range of nanograms per millilitre, reflecting the excellent sensitivity of the EOT biosensor. Such a low LOD suggests that the EOT biosensor could potentially serve as a means for ultrasensitive *C. difficile* toxins detection.

Currently, EOT biosensors require complex instrumentation and are not portable, making application difficult at clinical or point-of-care sites. To overcome this challenge, fibre-optic SPR-EOT was employed as the biosensing platform to provide a portable and straightforward diagnostic method for point-of-care or resource-restricted environments. Toxin B was chosen as the target analyte because it mediates a full spectrum of CDI symptoms (Shen et al., 2020), and it is more clinically relevant than toxin A (Luo and Liu, 2020). Our experimental results demonstrate that the fibre-optic SPR-EOT biosensor can offer label-free toxin B detection at a very low concentration in a short timeframe.

4.2.3. Method and Materials

4.2.3.1. Template Cleaning

A gold sensing surface was fabricated from a silicon template with a premade nanohole lattice (Lightsmyth, S2D-18D3-0808-350-P, USA). The template was thoroughly cleaned by following a three-stage cleaning procedure with Piranha, Aqua Regia, and then Piranha solutions, consecutively. For cleaning with the Piranha solution, each template was placed into a glass vial. 0.3 mL of 98% w/w sulfuric acid and then 0.7 mL of 30% w/w hydrogen peroxide were added into the vial. The mixture was mixed thoroughly before sonicating in a sonication bath for 30 min. After cleaning, the template was rinsed with Mili Q water three times and blow-dried completely with nitrogen. For the cleaning process using Aqua Regia, the template was emersed in a solution of 0.2 mL of water, 0.3 mL of 32% hydrochloric acid (RCILabscan Limited, Thailand), and 0.1 mL of 70% w/w nitric acid (Chem-supply, Australia). This vial was in a sonication bath for 30 min, and the template was rinsed with MiliQ water three times before blow-drying with nitrogen. The Piranha solution was applied to remove organic contaminants on the template before coating.

4.2.3.2. Fabricating the Flow Cell for the Biosensor

Two steps were undertaken to fabricate a complete flow cell: preparing the sensing surface and assembling all the components into a flow cell. After cleaning the template, it was coated with a 100 nm-thick gold layer using a thermal evaporator (Quorum Technology-K975X Turbo-Pumped Thermal Evaporator, UK) to prepare a sensing surface. The coating rate was kept at 0.2 nm/s. The optical fibre was polished using two types of polish paper (9 µm silicon carbide and 0.3 µm aluminium oxide) before template transfer. The optical fibre's tip and the gold film on the template were joined with epoxy glue. After that, everything was left at 60 °C for 4 h to cure the epoxy glue, and aged for 24 h at room temperature. Subsequently, the optical fibre with a 100 nm gold film was peeled from the template to obtain a sensing probe.

Finally, the sensing probe, a signal-collecting optical fibre, and two microfluidic tubes were affixed to a customised 3D-printed chamber to assemble the flow cell. The distance between the two optical fibre's facets were controlled to be 100 µm to ensure efficient collection of transmitted light. **Figure 4-1** shows a pictorial representation of how to control the space between the two optical fibres. The microscope focuses on the distance between the two facets through an aperture of the flow cell. The aperture is the insert for microfluidic tubes, which has a diameter of 1 mm. The aperture is large enough to allow the microscope to focus entirely on the two optical fibres. The distance is measured by the microscope and adjusted accordingly until the desired distance of 100 µm is achieved. Finally, all joins were sealed airtight using superglue.

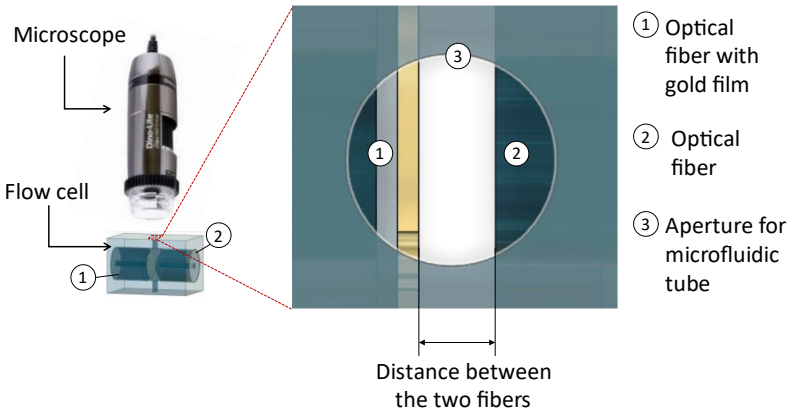

Figure 4-1 Depiction of how the distance between the two fibres' facets is measured and controlled

4.2.3.3. Data Interpretation

The transmission data were collected by using two approaches during the experiment. An optical spectrometer (Ocean Insights, USB4000, USA) was used to digitalise the optical signal. The data were exported automatically by SpectraSuite software (Ocean Insights, USA) every 5 s, and they were immediately imported to Matlab (Mathworks, USA) and processed to plot a real-time sensorgram. Simultaneously, the transmission data were collected manually using SpectraSuite software (Ocean Insights, USA) after every

experimental step. They were analysed using Origin software (Originlab, USA) at the end of the experiment.

4.2.3.4. Sensitivity Test

Sodium chloride solutions at a concentration of 0%, 5%, 10%, 15%, and 20% were introduced to the flow cell for 5 mins in ascending order of concentration. The wavelength shift of the transmission peak was calculated and linearly fitted with the solutions' refractive index to evaluate the biosensor's sensitivity.

4.2.3.5. Optimising Functionalisation

Four silicon wafers coated with a 100 nm gold film were washed in a Piranha solution and then immersed in water, ethanol, 10 mM 3-Mercaptopropionic acid (3-MPA) in water, and 10 mM 3-MPA in ethanol, respectively. After 5 h, the wafers were rinsed with the above corresponding solvents, blow-dried with nitrogen, and used for contact angle measurements. 1 µL of Mili Q water was dropped onto the functionalised gold surface, and the contact angle was measured using a Tantec CAM-F1 Contact Angle Meter (USA).

4.2.3.6. Antibody Immobilisation

The sensing surface was functionalised with a self-assembled monolayer of 3-MPA by incubating the surface with a 10 mM 3-MPA in water overnight. The surface was rinsed with water, and the running buffer was changed to a PBS buffer (pH=7.4). 200 µL of a mixture solution of 0.2 M 1-ethyl-3-(3-dimethyl aminopropyl) carbodiimide hydrochloride (EDC) and 0.05 M N-hydroxysulfosuccinimide (Sulfo-NHS) was introduced to activate the carboxylic functional groups of 3-MPA, and the surface was quickly rinsed with the PBS buffer for 1 min. Next, 1 mL of anti-toxin B (ab83066, Abcam, UK) in a PBS buffer was injected into the flow cell to enable immobilisation of the antibody onto the gold sensing surface.

Subsequently, the immobilising reaction was quenched using 10 mM Tris buffer (7 min, 20 µl/min), and the surface was rinsed with the PBS buffer for 20 min.

4.2.3.7. Toxin B Detection

Thirteen toxin B samples at concentrations ranging from 0.001 pM to 50 nM were prepared from a 740 nM toxin B stock (ab124001, Abcam, UK). Samples were injected in ascending concentrations into the flow cell for 9 min. Between two consecutive injections, the surface was rinsed with the PBS buffer for 5 min.

4.2.4. Results

4.2.4.1. Sensitivity Test

The bulk sensitivity of three probes was determined using NaCl solutions at different concentrations. **Figure *4-2*** describes the shift of transmission spectra acquired when a NaCl solution was injected into the flow cell at a concentration of 0%, 5%, 10%, 15%, and 20%, with a corresponding refractive index (RI) of 1.3330, 1.3418, 1.3505, 1.3594, and 1.3684, respectively. Transmission peaks at 750 nm, 830 nm, and 900 nm exhibited redshifts when the RI of the NaCl solution increased (**Figure 4-2 (a)**). The averaged shifts from three probes were plotted against the RIs, and the curves are shown in **Figure 4-2 (b)**. The peak shifts at three wavelengths have an excellent linear correlation with the RI values (R^2 = 0.999). A one-way ANOVA statistical analysis shows that the average sensitivity of the peak at 830 nm is significantly different from that of other peaks ($p = 7.65 \times 10^{-8}$). A sensitivity value of 516±7 nm/RIU is obtained, in comparison with 410±50 nm/RIU and 379±20 nm/RIU for peaks at 750 nm and 900 nm, respectively. The peak at 830 nm was chosen for monitoring the peak shift for toxin-B detection experiments due to its excellent sensitivity and minimum

variations.

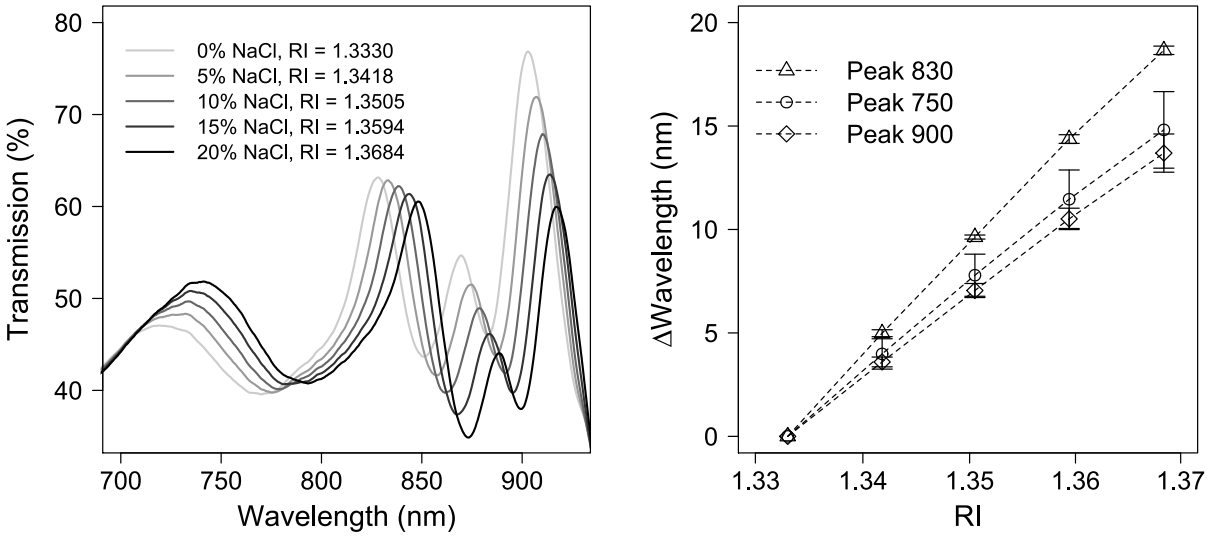

Figure 4-2 (a) Shift of transmission spectra for NaCl solutions at different RIs from one sensing probe; **(b)** The average sensitivity of three prominent peaks from three sensing probes.

4.2.4.2. Optimising Functionalisation and Antibody Immobilisation

The first step for antibody immobilisation is to functionalise the sensing gold film with functional groups. 3-MPA was employed to coat a self-assembled monolayer (SAM) with carboxyl groups on the gold sensing surface. Initially, a 3-MPA solution at 10 mM was prepared in ethanol for the coating process, since ethanol is the most popular solvent for SAM fabrication (Tokel et al., 2015, Wei et al., 2010, Wang et al., 2009, Vaisocherová-Lísalová et al., 2016, Chen et al., 2015), creating a highly organised and stable SAM (Singh et al., 2020). Unfortunately, ethanol damaged the sensing gold film, evidenced by degradation of the crosslinkers of the epoxy glue and distortion of the sensing probe (Supplementary **Figure *4-8***). Water was then explored as a potential alternative given its favourable action of maintaining crosslinking from the glue and establishing a SAM with comparable quality to ethanol (Noh et al., 2005). Four silicon wafers with a 100 nm gold film were immersed in either water, ethanol, 10 mM 3-MPA in water, or 10 mM 3-MPA in

ethanol to evaluate the possibility of using water as a solvent for 3-MPA. After five hours, the contact angle of water on these wafers was measured. The results are shown in **Table 4-1**.

Table 4-1 Contact angles of four gold-coated silicon wafers before and after SAM formation.

	Water (Blank)	Ethanol (Negative control)	10 mM 3-MPA in water (Sample)	10 mM 3-MPA in ethanol (Positive control)
Before SAM formation	77.3°	70°	80.7°	80°
After SAM formation	75.3°	74.3°	44°	39.2°

Before the experiment, the four wafers with gold film had contact angles (Θ_c) ranging from 70° to 80.7°. After SAM formation, the Θ_c for the blank and negative controls had a negligible change, indicating the gold surface remained intact. In contrast, the Θ_c of wafers incubated in the 3-MPA aqueous solution and the 3-MPA ethanolic solution dropped significantly to 44° and 39.2°, respectively. A smaller Θ_c suggests that the gold film becomes more hydrophilic due to the successful formation of a 3-MPA SAM. The results of the Θ_c values using water and ethanol as solvents agree well with those from a previous study (Noh et al., 2005). Most importantly, water as a solvent in the functionalisation process avoids damage to the sensing probe, as shown in **Figure 4-9**.

After functionalisation of a 3-MPA SAM on the gold film using 10 mM 3-MPA in MiliQ water, the carboxyl functional groups were activated by a mixture of EDC and NHS for the carbodiimide crosslinking reaction. EDC and NHS react with the carboxyl functional group to create a stable intermediate for efficient antibody immobilisation at a physiologic pH (pH = 7.4). A 1:100 anti-toxin B antiserum dilution was introduced into the flow cell at a

flow rate of 20 µL/min to deposit the antibody for toxin-B onto the sensing gold film. After antibody immobilisation, three sensing probes acquired a peak shift of 1.1 ± 0.4 nm. The sensorgrams obtained from three sensing probes after antibody immobilisation are shown in **Figure 4-10**. The results confirm that antibody immobilisation on the gold film has been accomplished, and water can be the solvent for surface functionalisation.

4.2.4.3. Toxin B Detection

Figure 4-3 shows the wavelength change of the peak at 830 nm of the transmission spectra acquired during toxin B detection from three sensing probes. Thirteen toxin B samples at concentrations ranging from 10^{-7} nM to 50 nM were injected into the flow cell in ascending order of concentration. The sensing surface was rinsed with a PBS buffer between sample injections to remove excess toxin B from the sensing surface. Consequently, one dataset for each toxin B detection was acquired immediately after sample injection and another after the PBS rinse, as shown in **Figure 4-3**.

According to **Figure 4-3**, the transmission signal redshifts (shifts toward longer wavelengths) proportionally to the toxin B concentrations. Negligible signal changes are seen before and after the PBS rinse, except for those at three high toxin B concentrations greater than 5 nM, highlighted with a red colour in **Figure 4-3**. When the toxin B concentration is beyond the red dash vertical line in **Figure 4-3**, the signal experienced blueshift (a shift toward shorter wavelengths) after the PBS rinse. The signal drops are consistent for three sensing probes for toxin B detection. They become more evident at a higher toxin B concentration, indicating that the antibody binding sites on the gold film for toxin B may be saturated. Additionally, the singal change acquired during the injection of the toxin B samples (10 nM, 25 nM, and 50 nM) might be mainly due to the physical adsorption of toxin B onto the sensing surface. In this context, the upper limit of detection from these sensing probes is around 5 nM (equivalent to 1.35 µg/mL). It appears that there is a linear

relationship between the peak shift and the toxin B concentration at a semi-log scale when the toxin B concentration is in the range from 10^{-7} nM to 5 nM. Linear fitting of the signal shift after PBS rinses returned a correlation coefficient R^2 of 0.98, 0.99, and 0.98 for the three sensing probes.

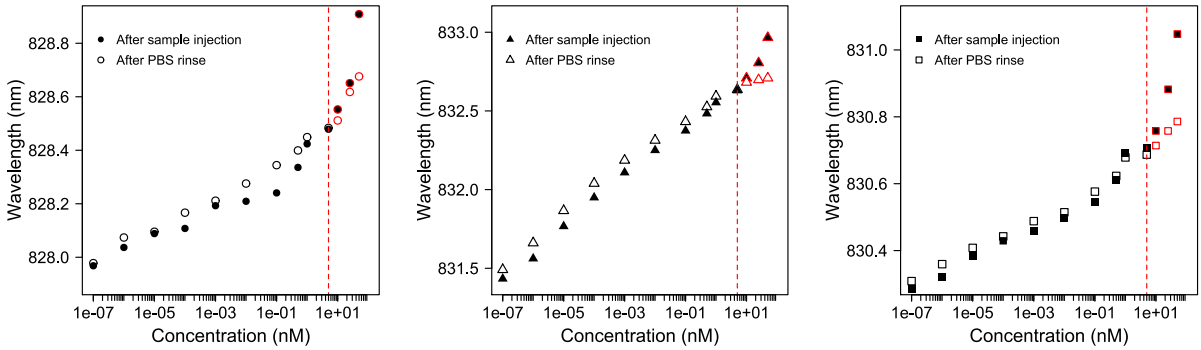

Figure 4-3 Results of toxin B detection from three sensing probes. The red dash line in each plot indicates where signal change mainly governed by physical adsorption instead of antigen-antibody interaction.

Data analysis for toxin B detection was carried out for the toxin B concentrations ranging from 10^{-7} nM to 5 nM to determine the detection limit and evaluate the sensing performance. Since these sensing probes were prepared manually, each probe may have a slightly different antibody density on the gold film. Data normalisation was applied to diminish the differences in the wavelength shifts for toxin B detection, generated from variations in antibody immobilisation. Normalisation was conducted by dividing the wavelength shift of toxin B detection by that from the antibody immobilisation. **Figure 4-4 (a)** compares the wavelength shift results of toxin B detection before and after data normalisation. The white scatter plots represent the data before normalisation, while the black scatter plots show the data after normalisation. It can be seen from **Figure 4-4 (a)** that the variations between toxin B detections became less significant after data normalisation.

Despite the variations in the shifts for the three probes, the average wavelength shifts after normalisation in **Figure 4-4 (b)** have an excellent linear relationship with the toxin B

concentrations from fibre-optic SPR-EOT biosensors. These data points were regressed into a straight line, with a correlation coefficient R^2 of 0.99. The LOD is calculated to be 1.79×10^{-5} nM (4.8 pg/ml), at which point the wavelength shift is three times the standard deviation of blank ($\sigma_{blank} = 0.0653$ nm). Thus, a fibre-optic SPR-EOT biosensor could be employed to detect toxin B at low concentrations through sensitive wavelength shifts of the transmission spectra.

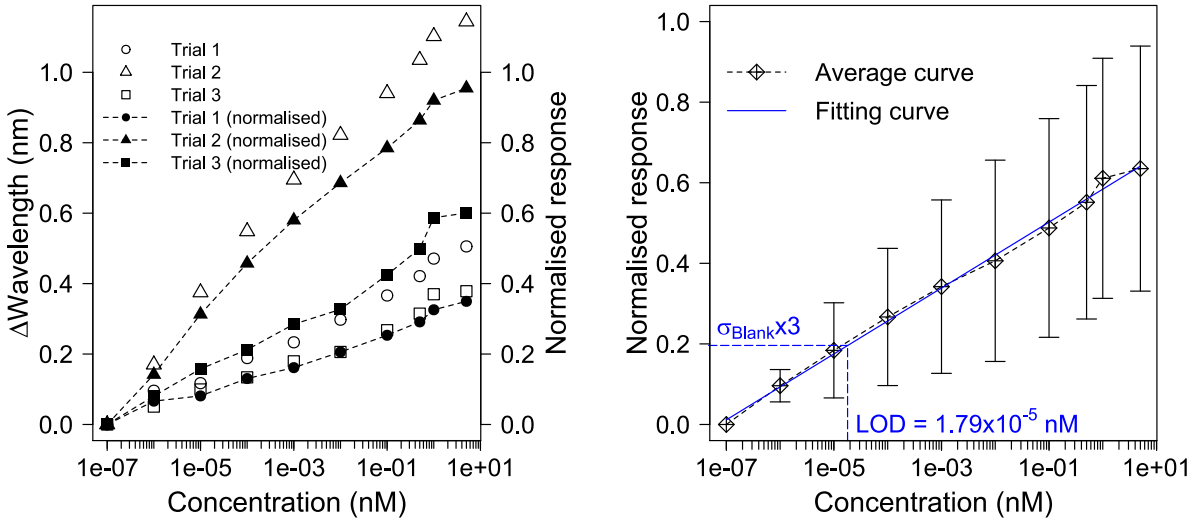

(a) **(b)**

Figure 4-4 (a) Toxin B detection in triplicates before and after data normalisation; **(b)** Average wavelength shifts for toxin B detection using a fibre-optic SPR-EOT biosensor with standard deviation.

4.2.5. Discussion

The results demonstrate that a fibre-optic SPR-EOT biosensor is highly sensitive for label-free and rapid toxin B detection. Fibre-optic SPR-EOT has excellent potential for point-of-care diagnosis of CDI because it is cheap, compact and straightforward to operate. Many *C. difficile* detection methods have been developed, although not many have been applied in the CDI diagnosis algorithm. The LOD of a commercial rapid toxin assay kit (*C. diff* Quik Check Complete, TechLab, Inc., Blacksburg, VA, USA) is 630 pg/mL for toxin A and 160 pg/mL for toxin B (Sandlund et al., 2020). Unfortunately, this LOD is much greater than that of

other ultrasensitive detecting methods that are under development. The most extensively studied *C. difficile* toxin detection method is a Single Molecular Array (SIMOA) or a single immunocomplexes digital enzyme-linked immunosorbent assay (ELISA). The SIMOA employs a Simoa HD-1 analyser (Quanterix Corporation, USA) to test samples and generate results automatically (Song et al., 2015, Banz et al., 2018, Pollock et al., 2019). The target analyte is captured onto paramagnetic beads with a fluorescent label to form immunocomplexes on the beads. These beads are then loaded into femtoliter-sized wells, and the fluorescent signal is detected by the Simoa HD-1 (Rissin et al., 2010). The SIMOA method provides decent sensitivity with an LOD as low as 2.9 pg/mL in the stool (Banz et al., 2018). Similar to the SIMOA, the Single Molecule Counting (SMC) *C. difficile* toxin A/B assay employs microbeads to capture and label the target molecule for toxin A and toxin B detection. A Singulex Clarity instrument (SMCxPRO™ Instrument) automatically processes the samples (Sandlund et al., 2018, Hansen et al., 2019). Instead of measuring the fluorescent signal from the immunocomplexes in the multiwells, the SMC has the extra step of disassociating the immunocomplex, whilst the fluorescence is measured for the elution samples (Sandlund et al., 2018). The SMC has an LOD for toxin B at 0.3 pg/mL in a buffer and 0.7 pg/mL in stool samples. The multipath method reported by Gite et al. (2018) shares the same detecting mechanism as SIMOA and SMC. The sample is mixed with a diluent that contains immunoreagents to form immunocomplexes. Afterwards, the mixture is loaded to a microtiter well with a visible light-blocking gel cushion at the bottom. The immunocomplexes are anchored to the gel cushion by a magnetic force, and the fluorescent signal is read from the bottom of the well. The gel cushion blocks any possible fluorescent signal in the diluent from unbound fluorescent nanoparticles; thus, no additional washing step is required. This multipath method has the most minimal process steps among these novel ultrasensitive toxin B detection methods and offers an LOD of 45 pg/mL in stool samples

(Gite et al., 2018). The most recent method for toxin B detection was reported by (Luo and Liu, 2020). The study employed magnetic beads hybridised with an aptamer that is labelled with horseradish peroxidase (HPR). In the presence of toxin B, the aptamer selectively binds to toxin B in the sample and decouples from the magnetic beads. When the aptamer binds to toxin B, the HPR label cannot react with the TMB, a chromogenic substrate; therefore, the HPR catalytic reaction decreases, as does the absorption intensity at 450 nm, produced from TMB via an HPR catalytic reaction. In brief, the absorption intensity is negatively correlated with the toxin B concentration. This aptamer-mediated colourimetric assay (AMCA) reports an LOD of 5 ng/mL for toxin B detection, which is a magnitude greater than for other methods (Luo and Liu, 2020).

A standalone test for CDI diagnosis via ultrasensitive detection of *C. difficile* toxin A or B in the stool sample must satisfy a few crucial criteria, including sensitivity, selectivity, and turnaround time (Bollam et al., 2020). Criteria for each method are shown in **Table 4-2**. Our proof-of-concept data have shown the potential of this ultrasensitive toxin B detection method using a fibre-optic SPR-EOT biosensor. The lower LOD of our biosensor is 4.8 pg/mL, which is comparable with SIMOA and SMC. The redshifts in the transmission spectra are linearly correlated with the toxin B concentration. The upper LOD is 1.35 µg/mL; hence, the detection range covers the concentration range of toxin B for CDI clinical diagnosis, which was estimated to be from 23.3 pg/mL to 10000 pg/mL (Song et al., 2015). The turnaround time of our biosensor is 15 min, which is the shortest amongst these detection methods.

Table 4-2 Methods of toxin B detection with LOD, sensitivity, specificity, and turnaround time

Method of toxin B detection	Limit of detection	Sample matrix	Turnaround time	Sensitivity	Specificity	Reference method	Reference
Cytotoxicity neutralisation assay (CCNA)	50 to 100 pg/ml	Stool	<24 h				(Sandlund et al., 2020) (Lübbert et al., 2014)
Enzyme immunoassay (EIA)	0.8 to 2.5 ng/ml	Stool	60 min	66.9-83.2%	98.8-99.3%	CCNA	(Sandlund et al., 2018) (Planche et al., 2013)
Single Molecular Array (SIMOA)	2.9 pg/ml	Stool	69 min	95.5-100%	83,3-87.0%	CCNA	(Banz et al., 2018) (Song et al., 2015)
Single Molecule Counting (SMC)	0.7 pg/mL	Stool	32 min	96.3%	93%	CCNA	(Sandlund et al., 2020)
Multipath technology	45 pg/ml	Stool	30 min	97%	98.3%	CCNA	(Gite et al., 2018)
Aptamer-mediated colorimetrc assay (ACMA)	5 ng/mL	Stool	45 min	66%	97%	TC and NAAT	(Luo and Liu, 2020)
Fibre-optic SPR-EOT biosensor (this method)	4.8 pg/ml	Buffer	15 min				

Other factors may also contribute to the practical applicability of a rapid toxin B detection method, such as affordability, user-friendliness, instrumentation simplicity, and portability (Land et al., 2019). The fibre-optic SPR-EOT biosensor does not require complicated instrumentation. It can be accommodated in a laboratory with a standard halogen light source, a portable USB spectrometer, and a computer to display and process data. In contrast, SIMOA and SMC demand specific and expensive instruments, such as a Simoa HD-1 analyser and SMCxPRO™ Instrument (Song et al., 2015, Sandlund et al., 2018). Moreover, toxin B detection via our biosensor is conducted at room temperature, while Multipath and AMCA require precise temperature control at 37 ^{o}C to incubate the sample with

immunoreagents (Gite et al., 2018, Luo and Liu, 2020), which affects applicability dramatically. This optic biosensor is highly portable. Therefore, our fibre-optic SPR-EOT biosensor has excellent potential for rapid toxin B detection in resource-limited conditions: for example, in point-of-care facilities.

Although the proof-of-concept using the fibre-optic SPR-EOT biosensor to detect toxin B in the buffer has been demonstrated, a few issues remain unresolved. First, the sensitivity and specificity of our sensor for toxin B in stool samples, and the process for stool preparation, needs to be assessed to demonstrate further the competency of the fibre-optic SPR-EOT biosensor for point-of-care CDI diagnosis. The sensitivity could be improved through optimisation of the antibody immobilisation process. Although using EDC and NHS allows effective antibody immobilisation through amine coupling reaction at physiologic pH (pH=7.4) (Thermo Fisher Scientific, 2021), changing the pH of the buffer to pH=5 or below might enhance the reaction efficiency (Fischer, 2010) and increase the antibody density on the sensing surface. Moreover, the repeatability of our sensors for toxin B detection in stool samples needs to be improved. Variations in the peak shift for three probes could be due to quality changes in one critical reagent used during antibody detection: EDC. EDC is prone to hydrolysis (Nam et al., 2008), and the EDC solution is recommended to be used within two months from preparation (Cytiva Life Sciences, 2020). The efficiency of the antibody immobilisation on the gold film is reduced when EDC experiences hydrolysis. Although the variations in wavelength shifts due to the differences in the antibody immobilisation process could be partially mitigated through data normalisation, the divergence in the wavelength shifts from the three probes is still quite significant. In the future, the study must apply better quality control for the reagents to obtain better repeatability. The fibre-optic SPR-EOT biosensor should be applied in a clinical setting to assess the applicability, sensitivity, specificity, and reproducibility.

There is an apparent demand for ultrasensitive *C. difficile* toxin detection to assist in rapid CDI diagnosis and replace current multi-phase diagnosis algorithms. Although many ultrasensitive toxin B detection methods have been explored, none of these methods has been approved for clinical application (Sandlund et al., 2020, Mizusawa and Carroll, 2021). More studies are required to develop a robust strategy for implementing these ultra-sensitive toxin B assays in routine clinical practice (Sandlund et al., 2018). Moreover, these toxin B assays need to address the emergence of new toxin B variants because they themselves may affect the binding affinity between toxin B and immunoreagents, thereby altering any established sensitivity and specificity (Shen et al., 2020). Our sensor has LOD comparable with SIMOA and SMC and shows great sensitivity to toxin B concentrations below 5 nM (1.35 µg/mL); therefore, it allows ultrasensitive and rapid CDI diagnosis. More importantly, our sensor is cheap, simple to implement, and adaptable for clinical settings. Fibre-optic SPR-EOT biosensors can be ready for clinical use as soon as the sensitivity, specificity and reproducibility are demonstrated in toxin B-containing stool samples.

4.2.6. Conclusion

This proof-of-concept study demonstrates the feasibility of using a fibre-optic SPR-EOT biosensor for ultrasensitive toxin B detection. After improving the stability and portability of the sensor by optimising the processes of flow cell preparation and surface functionalisation, three sensors with a simple instrument were applied to detect toxin B in a label-free manner at a concentration range up to 6 orders of magnitude. An LOD of 4.8 pg/m is achieved from these sensors, and the wavelength shifts in the transmission spectra are well correlated with the toxin B concentration when lower than 1.35 µg/mL. A fibre-optic SPR-EOT biosensor may well emerge as a novel platform for rapid toxin B detection; however, further studies on improving the reproducibility of the detection method and assessment of sensitivity and specificity of the biosensor in toxin B stool samples will be required.

4.3. Supplementary Materials

4.3.1. Fabrication of the Gold Sensing Surface

For template stripping, the template must be cleaned thoroughly before reuse to maintain a consistent quality of the sensing surface. The standard template cleaning procedure is described in the Materials and Methods section. **Figure 4-5** shows that the sensing surface is fabricated from a contaminated (left) and a clean template (right). Both photos were taken at the sample microscope objective, but the two sensing probes were fabricated with different sizes (Left: d = 3.2 mm; Right: d = 2.5 mm); therefore, they appear different in size from the photos. The contaminated template produces a sensing probe with a rough surface and has contaminant residues on the surface. In contrast, the sensing surface fabricated from a thoroughly cleaned template is smooth, without noticeable scratches and contaminants on the surface. High-quality sensing surfaces ensure the consistency of the experimental results.

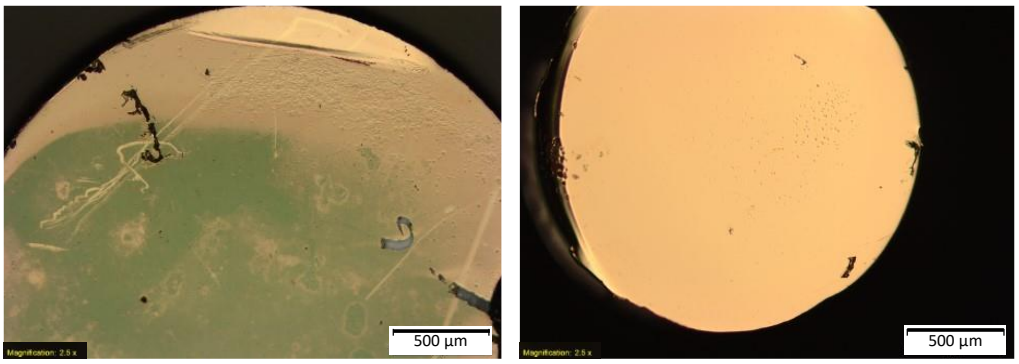

(a) **(b)**

Figure 4-5 Photos of sensing surfaces made from a contaminated **(a)** and a clean template **(b)**.

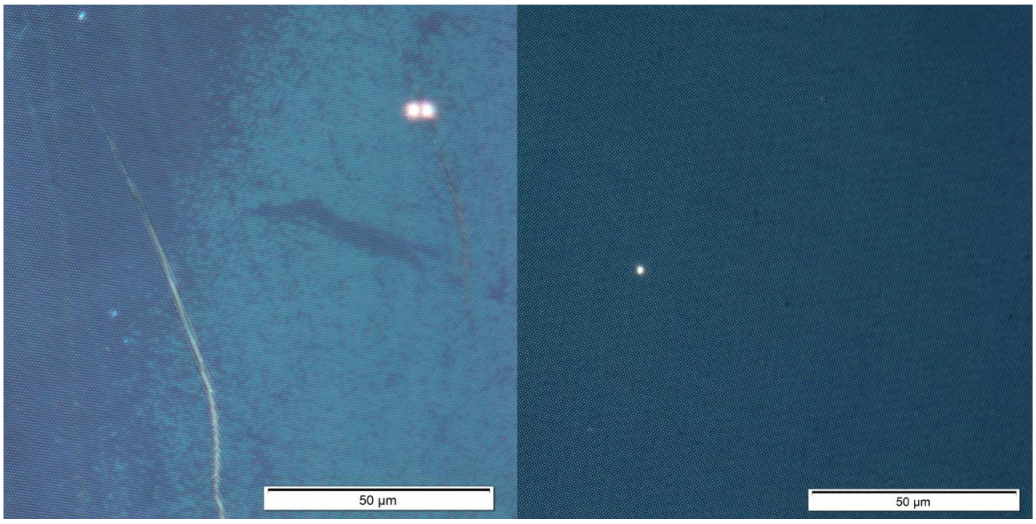

(a) **(b)**

Figure 4-6 Templates before **(a)** and after cleaning **(b)** (25X magnification).

Ultimately, the nanohole array of the gold film after template transfer can be observed under 25X magnification. After fabrication, **Figure 4-7** shows the gold nanohole array on an optical fibre's facets. The figure confirms the quality of the gold sensing surface with a well-characterised nanostructural pattern. An SEM image of the nanostructural sensing surface can be found in a collaborative work with Du et al. (2020a).

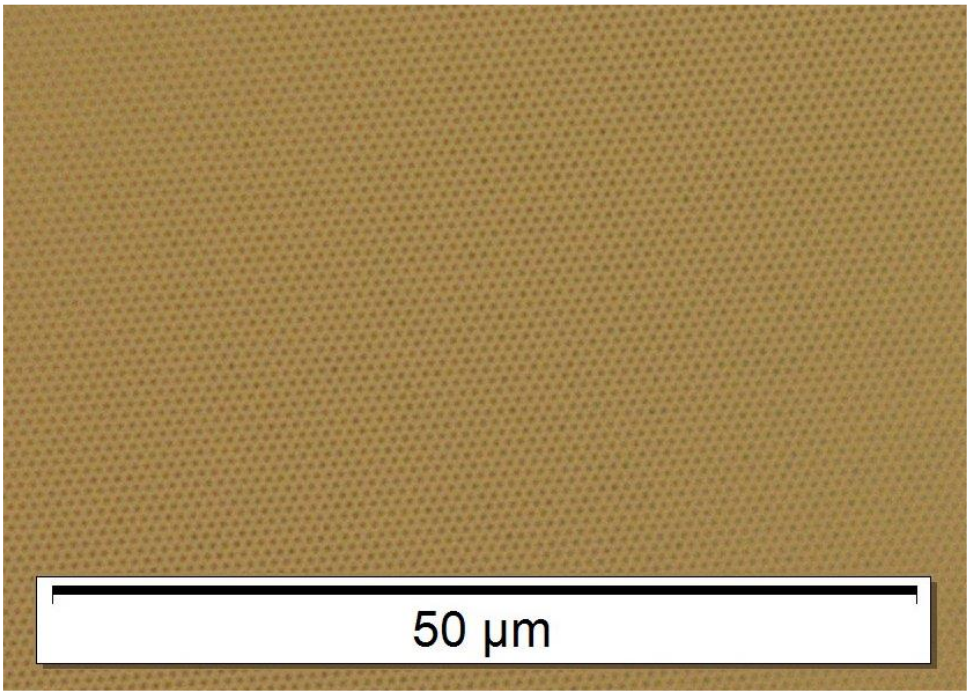

Figure 4-7 Gold nanohole array on the optical fibre tip after a successful template transfer

4.3.2. Optimising Surface Functionalisation

Figure 4-8 depicts a sensing probe before and after surface functionalisation with ethanol as a solvent. Due to the dissolution of epoxy glue in ethanol, the gold film is deformed after surface functionalisation. The photos demonstrate that ethanol as a solvent could weaken the crosslinks in the epoxy glue layer and damage the sensing surface.

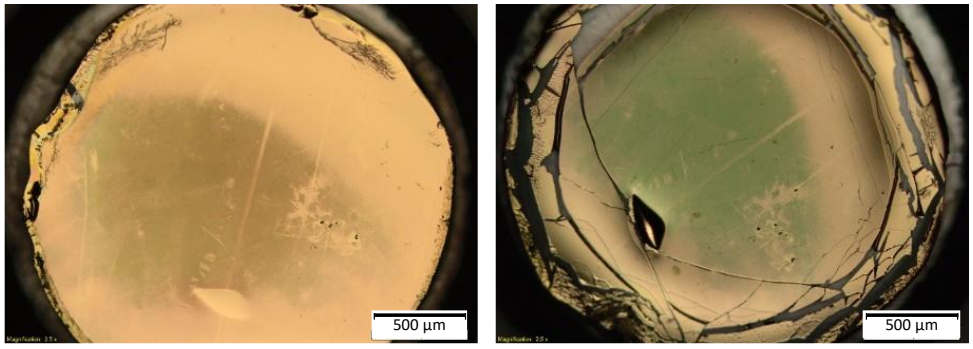

(a) **(b)**

Figure 4-8 A gold sensing surface before **(a)** and after **(b)** functionalisation with 3-MPA in ethanol.

Figure 4-9 illustrates a sensing probe before and after surface functionalisation using water as a solvent. After functionalisation, the sensing surface remained intact, indicating that water is an excellent alternative to ethanol for surface functionalisation. **Figure 4-9** also confirms that the damage on the sensing surface in **Figure 4-8** could be due to the use of ethanol as a solvent.

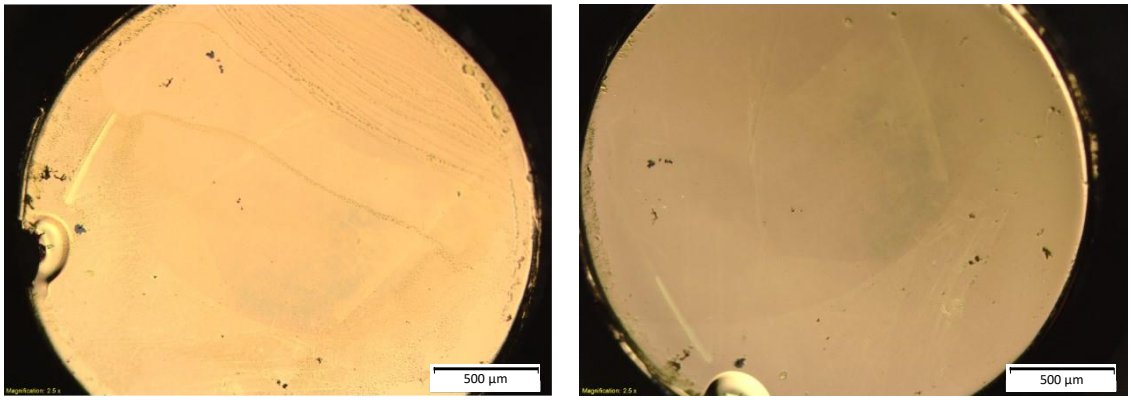

(a) **(b)**

Figure 4-9 A gold sensing surface before **(a)** and after **(b)** functionalisation with 3-MPA in water.

4.3.3. Sensorgrams during Antibody Immobilisation and Toxin B Detection

The data were automatically exported by SpectraSuite software during experimentation, and were then imported to Matlab to process and plot the real-time sensorgram. **Figure 4-10 (a)** shows the sensorgrams from three sensing probes obtained during antibody immobilisation. The signal peak in the sensorgram appears immediately after EDC/NHS injection. The peak sharply drops after the surface is rinsed with a PBS buffer and it reaches a plateau. After injection of the antibody solution into the flow cell, the signal gradually increases.

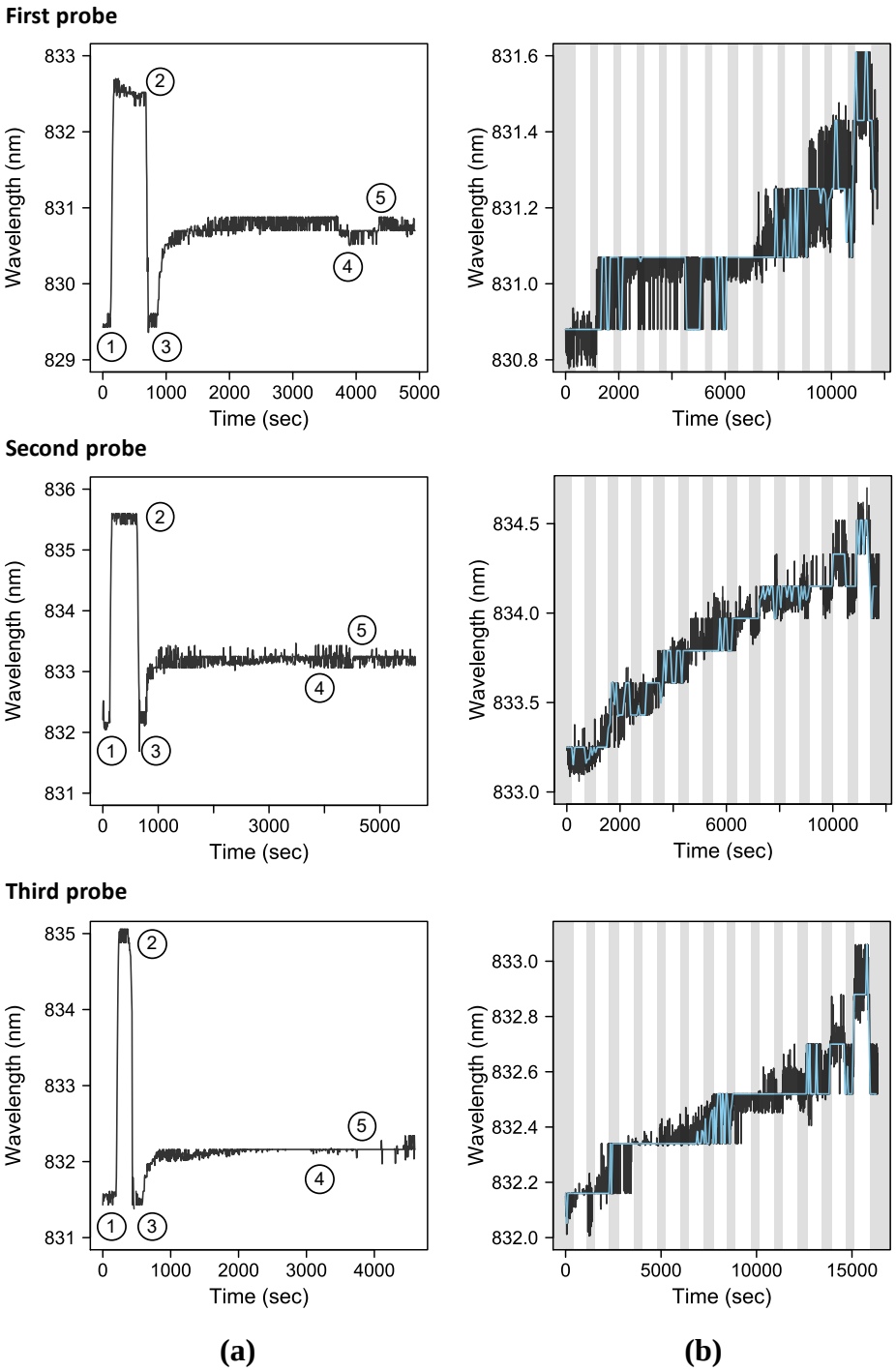

Figure 4-10 Sensorgrams monitoring signal changes **(a)** during antibody immobilisation from three sensing probes: (1) EDC/NHS, (2) PBS buffer, (3) Antibody, (4) Tris buffer, (5) PBS buffer; **(b)** during toxin B detection: grey areas indicate PBS rinse between sample injection; white areas indicate sample injections; blue line is the sensorgram signal after noise removal

Figure 4-10 (b) illustrates the sensorgrams from three sensing probes during toxin B detection. The blue line represents the signal after noises was removed. From experimental observance, the signal always fluctuates around a certain value, therefore, the filter was

applied to pick out the value that have the highest appearing frequency among twelve data points. Each data point was acquired and calculated every five seconds, therefore, each filtered data point constitute the data acquired in one minute. Due to the limitations of the pre-scripted curve fitting function in Matlab, the sensorgrams cannot distinctively display small signal changes when the toxin B concentration increases. However, the sensorgrams are still able to illustrate the overall redshift of the peak at 830 nm. It is noticeable that the signal drops during PBS rinses at the end of the sensorgrams, indicating that saturation of the binding sites has occured. Although the sensorgrams are competent for monitoring signal changes during antibody immobilisation, the data need to be pre-processed in a subsequent study to improve the signal/noise ratio. We performed continuous injections of toxin B samples and rinses with a PBS buffer; thus, the sensorgrams for toxin B detection have high noise levels. The noises could be mitigated if a disposable sensing probe were to be used for a single sample.

5. Chapter 5

RAPID COVID-19 DIAGNOSIS USING A FIBRE-OPTIC SPR-EOT BIOSENSOR

5.1. Statement of Authorship

Title of paper	Rapid COVID-19 Diagnosis Using a Fibre-optic SPT-EOT Biosensor
Publication Status	Unpublished
Publication Details	

Principal Author

Name of Principal Author (Candiate)	Thai Thao Ly		
Contribution to the Paper	Outlined the conceptualisation and methodology; ran the experiments; analysed the data, designed experimental optimisation; wrote the original draft		
Overall percentage	80%		
Certification	This paper reports on original research I conducted during the period of my Higher Degree by Research candidature and is not subject to any obligations or contractual agreements with a third party that would constrain its inclusion in this thesis. I am the primary author of this paper.		
Signature		Date	19/10/2021

Co-author Contributions

By signing the Statement of Authorship, each author certifies that:

i. the candidate's stated contribution to the publication is accurate (as detailed above);
ii. permission is granted for the candidate in include the publication in the thesis; and
iii. the sum of all co-author contributions is equal to 100% less the candidate's stated contribution.

Name or Co-Author	Yinlan Ruan		
Contribution to the Paper	Initiated the project and conceptualisation; executed data validation; provided resources; supervised the project; edited the manuscript.		
Signature		Date	20 Oct 2021

Name or Co-Author	Hu Zhang		
Contribution to the Paper	Evaluated the methodology; supervised the project, provided resources, edited the manuscript.		
Signature		Date	Oct 17,2021

5.2. Publication

5.2.1. Abstract

The potential of a fibre-optic surface plasmon resonance-extraordinary optical transmission (SPR-EOT) biosensor for early phase COVID-19 diagnosis was investigated. The biosensor detects the nucleocapsid protein (N protein) of SARS-CoV 2 since the N protein in the human serum can be detectable at an early phase of infection. Antibodies for N proteins are covalently bound to a gold film via a functionalised agent 3 -MPA and the gold film is transferred to the tips of an optic fibre with the assistance of an epoxy glue. Consistent redshifts in the transmission spectrum are observed from three biosensing probes when they are applied to detect the N protein in a PBS buffer and the biosensors have a limit of detection (LOD) of 1.77 μg/mL. The biosensing probe cannot withstand more than 9 times of regeneration using 50 mM NaOH. The presence of free epoxide rings in the epoxy glue that is used during the fabrication process for our biosensors may be account for such an undesirable LOD. Since antibodies may be entrapped in the epoxy layer due to the reaction between 3-MPA and free epoxide rings, blueshifts of the peaks in the transmission spectra are observed after the N protein interacts with the antibodies in the epoxy layer. Interference of blueshifts with redshifts results in a poor sensitivity of our sensors fabricated with the epoxy glue. An epoxy-free fabrication process was developed for the SPR-EOT biosensor, and it significantly improved sensitivity with a LOD down to 0.046 pg/mL. However, the quality of the epoxy-free biosensors is not consistent, thus, the reproducibility of redshifts of three sensors is quite low. After consistent quality of our epoxy-free sensors is achieved, our fibre-optic SPR-EOT biosensors could have an enhanced sensitivity for N protein detection and excellent repeatability, and they could become a potential device for rapid point-of-care testing (POCT) for COVID-19 due to its compact size, simple set-up, and low cost.

5.2.2. Introduction

Since March 2020, the COVID-19 (Corona Virus Disease -2019) pandemic has become the biggest global concern. COVID-19 was first reported in December 2019 in Wuhan Province, China, and a global pandemic was declared by WHO in March 2020 (Bhalla et al., 2020). By August 11, 2021, it had caused over 4 million deaths globally, with over 180 million confirmed cases. COVID-19 is an acute respiratory disorder with typical symptoms of fever, shortness of breath, and cough (Kabir et al., 2021). Currently, the two most common methods for confirming COVID-19 are detection of viral nucleic acids and serological assays (Carter et al., 2020).

Reverse transcriptase-polymerase chain reaction (RT-PCR) is the recommended method to detect viral nucleic acids in the host body (Porte et al., 2020). RT-PCR offers good sensitivity and specificity (Kabir et al., 2021). However, it requires expensive equipment, well-trained personnel, multiple reagents, and designated laboratories; thus, it is unsuitable for point-of-care or on-site diagnosis (Li et al., 2020b, Shrivastav et al., 2021). The disadvantages of RT-PCR include low sensitivity due to sample handling and storage conditions (Bhalla et al., 2020), sample type (Ji et al., 2020) and ultimately, inconsistent limit of detection (LOD) between different RT-PCR assays (Kabir et al., 2021). These limitations make RT-PCR have a remarkable high risk of false-negative results (Li et al., 2020a), especially in the early phase of infection (Shan et al., 2021).

Serological assays are a cheap and rapid alternative to nucleic acid detection (Kabir et al., 2021) and they are more practical for COVID-19 surveillance (Taleghani and Taghipour, 2021). They detect the anti-SAR-CoV-2 antibodies produced by a human host. The antibodies loads provide information to monitor COVID-19 progression and identify a recent or old infected case (Bhalla et al., 2020). Moreover, serological tests can identify asymptomatic carriers (Kabir et al., 2021). Serological tests, in general, have few limitations.

First, the accuracy of these tests mostly depends on the phase of detection. The result could be false-negative for early detection but false positive for an old case (Taleghani and Taghipour, 2021, Yuan et al., 2020). Second, serological tests lack of specificity. Patients infected with other coronavirus types could be seropositive for the COVID-19 test (Kabir et al., 2021, Taleghani and Taghipour, 2021). Lastly, these tests have lower sensitivity than nucleic acid-based methods (Bhalla et al., 2020). Serological tests have been widely used as complementary to RT-PCR for efficient and accurate COVID-19 diagnosis. They hold great potential for cheap and rapid screening of SARS-CoV-2 infection under limited-resource conditions; however, the main drawbacks are false-positive results due to cross-reactivity and poor detection sensitivity for early phase diagnosis (Taleghani and Taghipour, 2021).

Early and rapid diagnosis is critical for mitigating the spread and allowing medical practitioners to apply appropriate treatment for high-risked patients (Rong et al., 2020). As a result, there is an urgent need to establish rapid, cheap, and sensitive COVID-19 point-of-care testing (POCT) to effectively identify and trace the infected cases effectively and then to isolate them promptly (Ji et al., 2020). Here in this study, we utilised a highly sensitive surface plasmon resonance (SPR) biosensor to detect N proteins on the surface of SAR-CoV-2 for early and rapid diagnosis of COVID-19.

SPR biosensors are excellent candidates for rapid and ultrasensitive COVID-19 diagnosis because they provide superior sensitivity and quick turn-around times. Nevertheless, SPR biosensors are not suitable for POCT due to their substantial size and high instrumentation cost (Bhalla et al., 2020). The biosensor proposed in this study is based on a nanoplasmonic phenomenon- extraordinary optical transmission (EOT)- which enables it to overcome the limitations of SPR biosensors but to maintain comparable sensitivity.

EOT occurs when light transmits through a metallic film with a subwavelength nanohole array. The transmission spectrum has peaks and dips corresponding to the dimensional characteristics of the metal film. EOT biosensors are highly sensitive because the peaks of the transmission spectrum are sensitive to changes in the local or bulk refractive index. Due to its excellent sensitivity, EOT biosensors have been studied for various protein-protein interactions (Jackman et al., 2017). Additionally, the EOT biosensor employs a more straightforward and flexible optical setup to replace a bulky prism and a strictly controlled angle of incident light in the conventional SPR optical settings. This simple optical setup allows miniaturisation through engineering modifications. In this study, optical fibres were used to fabricate the EOT biosensor, which was named a fibre-optic SPR-EOT biosensor. The fibre-optic SPR-EOT biosensor is exceptionally portable, as it requires few simple components for detection of N protein- a light source, a portable spectrometer, and a computer, while it offers good sensitivity and repeatability.

The target antigen for early COVID-19 diagnosis is the N protein of SARS-CoV-2. The N protein is chosen instead of other SARS-CoV-2 structural proteins (spike glycoprotein, envelope protein, and membrane protein) because it is the most abundant protein available in the host body at the early phase of infection (Hodge et al., 2021). Che et al. (2004) reported that the N protein of SARS-CoV could be detected in human serum as early as day 1 of symptom onset. Li et al. (2005) concluded that the SARS-CoV N protein had a higher detection rate than SARS-CoV RNA and anti-SARS-CoV antibodies during the first 15 days after symptom onset. A recent study by Shan et al. (2021) for SARS-CoV-2 also reached the same conclusion. Utilisation of the fibre-optic SPR-EOT biosensor for N protein detection may offer a promising method for portable COVID-19 detection at an early phase. Additionally, it can be used as a rapid detection method to identify potential infectious cases to mitigate the spread of COVID-19. Advanced diagnosis methods such as RT-PCR could be

used as a secondary diagnosis step to identify the viral strain and confirm the diagnostic results.

This study was carried out to investigate the feasibility of using a fibre-optic SPR-EOT biosensor for COVID-19 diagnosis by detecting the N protein on the viral surface. The gold film functionalised with anti-N protein antibodies was bound to the fibre tips with an epoxy glue. Transmission spectra were generated after the N protein in a PBS solution was captured with the antibodies on the gold film. Regeneration of the probe surface was also implemented to examine the reusability and durability of the biosensor for N protein detection. The results confirm that the biosensor fabricated with the epoxy glue can detect the N protein of SARS-CoV-2 with excellent repeatability and reproducibility, while the LOD is far above that from previous reports. Free epoxide rings in the epoxy glue may be a contributing factor for such a high LOD. Epoxy-free biosensors are demonstrated to improve the LOD of the sensor, but the quality of epoxy-free biosensors is inconsistent. Overall, our fibre-optic SPR-EOT biosensor holds great potential for early SARS-CoV-2 detection; however, there is still plenty of room for improvement before the biosensor can be used for clinical applications.

5.2.3. Method and Materials

5.2.3.1. Sensor Fabrication

The nanopatterned sensing gold film was purchased from Lightsmyth (USA). The silicon template (Product code: S2D-18D3-0808-350-P) had nanoholes arranged in a hexagonal lattice with spacing of 700 nm. The diameter of the nanohole was 200 nm. The template was first cleaned with a Piranha solution for 30 min to remove the residual of an epoxy glue, followed by an Aqua Regia to clean the gold residue, and finally a Piranha solution for 30 min to ensure the surface was free of organic contamination.

After cleaning, gold at a size of 100 nm was deposited onto the template using a thermal evaporator (Quorum Technology-K975X Turbo-Pumped Thermal Evaporator, UK). The template coated with gold was aligned to be parallel with an optical fibre, and 0.8 µL of epoxy glue was deposited onto the tip of the optical fibre. The template and optical fibre were firmly pressed until the epoxy glue was evenly distributed on the ferrule. The epoxy glue was cured under a heating lamp at approximately 60 ℃ for 4 h, then left at room temperature for 24 h. After the glue was cured, the optical fibre was peeled from the template. The gold film with the epoxy glue was transferred to the optical fibre, resulting in an optical fibre with a nanopatterned gold film on the tip.

Fabrication of an epoxy glue-free sensing probe was slightly modified from the approaches reported by Polley et al. (2019) and Arghir et al. (Arghir et al., 2015). The nanopatterned gold film was chemically fixed onto an optical fibre due to the interaction between the thiol group on the optical fibre and the gold film. A silicon template with the gold film was immersed in 0.1 M NaOH overnight to cleave the chemical bond between the silicon template and the gold film. The template with the gold film was transferred from the NaOH solution to MiliQ water. A small scratch was made across the gold film, and the gold film released from the template floated on the water's surface. The optical fibre with a ferrule jacket was cleaned thoroughly in ethanol in a sonication bath. It was silanised in a solution of 0.3 M acetic acid and 0.08 mM (3-mercaptopropyl) trimethoxysilane (MPS) in toluene for 2 h. The floating gold film was attracted and attached to the functionalised optical fibre due to the chemical reaction between the thiol group and gold (Xue et al., 2014). The optical fibre with the gold film was dried in an oven at 70 ^{o} C for 1 h.

After the sensing gold film was firmly attached onto the optical fibre, either with or without an epoxy glue, the optical fibre was assembled with a 3-D printed chamber, a bare

optical fibre was used to collect the transmitted light signal, and two stainless steel microfluidic tubes were used to make a flow cell.

5.2.3.2. Data Interpretation

The optical transmission spectra were measured by a spectrometer (Ocean Insights, USB4000, USA), automatically recorded every 5 s by SpectraSuite software (Ocean Insights, USA), and they were processed by a customised Matlab (Mathworks, USA) script to real-time monitor the shift of the peak at 830 nm. Simultaneously, optical transmissions were manually collected after every sample injection, and these data were analysed using Origin software (Originlab, USA). All plots were made based on the wavelength shift of the transmission peak at 830 nm.

5.2.3.3. Antibody Immobilisation

The gold sensing surface was first functionalised with aqueous 10 mM 3-mercaptopropionic acid solution (Sigma Aldrich M5801) overnight and rinsed with Milia-Q water. The running solution was then changed to a PBS buffer. A mixture of 0.2 M (1-ethyl-3-(3-dimethylaminopropyl)carbodiimide hydrochloride) (EDC) and 0.05 M N-hydroxysuccinimide (NHS) (Cytiva Life Sciences- Amine Coupling Kit) in water was introduced into the flow cell for 7 min to activate the EDC/NHS amine coupling reaction. The sensing surface was quickly rinsed with the PBS buffer, and 0.01 mg/mL antibody solution (Rabbit anti-SARS-CoV-2 N-Protein antibody, 130-10760-100, RayBiotech, US) in 0.01 M sodium acetate buffer (pH = 5) which was pumped through the flow cell for 30 min at a flow rate of 20 µL/min. The surface was rinsed with the PBS buffer to remove the excess antibodies. The coupling reaction was quenched by 0.05 M Tris buffer (pH=7.4) for 7 min, and non-specific binding sites on the sensing surface were blocked by 1% BSA in the PBS buffer (pH = 7.4) for 15 min. Finally, the sensing surface was rinsed with the PBS buffer for 5 min.

5.2.3.4. N Protein Detection

Recombinant SARS-CoV-2 nucleocapsid protein (N protein) was purchased from RayBiotech (230-01104-100, US). Each experiment was carried out in triplicate. To evaluate the feasibility of using a fibre-optic SPR-EOT biosensor for rapid detection of N protein on the SARS-CoV 2 viruses, N protein was prepared in a series of dilutions to have a concentration ranging from 9.1×10^{-12} mg/mL to 1.1×10^{-2} mg/mL. The samples were injected into the flow cell from low to high concentrations with interval rinses with a PBS buffer. A similar experimental approach was applied to N protein detection using a sensing probe fabricated without an epoxy glue. The repeatability of the biosensor for N protein detection was also assessed by regenerating the sensing surface after each sample measurement. The sensing surface was regenerated via a quick flush of a 50 mM sodium hydroxide solution between sample injections. Three different sensing probes were used to measure the N protein concentration of 9.1×10^{-10} mg/mL, 9.1×10^{-8} mg/mL, and 9.1×10^{-6} mg/mL respectively to confirm transmission signal changes at a low N protein concentration.

5.2.4. Results

5.2.4.1. Feasibility of using a Fibre-optic SPR-EOT Biosensor for N Protein Detection

We first evaluated the feasibility of using the fibre-optic SPR-EOT biosensor for rapid Covid-19 diagnosis by detecting the N protein on the viral surface. It is worth mentioning that the N protein concentration range varies across the three replicates. In the first trial, the concentration range was from 9.1×10^{-12} mg/mL to 1.1×10^{-2} mg/mL. The preliminary signal analysis from the first sensing probe suggests that the signal change is negligible when the N protein concentration is lower than 9.1×10^{-5} mg/mL. Therefore, for the second and third sensing probes, the concentration range was changed to be between 9.1×10^{-8} mg/mL and 9.1×10^{-3} mg/mL but more data points were added to confirm the signal change.

After the N protein solution at the above concentration range flows through the optical fibre in the flow cell, the transmission spectra generated from the fibre were acquired and analyzed. The wavelength shifts of the transmission spectra peak at 830 nm are displayed in **Figure 5-1** (**a**). Each black dashed line indicates the N protein detection results from one individual sensing probe, and a thick black line represents the curve-fitting line. The limit of detection (LOD) is shown as a dashed red line. The LOD was calculated from three times the standard deviation of the blank sample. Despite a different range of N protein concentrations, the trend of signal shifts across the three sensing probes is very consistent. There is an apparent positive correlation between the N protein concentration and the shift of the signal transmission peak at 830 nm. There are negligible changes in the signal shift of the transmission peak at 830 nm at a low N protein concentration; however, when the N protein concentration is greater than 9.1×10^{-5} mg/mL, the signal shifts escalate sharply. The results show that our biosensor system can detect the N protein with excellent repeatability, but it suffers from low detection sensitivity. The limit of detection (LOD) is calculated to be 1.77 µg/mL, which is much greater than that obtained from other studies.

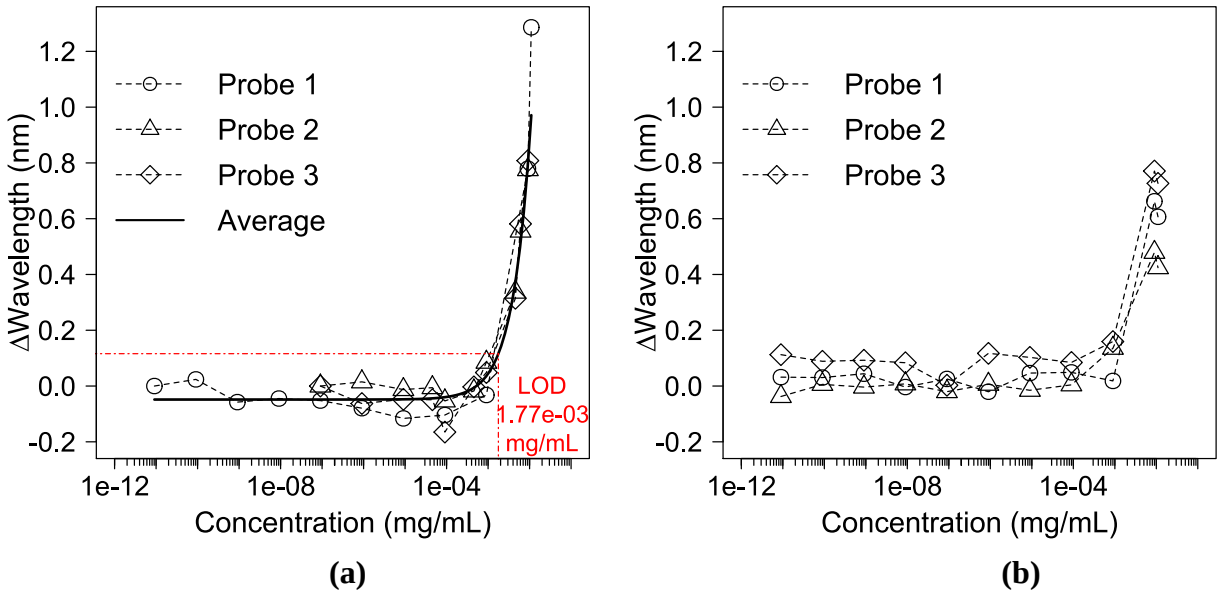

Figure 5-1 (**a**) Wavelength shifts of the transmission spectral peak at 830 nm acquired from three antibody-based fibre-optic SPR-EOT biosensors for N protein detection.

Dashed black lines from three individual sensing probes, a solid black line for curve-fitting and a red dashed line for an average LOD of three sensors. (**b**) N protein detection using antibody-based fibre-optic SPR-EOT biosensors in triplicate with regeneration between sample injections.

To confirm the trend and repeatability of our biosensor system for N Protein detection, the sensing surface of each sensing probe in **Figure 5-1 (a)** was regenerated by 50 mM NaOH between each sample injection and the result is shown in **Figure 5-1** (**b**). The regenerating solution of 50 mM NaOH was chosen from a separate regenreation test, in which different concentrations of NaOH (10 mM, 25 mM, and 50 mM) were used find the most efficient solution. Details about the regeneration test can be found in section **5.3.1** of the **Supplementary Materials**. In **Figure 5-1** (**b**), the trend of signal shifts is similar to that in **Figure 5-1 (a)**; however, the wavelength shifts of all three sensing probes experience a significant drop during detection of N protein at 1.1×10^{-2} mg/mL. The average wavelength shift is 0.568 ± 0.15 nm in comparison with 1.28 nm in **Figure 5-1 (a)** at the same N protein concentration (See the Supplementary doccument for the detailed data). This signal drop indicates that the immobilised antibody cannot withstand more than nine instances of regeneration with 50 mM NaOH. **Figure 5-1 (a)** and **Figure 5-1 (b)** confirm the reproducibility of our biosensor system, suggesting its potential in detecting the N protein of coronaviruses. However, the detecting sensitivity of our biosensor system needs to be improved, so that the system can be used for coronavirus detection.

5.2.4.2. Effect of Epoxy Residues on the Sensitivity of our Sensors for N Protein Detection

To probe the sensor performance at a low concentration and improve the detecting sensitivity of our sensing probes, three sensing probes were used to measure the signal change at three N protein concentrations. Probe 1 measured the N protein concentrion at 9.1×10^{-10} mg/mL, probe 2 for the N protein concentration at 9.1×10^{-08} mg/mL, and probe 3 for the

concentration at 9.1×10^{-06} mg/mL. The wavelength shifts of the three sensing probes are shown in **Figure 0-2** (**a**).

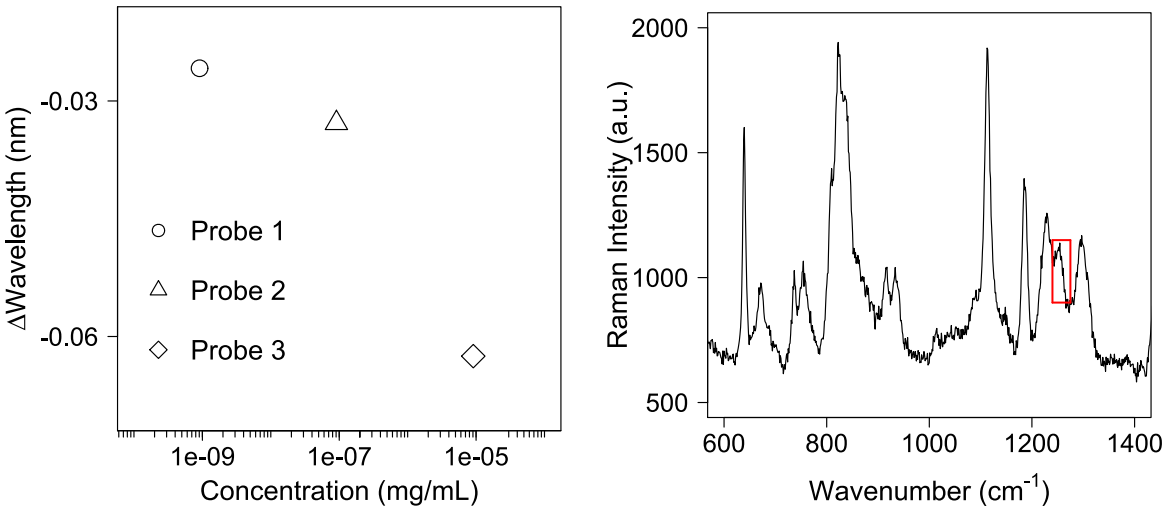

(a) **(b)**

Figure 5-2 (**a**) N protein detection at low concentrations of N protein using three individual sensing probes. (**b**) Raman spectrum of cured epoxy, the peak at 1255 cm^{-1} corresponds to free epoxide rings

It is interesting to note in **Figure 0-2 (a)** that the transmission peak experiences a blueshift (or negative shift) as the N protein concentration increases. Moreover, it can be observed that the signal shifts drop slightly and then increase during N protein detection at low N protein concentrations in **Figure 5-1 (a)**. It was hypothesised that the epoxy layer for fabricating the sensing film might be responsible for this unexpected signal change. Du et al. (2020a) used a fibre-optic SPR-EOT biosensor to detect methanol in gas and reported that the blueshifts were observed when methanol molecules bound to the epoxy layer. After the epoxy layer reacted with methanol in the gas phase, they were able to detect and quantify the concentration of methanol in the gas phase by monitoring the blue shift of the transmission signal. Consequently, negative shifts of the transmission peak at a low concentration of N protein may be due to capture of the N protein in the epoxy layer. After the N protein becomes saturated at the epoxy layer, the blue shift reaches the maximum value. The N protein starts to bind to the gold film, resulting in a positive shift in the transmission peak.

The positive shift counteracts the negative shifts from the epoxy layer, and the signal shifts start to increase as the concentration of N protein increases. When the N protein concentration is high enough to cover the binding sites on both the epoxy layer and the gold layer, there is a positive signal shift.

To examine the interaction of N proteins with epoxy, the Raman spectroscopy of the cured epoxy (**Figure 0-2 (b)**) was acquired. A distinguished peak for the epoxide ring at 1255 cm^{-1} is detectable for the cured epoxy. During the curing process, free epoxide rings interact for crosslinking and the number of free epoxide rings decreases; therefore, the intensity of the peak at 1255 cm^{-1} decreases during the curing process (Vaskova and Křesálek, 2011, Andrade et al., 2013). Since the peak at 1255 cm^{-1} is still distinct; it can be concluded that there were a small number of unreacted epoxide rings in the epoxy layer after completion of the fabrication process for our biosensors.

Grazu et al. (2012) reported that these unreacted epoxide groups readily react with thiol functional groups under any pH conditions. Therefore, it can be hypothized that the unreacted epoxide groups in the epoxy layer might react with the thiol group of 3-MPA during functionalisation through a β-hydroxythio-ether linkage. A scheme for the reaction between 3-MPA and epoxy rings is shown in **Figure 5-3**. After 3-MPA is bound to the epoxy layer, the antibody might react with 3-MPA and immobilise onto the epoxy layer during antibody immobilisation. Accordingly, the N protein might bind to the antibody immobilised on the epoxy layer and cause the blueshifts.

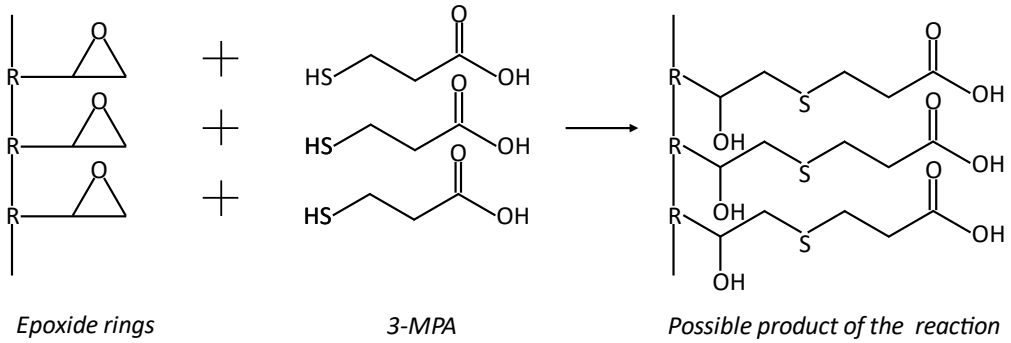

Figure 5-3 Proposed reaction between 3-MPA and the residual epoxide rings during functionalisation

5.2.4.3. N Protein Detection using Epoxy-free Sensing Probes

Since the epoxy glue may interfere with N protein detection, we developed a method to fabricate the sensing probes for N protein detection. The detailed procedure for fabricating the epoxy-free biosensing probe is included in the methodology section.

Du et al. (2020c) fabricated an epoxy-free sensing probe to monitor humidity by transferring a free-standing gold film onto an optical fibre ferrule simply by physical adsorption. Unfortunately, this method is not applicable to liquid samples because the gold film is not firmly fixed onto the optical fibre, and it is prone to detach from the fibre under shear stress of liquid flow. We modified the methods proposed by Polley et al. (2019) and Arghir et al. (2015) to chemically adsorb the gold film onto an optical fibre. The silica optical fibre was silanised with MPS so that the optical surface is covered with thiol groups. The thiol groups react with the gold film to create chemical bonds between the gold film and the optical fibre. These thiol-gold bonds secure the gold film in place when the liquid samples flow over it. The durability of the sensing probe without the epoxy glue was tested. They are demonstrated to be robust at a high flow rate up to 1 ml/min. These sensing probes were then applied for N protein detection. The results are depicted in **Figure 5-4.**

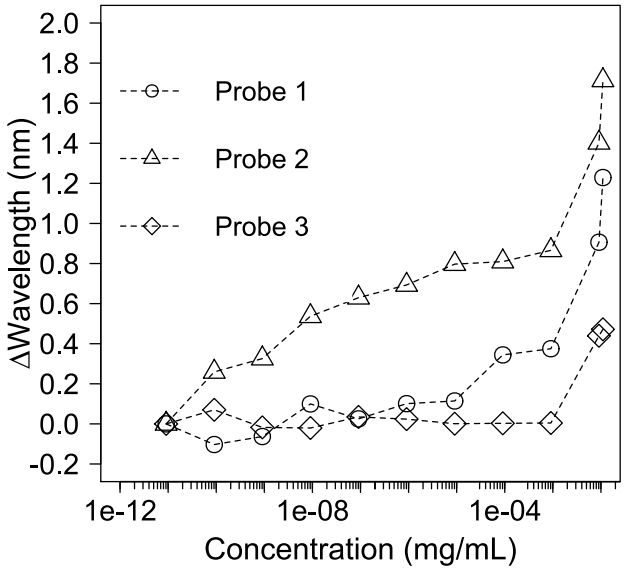

Figure 5-4 N protein detection using three epoxy-free fibre-optic SPR-EOT biosensors

It can be seen that the sensitivity of the sensing probes without the epoxy glue is improved significantly, while their repeatability is reduced in comparison with **Figure 5-1 (a)**. There is a significant redshift at a low N protein concentration. A significant increase in the wavelength shift is found for the second probe even at an N protein concentration down to 9.1×10^{-11} mg/mL, and the LOD for the probe is estimated to be 4.6×10^{-11} mg/mL (0.046 pg/mL). This LOD is eight orders of magnitude lower than the LOD from sensing probes with epoxy (1.77 μg/mL). The epoxy-free sensing probe displays a much more significant signal change, up to 1.7 nm at a N protein concentration of 1.1×10^{-2} mg/mL, in comparison with the maximal change of 1.2 nm of the sensing probe with the epoxy glue at the same N protein concentration. Therefore, the epoxy-free sensing probe offers better sensitivity for N protein detection.

However, the signal shifts vary among three sensing probes. The signal change of the first probe increases slightly but noticeably, while no such improvement is found for the third probe. Repeatability might be impaired due to operational variations during fabrication. When the gold film is only physically bound to the optical fibre via the epoxy glue, it can

easily be adjusted until it is placed perfectly flat and smooth onto the optical fibre (Du et al., 2020b). However, it is impossible to adjust and align the gold film when it is chemically adsorbed to the optical fibre. Three epoxy-free probes are partially defective with wrinkles on the gold film (see the supplementary doccument). Although they still can provide extraordinary optical transmission and improve the detecting sensitivity, the quality of the three biosensors is not consistent, thus, the repeatability of the signal shifts is very poor.

We have demonstrated that the sensitivity of the fibre-optic SPR-EOT biosensor could be improved by eliminating the epoxy glue; however, the fabricating procedure needs to be improved to ensure consistent quality for all sensing probes and better repeatability of N protein detection.

5.2.5. Discussion

Previous studies for N protein detection for COVID-19 diagnosis can be divided into four groups: ELISA-based methods, lateral flow assays (LFAs), other methods, and novel ligands for the N protein. **Table 5-1** summarizes recent N protein detection studies in these four groups with their sensitivity, specificity, LOD, and turn-around time.

Excellent sensitivity and specificity for N protein detection have been reported; however, most of these methods are not applicable for POCT. As shown in **Table 5-1**, except for LFA, other N protein detection methods require specific instruments to conduct the test. These instruments often require a substantial space and a high capital cost; thus, they face great challenges for POCT. For example, the sensitive single-molecule array immunoassay or Simoa was approved for Emergency Use Authorization (EUA) by the Food and Drug Administration (FDA) in 2021 (U.S. Food and Drug Administration 2021). Simoa requires an HD-X analyser (Quanterix Corporation, USA); therefore, the Simoa SARS-CoV-2 N protein antigen test can only be conducted at those laboratories in which there is an HD-X analyser.

Our biosensor can be delivered and installed at POCT thanks to its compact size and low capital cost. The fibre-optic SPR-EOT biosensor requires a visible light source, a portable spectrometer, a small pump (optional), and a computer or laptop to process and analyse the data.

Additionally, the turn-around time for our biosensor is 15 minutes, which is faster than other N protein detection methods shown in **Table *5-1***. ELISA assays with multiple washing steps typically take more than 2 hours, making the process time-consuming and complicated. However, the fibre-optic SPR-EOT biosensor system has the potential to allow high-throughput analysis by processing multiple samples simultaneously with parallel biosensors within one system. Finally, our biosensor detection method is label-free, and it does not require additional chemical/biochemical reagents to enhance the detecting signal, unlike ELISA and LFA. Secondary antibodies, a horseradish peroxidase (HRP) marker, a fluorescent marker, or gold nanoparticles are utilised to enhance the detection signal of ELISA assays. The additional materials for markers or signal enhancers require extra steps and more processing time for the COVID-19 test. They also account for the extra cost of the analytical method, which contributes to the final cost of the test. Label-free detection using fibre-optic SPR-EOT biosensors helps to reduce the processing time and cost of the test.

Our detection method could be an alternative promising method for POC COVID-19 tests to the current LFAs. Among 32 EUA antigen diagnostic tests approved by the FDA, 25 are LFAs. In 2021, the FDA has approved 8 LFA tests for at-home COVD-19 tests (U.S. Food and Drug Administration 2021). However, the accuracy of some LFA tests is not reliable, especially for those that are not FDA-approved and available outside of the USA. Porte et al. (2020) evaluated the accuracy of Bioeasy 2019-Novel Coronavirus (2019-nCoV) Fluorescence Antigen Rapid Test Kit (Bioeasy Biotechnology Co., China) against RT-PCR and reported an excellent accuracy of 96.1%. However, another rapid N protein detection kit,

BIOCREDIT COVID-19 Ag (RapiGEN Inc, Korea), is one thousand times less sensitive than RT-PCR (Mak et al., 2020). Although LFA rapid test kits have the advantages of ease use and great accessibility, they need to be carefully validated for early COVID-19 diagnosis.

Besides development of ELISA alternatives for N protein detection, specific binding agents to capture the SARS-CoV-2 N protein have been prepared to improve detection sensitivity (Bhalla et al., 2020, Surjit and Lal, 2008). The novel ligands include recombinant antibodies, antibodies or antibody fragments from immunised animals, and aptamers (as shown in **Table 5-1**). The immunoassays utilising novel ligands can achieve an LOD in the range of picograms per millilitre to nanogram per millilitre, which is comparable to the LOD of other studies in **Table 5-1**. These novel ligands could be implemented in our fibre-optic SPR-EOT biosensors for N protein detection to provide ultrasensitive tests for COVID-19 diagnosis in an early phase of infection.

Compared with ELISA and mass spectrometry, the fibre-optic SPR-EOT biosensor is more suitable for POCT due to its small size, simple setup, and simple operation. Although SPR biosensors hold great potential for viral detection, their use for POCT is still at the infancy stage (Shrivastav et al., 2021). The sensitivity of our fibre-optic SPR-EOT biosensor needs to be improved before it can be applicable for ultrasensitive N protein detection as the LOD of the fibre-optic SPR-EOT biosensor with epoxy glue is significantly greater than that from other methods in **Table 5-1**. We have demonstrated that the sensitivity of fibre-optic biosensors could be improved by use of the epoxy-free fabrication process, but the fabrication process without epoxy glue is not consistent. Additionally, novel antibody better affinity ligands to the SARS-CoV-2 N protein could be implemented in our sensor to boost the detection sensitivity.

5.2.6. Conclusion

In this study, we have demonstrated the feasibility of using a fibre-optic SPR-EOT biosensor to detect the N protein of SARS-CoV-2. The biosensor fabricated with the epoxy glue can detect the N protein with excellent repeatability and it can be regenerated up to nine times using 50 mM sodium hydroxide. However, the sensitivity of the biosensor is far below the threshold values for ultrasensitive N protein detection. The LOD of our biosensor is 1.77 µg/mL, while the LOD values from other ultrasensitive N protein detection methods are at the level of nanograms per millilitre. Such a high LOD might be due to the presence of free epoxide rings in the epoxy glue. Free epoxide rings may react with the functionalised reagent 3 -MPA, thus antibodies for detecting the N protein may be also in the epoxy layer, as well as on the gold film. After the N protein is bound to the antibodies in the epoxy layer, blueshifts of the peaks in the transmission spectra interfere with redshifts when the N protein is bound to antibodies on the gold film. An epoxy-free fabrication method is developed for our sensors to eliminate blueshifts during N protein detection. The sensing probe from this epoxy-free method has a better sensitivity, but the repeatability of wavelength shifts across the three probes is poor due to the inconsistent fabrication process.

Compared with other N protein detection methods, such as ELISA and mass spectrometry, the fibre-optic SPR-EOT biosensor has great potential for POCT due to its small size and simple setup. It can detect the N protein of SARS-CoV-2 in a label-free approach within a short time, and it does not require complicated instrumentation or chemical or biochemical reagents. The sensitivity could be improved via a consistent epoxy-free fabrication method and novel bioagents for N protein detection that are only bound to the gold film.

Table 5-1 Recent studies on N protein detection for COVID-19 diagnosis

No	Type of study	Method of detection	Sensitivity	Specificity	LOD	Turn-around time	Label/ secondary antibody	Complicated equipment	Reference
1	ELISA-based method	Sandwich and indirect ELISA	94%	99.9%	N/A	3 hours	HRP	Safety cabinet	(Che et al., 2004)
2	ELISA-based method	Sandwich and indirect ELISA	N/A	96.7%	0.2 ng/mL	3 hours	HPR	Safety cabinet	(Lau et al., 2004)
3	ELISA-based method	Sensitive single molecule array (Simoa) immunoassay	90%	98%	0.1 pg/mL	N/A	Paramagnetic beads	HD-X instrument	(Shan et al., 2021)
4	Novel capture ligand for N protein and ELISA-based method	Antibody-aptamer hybrid sandwich ELISA	N/A	N/A	1 ng/mL	3 hours	HPR	Safety cabinet	(Zhang et al., 2020a)
5	Novel capture ligand for N protein and ELISA-based method	Sandwich ELISA using antibodies generated by animals	N/A	N/A	100 ng/mL	1 hour	HRP	Safety cabinet	(Li et al., 2020a)
6	LFA	Fluorescence immunochromatographic assay	75.6%	100%	N/A	10 minutes	Fluorescence		(Diao et al., 2021)
7	Novel capture ligand for N protein and LFA method	Antibody-aptamer hybrid gold nanoparticle immunochromatographic strip	N/A	N/A	1 ng/mL	15 minutes	Gold colloid		(Zhang et al., 2020a)
8	Novel capture ligand for N protein and LFA method	Quantum dots-chromatographic assay using antibodies generated by animals	N/A	N/A	10 ng/mL	15 minutes	Quantum dots		(Li et al., 2020a)
9	Other methods	Localised surface plasmon coupled fluorescence fibre-optic biosensor and sandwich			1 pg/mL	2 hours	Fluorescence and gold nanoparticle	Laser source, photomultiplier tube, and lock-	(Huang et al., 2009)

		immunoassay						in amplifier	
10	Other methods	Optical quantum dots-conjugated RNA aptamer chip	N/A	N/A	0.1 pg/mL	1 hour	Quantum dots		(Roh and Jo, 2011)
11	Other methods	Immunoaffinity purification and high-resolution mass spectrometry-based targeted qualitative assay	98%	100%	N/A	N/A	N/A	Ultimate 3000 RSLC nanosystem and Orbitrap Eclipse mass spectrometer	(Renuse et al., 2021)
12	Other methods	Mass Spectrometric Identification	N/A	N/A	N/A	3 hours	N/A	UltiMate RSLC 3000 and Orbitrap Fusion Tribrid mass spectrometer	(Ihling et al., 2020)
13	Novel capture ligand for N protein	MagPlex fluid array assays using single-domain antibodies against the SARS-CoV-2 N protein	N/A	N/A	50 pg/mL	2 hours	*R-phycoerythrin*	MAGPIX instrument	(Anderson et al., 2021)
14	Novel capture ligand for N protein	Modified ELISA using a monoclonal antibody against the N-terminal domain of N protein	N/A	N/A	In pg/mL range	2 hours	HRP	Safety cabinet	(Hodge et al., 2021)
15	Novel capture ligand for N protein	Double-antibody sandwich ELISA using antibodies derived from COVID-19 patients	N/A	N/A	0.78 ng/mL	1 hour	HRP	Safety cabinet	(Zhang et al., 2020b)
16	Novel capture ligand for N protein	Sandwich ELISA using recombinant antibodies	N/A	N/A	5500 PFU/mL	3 hours	HRP	Safety cabinet	(Terry et al., 2021)
17	Fibre-optic SPR-EOT biosensor (This study)	Label-free N protein detection	N/A	N/A	1.77 µg/mL	15 min	N/A	Halogen light source, portable spectrometer	

5.3. Supplementary Materials

5.3.1. Anti-N protein antibody regeneration

Before the experiment of N protein detection with regenerations between sample injections, the suitable concentration for regenerating solution was determined by a regeneration test. A sensing probe immobilised with rabbit anti-SARS-CoV-2 N-Protein antibody was used throughout the experiment and tested with different NaOH concentrations of 10 mM, 25 mM, and 50 mM. All the N protein samples had a concentration of 5 µg/mL. The sensor's flow cell was injected with N protein samples for 10 min then quickly flushed with NaOH solution to regenerate. For each NaOH concentration, sensor regenerations were carried out in triplicates. After each sample injection and regenerating flush, the sensing surface was rinsed with PBS buffer to remove the exceeded N protein and collect the signal. Before progressing to the higher NaOH concentrations, the sensing surface was regenerated by a quick flush of 50 mM NaOH.

Figure 5-5 shows the wavelength shifts collected during the regeneration test of three different NaOH concentrations. According to **Figure 5-5 (a)** and **(b)**, using 10 mM and 25 mM NaOH only partially regenerated the sensing surface; thus, the signal did not return to the baseline. In contrast, 50 mM NaOH solution worked well in unbinding the captured N protein from the sensing surface (**Figure 5-5 (c)**). It can be seen that as the NaOH concentration increased, the regeneration's efficiency also improved. Consequently, 50 mM NaOH solution was chosen as the regenerating solution.

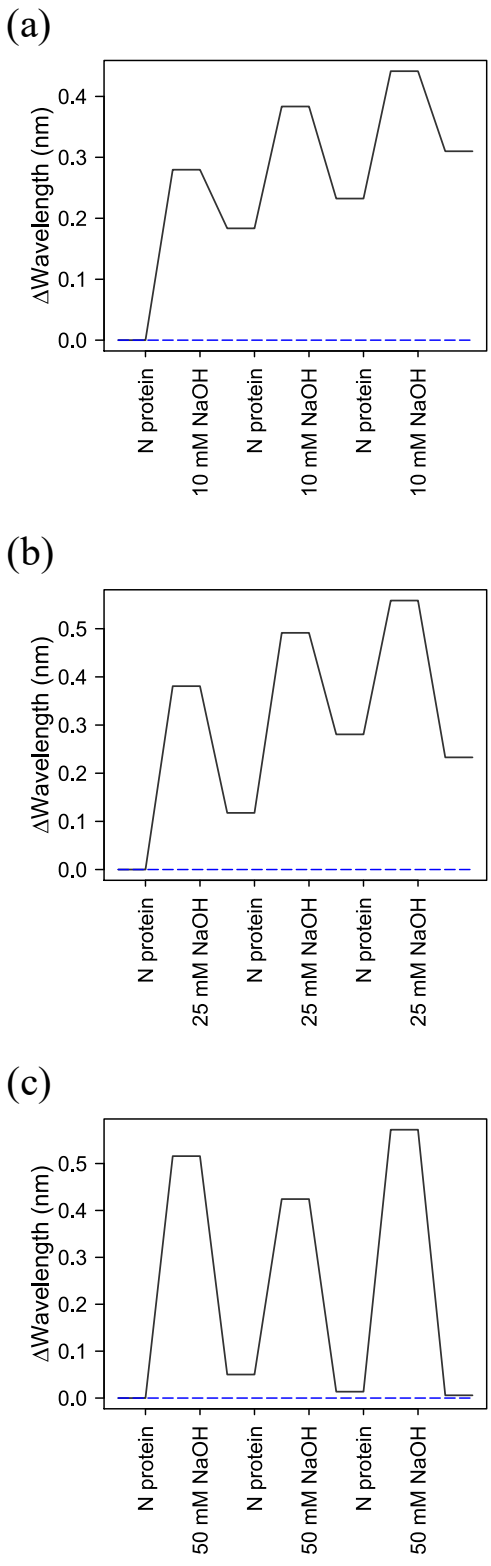

Figure 5-5 Line plots of wavelength shifts during the regeneration experiment with the regenerating solution of 10 mM **(a)**, 25 mM **(b)**, and 50 mM **(c)** NaOH. Blue dash line represents the baseline. The wavelength shift was recorded after PBS rinse.

5.3.2. Results of N Protein Detection

The numerical data of N protein detections in different approaches are displayed in **Table 5-2**, **Table 5-3**, and **Table 5-4**.

Table 5-2 Results of N protein detection using sensing probes made with epoxy glue, with no regenerations between sample injections.

Probe 1

Concentration (mg/mL)	Wavelength shift (nm)
9.10E-12	0.000
9.10E-11	0.024
9.10E-10	-0.058
9.10E-09	-0.045
9.10E-08	-0.052
9.10E-07	-0.079
9.10E-06	-0.116
9.10E-05	-0.104
9.10E-04	-0.032
9.10E-03	0.779
1.10E-02	1.286

Probe 2

Concentration (mg/mL)	Wavelength shift (nm)
9.10E-08	0.000
9.10E-07	0.015
9.10E-06	-0.013
4.55E-05	-0.006
9.10E-05	-0.053
4.55E-04	-0.018
9.10E-04	0.085
4.55E-03	0.337
6.07E-03	0.556
9.10E-03	0.776

Probe 3

Concentration (mg/mL)	Wavelength shift (nm)
9.10E-08	0.000
9.10E-07	-0.063
9.10E-06	-0.048
4.55E-05	-0.049
9.10E-05	-0.165
4.55E-04	-0.003
9.10E-04	0.048
4.55E-03	0.315
6.07E-03	0.581
9.10E-03	0.808

Table 5-3 Results of N protein detections using sensing probes made with epoxy glue. The probes were regenerated before each sample injection.

Probe 1

Concentration (mg/mL)	Wavelength shift (nm)
9.0E-12	0.032
9.0E-11	0.030
9.0E-10	0.044
9.0E-09	-0.004
9.0E-08	0.025
9.0E-07	-0.020
9.0E-06	0.046
9.0E-05	0.049
9.0E-04	0.018
9.0E-03	0.662
1.1E-02	0.607

Probe 2

Concentration (mg/mL)	Wavelength shift (nm)
9.0E-12	-0.038
9.0E-11	0.006
9.0E-10	-0.004
9.0E-09	0.008
9.0E-08	-0.020
9.0E-07	0.006
9.0E-06	-0.015
9.0E-05	0.004
9.0E-04	0.135
9.0E-03	0.479
1.1E-02	0.424

Probe 3

Concentration (mg/mL)	Wavelength shift (nm)
9.0E-12	0.113
9.0E-11	0.089
9.0E-10	0.092
9.0E-09	0.084
9.0E-08	0.003
9.0E-07	0.117
9.0E-06	0.103
9.0E-05	0.085
9.0E-04	0.159
9.0E-03	0.771
1.1E-02	0.727

Table 5-4 Results of N protein detections using epoxy-free sensing probes.

Probe 1

Concentration (mg/mL)	Wavelength shift (nm)
9.1E-12	0.000
9.1E-11	-0.103
9.1E-10	-0.063
9.1E-09	0.100
9.1E-08	0.025
9.1E-07	0.101
9.1E-06	0.114
9.1E-05	0.344
9.1E-04	0.375
9.1E-03	0.906
1.1E-02	1.229

Probe 2

Concentration (mg/mL)	Wavelength shift (nm)
9.0E-12	0.000
9.0E-11	0.259
9.0E-10	0.326
9.0E-09	0.537
9.0E-08	0.629
9.0E-07	0.693
9.0E-06	0.797
9.0E-05	0.810
9.0E-04	0.866
9.0E-03	1.402
1.1E-02	1.714

Probe 3

Concentration (mg/mL)	Wavelength shift (nm)
9.0E-12	0.000
9.0E-11	0.070
9.0E-10	-0.018
9.0E-09	-0.021
9.0E-08	0.035
9.0E-07	0.024
9.0E-06	0.001
9.0E-05	0.003
9.0E-04	0.004
9.0E-03	0.440
1.1E-02	0.472

5.3.3. Epoxy-free Sensing Surface

Figure 5-6 shows the sensing probe fabricated without epoxy. Without the support of a rigid adhesive layer, the gold film is not lying flat and has some wrinkles. The zoom-in inset shows a wrinkle at the optical fibre's core, which migh interfere with its sensing performance.

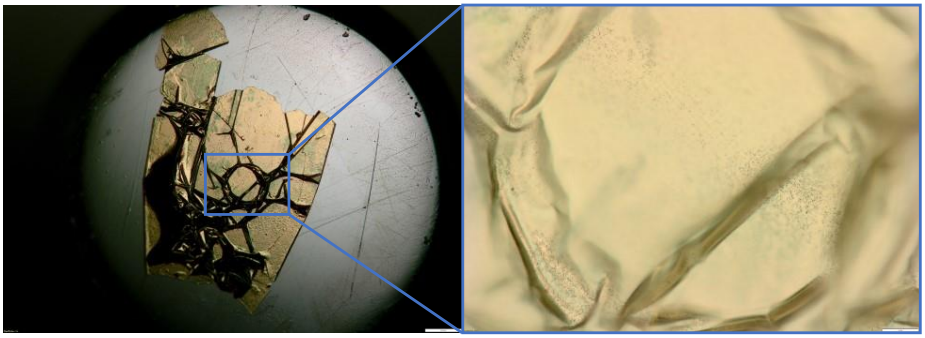

Figure 5-6 Sensing surface with gold film chemically bound to the optical fibre; the inset showns the gold film at the core of optical fibre.

6. Chapter 6

CONCLUSIONS AND FUTURE DEVELOPMENT

6.1. Conclusions

This research aims to improve the design of fibre-optic SPR-EOT biosensors, achieve a reliable biosensing platform, and demonstrate the biosensing potential for analytical and diagnostic applications. The design of the biosensor has been optimised for the detection of different biomolecules and the biosensing performance improved via different approaches.

The key conclusions of this thesis are:

1. The biosensing probes can achieve consistent sensitivity from batch-to-batch fabrication processes by implementing a standard template cleaning protocol with full control during the fabrication process.

2. The flow cell design in this thesis allows a stable sensing operation, minimises the presence of air bubbles in the flow cell, and lowers the cost. The 3D-printed chamber of the flow cell has a precisely controlled dimension and the potential for mass production.

3. The use of $SM(PEG)_2$ as a spacer arm for protein A immobilisation does not enhance the biosensor sensitivity for monoclonal antibody detection compared with the zero-length crosslinker. When detecting monoclonal antibodies at 0.01 mg/mL, the redshift was 0.333 nm and 0.375 nm for the sensing probe with and without spacer arm, respectively.

4. Immobilised Protein A can be regenerated ten times with 0.1 M glycine hydrochloride (pH=2.8) and the sensing surface remains stable after refrigeration storage for seven days at 4°C.

5. The protein A-based fibre-optic SPR-EOT biosensor can detect the monoclonal antibody (murine IgG2a) with a LOD of 0.44 µg/mL within 15 minutes.

6. Functionalisation of the sensing surface using 3-MPA can be conducted in an aqueous solution instead of an ethanolic solution.

7. The fibre-optic SPR-EOT biosensor can detect toxin B in the PBS buffer range from 4.8 pg/mL to 1.35 µg/mL.

8. The fibre-optic SPR-EOT biosensor can detect the N protein in PBS buffer with a consistent LOD of 1.77 µg/mL within 15 minutes. The anti-N protein antibodies cannot withstand more than nine regenerations using 50 mM NaOH.

9. The presence of an adhesive epoxy layer might reduce the sensing sensitivity due to the binding of bioreceptors and analytes to the residual epoxide rings. The LOD for N protein detection could be lowered to 0.046 pg/mL when the sensing probe is fabricated without the epoxy glue.

My experimental results have supported the potential of the fibre-optic SPR-EOT biosensor as a highly sensitive biosensing device for analytical and diagnostic applications. The biosensor can detect different biomolecules at low concentrations in a label-free and real-time manner. The findings from this study can contribute to the development of a commercial fibre-optic SPR-EOT biosensor in the future.

6.2 Recommendations for future studies

The results have demonstrated the feasibility of using a fibre-optic SPR-EOT biosensor as a label-free, real-time, and sensitive biosensing device. The fabrication materials, procedure, and detecting analytes have a considerable impact on the biosensing sensitivity.

Since a stable fibre-optic SPR-EOT biosensing platform has been accomplished, the next phase of the biosensor development is to enhance the sensitivity, improve throughput, and obtain clinical evidential results. The sensitivity of fibre-optic SPR-EOT biosensors could be improved by hybridising with a micromachined Fabry-Perot interferometer reported by Tu et al. (2019), adjusting the incident angle using a bevelled fibre (Couture et al., 2016, Zhao et al., 2017), or fabricating free-standing gold nanohole arrays (Polley et al., 2019). Additionally, the sensing performance can be improved by using a better immobilisation strategy. The experimental results obtained from various biosensing projects have proved that immobilisation of the bioreceptors has a significant impact on sensing performance. The combination of polyelectrolyte adsorption and oriented immobilisation could ensure enhanced sensitivity and detection limit. Moreover, elimination of the epoxy layer or replacing it with an optically compatible and inert material could improve the sensitivity needed and reduce interference during the biosensing process.

The detecion throughput could be improved by designing flow cells that could be connected in a series or parallel to build multiplex or multichannel biosensors. A low throughput is the most significant disadvantage of fibre-optic SPR-EOT biosensors comparing with other EOT biosensors. However, optimisation of the biosensor throughput should not compromise the simplicity of the fibre-optic SPR-EOT biosensor.

Clinical evidence is the most critical determinant to rationalise the commercialisation of the biosensors. Clinical studies on the use of the biosensor for samples from patients will be carried out and a standard reference diagnostic method will be used for statistical analysis.

7. References

Abbas, A., Linman, M. J. & Cheng, Q. 2011. Sensitivity Comparison of Surface Plasmon Resonance and Plasmon-Waveguide Resonance Biosensors. *Sensors and actuators. B, Chemical,* 156**,** 169-175.

Afsheen, S., Iqbal, T., Aftab, M., Bashir, A., Tehseen, A., Khan, M. Y. & Ijaz, M. 2019. Modeling of 1d Au Plasmonic Grating as Efficient Gas Sensor. *Materials Research Express,* 6**,** 126203.

Aliberti, A., Ricciardi, A., Giaquinto, M., Micco, A., Bobeico, E., La Ferrara, V., Ruvo, M., Cutolo, A. & Cusano, A. 2017. Microgel Assisted Lab-on-Fiber Optrode. *Scientific Reports,* 7**,** 14459.

Anderson, G. P., Liu, J. L., Esparza, T. J., Voelker, B. T., Hofmann, E. R. & Goldman, E. R. 2021. Single-Domain Antibodies for the Detection of Sars-Cov-2 Nucleocapsid Protein. *Analytical chemistry,* 93**,** 7283-7291.

Andrade, J., Machado, R., Macêdo, M. & Cunha, F. 2013. Afm and Xrd Characterization of Silver Nanoparticles Films Deposited on the Surface of Dgeba Epoxy Resin by Ion Sputtering. *Polímeros, Ciência e Tecnologia,* 23**,** 19-23.

Arghir, I., Spasic, D., Verlinden, B. E., Delport, F. & Lammertyn, J. 2015. Improved Surface Plasmon Resonance Biosensing Using Silanized Optical Fibers. *Sensors and Actuators B: Chemical,* 216**,** 518-526.

Australian Commission on Safety and Quality in Health Care 2018. Clostridium Difficile Infection Monitoring the National Burden of Clostridium Difficile. Australian Commission on Safety and Quality in Health Care.

Baburin, A. S., Gritchenko, A. S., Orlikovsky, N. A., Dobronosova, A. A., Rodionov, I. A., Balykin, V. I. & Melentiev, P. N. 2019. State-of-the-Art Plasmonic Crystals for Molecules Fluorescence Detection. *Optical materials express,* 9**,** 1173-1179.

Bagra, B., Mabe, T., Tukur, F. & Wei, J. 2020. A Plasmonic Nanoledge Array Sensor for Detection of Anti-Insulin Antibodies of Type 1 Diabetes Biomarker. *Nanotechnology,* 31**,** 325503-325503.

Balsells, E., Shi, T., Leese, C., Lyell, I., Burrows, J., Wiuff, C., Campbell, H., Kyaw, M. H. & Nair, H. 2019. Global Burden of Clostridium Difficile Infections: A Systematic Review and Meta-Analysis. *Journal of global health,* 9**,** 010407-010407.

Banz, A., Lantz, A., Riou, B., Foussadier, A., Miller, M., Davies, K., Wilcox, M. & Carroll, K. C. 2018. Sensitivity of Single-Molecule Array Assays for Detection of Clostridium

Difficile Toxins in Comparison to Conventional Laboratory Testing Algorithms. *Journal of Clinical Microbiology,* 56**,** e00452-18.

Bdour, Y., Gomez-Cruz, J. & Escobedo, C. 2020. Structural Stability of Optofluidic Nanostructures in Flow-through Operation. *Micromachines (Basel),* 11**,** 373.

Belushkin, A., Yesilkoy, F., González-López, J. J., Ruiz-Rodríguez, J. C., Ferrer, R., Fàbrega, A. & Altug, H. 2020. Rapid and Digital Detection of Inflammatory Biomarkers Enabled by a Novel Portable Nanoplasmonic Imager. *Small (Weinheim an der Bergstrasse, Germany),* 16**,** e1906108-n/a.

Bhalla, N., Jolly, P., Formisano, N. & Estrela, P. 2016. Introduction to Biosensors. *Essays in Biochemistry,* 60**,** 1-8.

Bhalla, N., Pan, Y., Yang, Z. & Payam, A. F. 2020. Opportunities and Challenges for Biosensors and Nanoscale Analytical Tools for Pandemics: Covid-19. *ACS Nano,* 14**,** 7783-7807.

Bhardwaj, N., Bhardwaj, S. K., Nayak, M. K., Mehta, J., Kim, K.-H. & Deep, A. 2017. Fluorescent Nanobiosensors for the Targeted Detection of Foodborne Bacteria. *Trends in Analytical Chemistry,* 97**,** 120-135.

Blanchard-Dionne, A.-P. & Meunier, M. 2019. Multiperiodic Nanohole Array for High Precision Sensing. *Nanophotonics,* 8**,** 325-329.

Bollam, R., Desai, N. & Archbald-Pannone, L. 2020. Clostridium Difficile Diagnostics in Long-Term Care Facilities. *In:* CHOPRA, T. (ed.) *Clostridium Difficile Infection in Long-Term Care Facilities: A Clinician's Guide.* Cham: Springer International Publishing.

Briscoe, J. L., Cho, S. Y. & Brener, I. 2015. Part-Per-Trillion Level Detection of Microcystin-Lr Using a Periodic Nanostructure. *IEEE Sensors Journal,* 15**,** 1366-1371.

Carter, L. J., Garner, L. V., Smoot, J. W., Li, Y., Zhou, Q., Saveson, C. J., Sasso, J. M., Gregg, A. C., Soares, D. J., Beskid, T. R., Jervey, S. R. & Liu, C. 2020. Assay Techniques and Test Development for Covid-19 Diagnosis. *ACS Central Science,* 6**,** 591-605.

Cetin, A. E., Etezadi, D., Galarreta, B. C., Busson, M. P., Eksioglu, Y. & Altug, H. 2015. Plasmonic Nanohole Arrays on a Robust Hybrid Substrate for Highly Sensitive Label-Free Biosensing. *ACS Photonics,* 2**,** 1167-1174.

Che, X.-Y., Hao, W., Wang, Y., Di, B., Yin, K., Xu, Y.-C., Feng, C.-S., Wan, Z.-Y., Cheng, V. C. C. & Yuen, K.-Y. 2004. Nucleocapsid Protein as Early Diagnostic Marker for Sars. *Emerging infectious diseases,* 10**,** 1947-1949.

Chen, C. & Wang, J. 2020. Optical Biosensors: An Exhaustive and Comprehensive Review. *Analyst,* 145**,** 1605-1628.

Chen, P., Chung, M. T., McHugh, W., Nidetz, R., Li, Y., Fu, J., Cornell, T. T., Shanley, T. P. & Kurabayashi, K. 2015. Multiplex Serum Cytokine Immunoassay Using Nanoplasmonic Biosensor Microarrays. *ACS Nano,* 9**,** 4173-4181.

Chen, Y.-T., Lee, Y.-C., Lai, Y.-H., Lim, J.-C., Huang, N.-T., Lin, C.-T. & Huang, J.-J. 2020. Review of Integrated Optical Biosensors for Point-of-Care Applications. *Biosensors,* 10**,** 209.

Couture, M., Live, L. S., Dhawan, A. & Masson, J.-F. 2012. Eot or Kretschmann Configuration? Comparative Study of the Plasmonic Modes in Gold Nanohole Arrays. *Analyst,* 137**,** 4162-4170.

Couture, M., Ray, K. K., Poirier-Richard, H.-P., Crofton, A. & Masson, J.-F. 2016. 96-Well Plasmonic Sensing with Nanohole Arrays. *ACS Sensors,* 1**,** 287-294.

Couture, M., Zhao, S. S. & Masson, J.-F. 2013. Modern Surface Plasmon Resonance for Bioanalytics and Biophysics. *Physical Chemistry Chemical Physics,* 15**,** 11190-11216.

Cui, A., Liu, Z., Li, J., Shen, T. H., Xia, X., Li, Z., Gong, Z., Li, H., Wang, B., Li, J., Yang, H., Li, W. & Gu, C. 2015. Directly Patterned Substrate-Free Plasmonic "Nanograter" Structures with Unusual Fano Resonances. *Light: Science & Applications,* 4**,** e308-e308.

Cytiva Life Sciences. 2020. *Amine Coupling Kit, Type 2: Instructions for Use* [Online]. Available: https://www.cytivalifesciences.com/en/us/shop/protein-analysis/spr-label-free-analysis/spr-consumables/immobilization-reagents/amine-coupling-kit-type-2-p-06087 [Accessed 2021].

Dahlin, A. B., Mapar, M., Xiong, K., Mazzotta, F., Höök, F. & Sannomiya, T. 2014. Plasmonic Nanopores in Metal-Insulator-Metal Films. *Advanced Optical Materials,* 2**,** 556-564.

Damborský, P., Švitel, J. & Katrlík, J. 2016. Optical Biosensors. *Essays in Biochemistry,* 60**,** 91-100.

Daniel, S. & Bawuah, P. 2019. Plasmonic Implanted Nanogrooves for Optical Beaming. *Scientific reports,* 9**,** 391-391.

Davies, K. A., Longshaw, C. M., Davis, G. L., Bouza, E., Barbut, F., Barna, Z., Delmée, M., Fitzpatrick, F., Ivanova, K., Kuijper, E., Macovei, I. S., Mentula, S., Mastrantonio, P., von Müller, L., Oleastro, M., Petinaki, E., Pituch, H., Norén, T., Nováková, E., Nyč, O., Rupnik, M., Schmid, D. & Wilcox, M. H. 2014. Underdiagnosis of Clostridium Difficile across Europe: The European, Multicentre, Prospective, Biannual, Point-Prevalence Study of Clostridium Difficile Infection in Hospitalised Patients with Diarrhoea (Euclid). *Lancet Infect Dis,* 14**,** 1208-19.

Dhawan, A. & Muth, J. F. 2008. Engineering Surface Plasmon Based Fiber-Optic Sensors. *Materials Science and Engineering: B,* 149**,** 237-241.

Diao, B., Wen, K., Zhang, J., Chen, J., Han, C., Chen, Y., Wang, S., Deng, G., Zhou, H. & Wu, Y. 2021. Accuracy of a Nucleocapsid Protein Antigen Rapid Test in the Diagnosis of Sars-Cov-2 Infection. *Clinical microbiology and infection : the official publication of the European Society of Clinical Microbiology and Infectious Diseases,* 27**,** 289.e1-289.e4.

Ding, T., Hong, M., Richards, A. M., Wong, T. I., Zhou, X. & Drum, C. L. 2015. Quantification of a Cardiac Biomarker in Human Serum Using Extraordinary Optical Transmission (Eot). *PLOS ONE,* 10**,** e0120974.

Dore, C., Dörling, B., Garcia-Pomar, J. L., Campoy-Quiles, M. & Mihi, A. 2020. Hydroxypropyl Cellulose Adhesives for Transfer Printing of Carbon Nanotubes and Metallic Nanostructures. *Small (Weinheim an der Bergstrasse, Germany),* 16**,** e2004795-n/a.

Du, B., Ruan, Y., Ly, T.-T., Jia, P., Sun, Q., Feng, Q., Yang, D. & Ebendorff-Heidepriem, H. 2020a. Mos2-Enhanced Epoxy-Based Plasmonic Fiber-Optic Sensor for Selective and Sensitive Detection of Methanol. *Sensors and Actuators B: Chemical,* 305**,** 127513.

Du, B., Ruan, Y., Yang, D., Jia, P., Gao, S., Wang, Y., Wang, P. & Ebendorff-Heidepriem, H. 2020b. Freestanding Metal Nanohole Array for High-Performance Applications. *Photonics Research,* 8**,** 1749-1756.

Du, B., Yang, D., Ruan, Y., Jia, P. & Ebendorff-Heidepriem, H. 2020c. Compact Plasmonic Fiber Tip for Sensitive and Fast Humidity and Human Breath Monitoring. *Optics Letters,* 45**,** 985-988.

Du, B., Yang, Y., Zhang, Y., Jia, P., Ebendorff-Heidepriem, H., Ruan, Y. & Yang, D. 2019. Enhancement of Extraordinary Optical Transmission and Sensing Performance through Coupling between Metal Nanohole and Nanoparticle Arrays. *Journal of Physics D: Applied Physics,* 52**,** 275201.

Ebbesen, T. W., Lezec, H. J., Ghaemi, H. F., Thio, T. & Wolff, P. A. 1998. Extraordinary Optical Transmission through Sub-Wavelength Hole Arrays. *Nature,* 391**,** 667.

Escobedo, C., Brolo, A. G., Gordon, R. & Sinton, D. 2012. Optofluidic Concentration: Plasmonic Nanostructure as Concentrator and Sensor. *Nano Letters,* 12**,** 1592-1596.

Escobedo, C., Vincent, S., I K Choudhury, A., Campbell, J., Brolo, A., Sinton, D. & Gordon, R. 2011. Integrated Nanohole Array Surface Plasmon Resonance Sensing Device Using a Dual-Wavelength Source. *Journal of Micromechanics and Microengineering,* 21**,** 115001.

Esmonde-White, K. A., Cuellar, M., Uerpmann, C., Lenain, B. & Lewis, I. R. 2017. Raman Spectroscopy as a Process Analytical Technology for Pharmaceutical Manufacturing and Bioprocessing. *Analytical and Bioanalytical Chemistry,* 409**,** 637-649.

Falkowski, P., Lukaszewski, Z. & Gorodkiewicz, E. 2021. Potential of Surface Plasmon Resonance Biosensors in Cancer Detection. *J Pharm Biomed Anal,* 194**,** 113802.

Farcau, C. 2019. Metal-Coated Microsphere Monolayers as Surface Plasmon Resonance Sensors Operating in Both Transmission and Reflection Modes. *Scientific reports,* 9**,** 3683-3683.

Ferreira, J., Santos, M. J. L., Rahman, M. M., Brolo, A. G., Gordon, R., Sinton, D. & Girotto, E. M. 2009. Attomolar Protein Detection Using in-Hole Surface Plasmon Resonance. *Journal of the American Chemical Society,* 131**,** 436-437.

Fischer, M. J. E. 2010. Amine Coupling through Edc/Nhs: A Practical Approach. *In:* MOL, N. J. & FISCHER, M. J. E. (eds.) *Surface Plasmon Resonance: Methods and Protocols.* Totowa, NJ: Humana Press.

Fronczek, C. F. & Yoon, J.-Y. 2016. Chapter 12 - Detection of Foodborne Pathogens Using Biosensors A2 - Barros-Velázquez, Jorge. *Antimicrobial Food Packaging.* San Diego: Academic Press.

GE Healthcare 2016. Affinity Chromatography - Vol. 1 Antibodies. *Affinity Chromatography handbooks.* GE Healthcare Bio-Sciences AB.

Gite, S., Archambault, D., Cappillino, M. P., Cunha, D., Dorich, V., Shatova, T., Tempesta, A., Walsh, B., Walsh, J. A., Williams, A., Kirby, J. E., Bowers, J. & Straus, D. 2018. A Rapid, Accurate, Single Molecule Counting Method Detects Clostridium Difficile Toxin B in Stool Samples. *Scientific Reports,* 8**,** 8364.

Gody, J., Khouri, J., Durve, A., Zimmermann, E. & Furuya, K. 2019. Control of Protein a Column Loading During Continuous Antibody Production: A Technology Overview of Real-Time Titer Measurement Methods. *BioProcess International,* 17.

Grazu, V., López-Gallego, F. & Guisán, J. M. 2012. Tailor-Made Design of Penicillin G Acylase Surface Enables Its Site-Directed Immobilization and Stabilization onto Commercial Mono-Functional Epoxy Supports. *Process Biochemistry,* 47**,** 2538-2541.

Guh, A. Y., Mu, Y., Winston, L. G., Johnston, H., Olson, D., Farley, M. M., Wilson, L. E., Holzbauer, S. M., Phipps, E. C., Dumyati, G. K., Beldavs, Z. G., Kainer, M. A., Karlsson, M., Gerding, D. N., McDonald, L. C. & Emerging Infections Program Clostridioides difficile Infection Working, G. 2020. Trends in U.S. Burden of Clostridioides Difficile Infection and Outcomes. *The New England journal of medicine,* 382**,** 1320-1330.

Hackett, L. P., Ameen, A., Li, W., Dar, F. K., Goddard, L. L. & Liu, G. L. 2018. Spectrometer-Free Plasmonic Biosensing with Metal–Insulator–Metal Nanocup Arrays. *ACS Sensors,* 3**,** 290-298.

Hansen, G., Young, S., Wu, A. H. B., Herding, E., Nordberg, V., Mills, R., Griego-Fullbright, C., Wagner, A., Ong, C. M., Lewis, S., Yoon, J., Estis, J., Sandlund, J., Friedland, E. & Carroll, K. C. 2019. Ultrasensitive Detection of Clostridioides Difficile Toxins in Stool by Use of Single-Molecule Counting Technology: Comparison with Detection of Free Toxin by Cell Culture Cytotoxicity Neutralization Assay. *Journal of clinical microbiology,* 57**,** e00719-19.

Hegner, M., Wagner, P. & Semenza, G. 1993. Ultralarge Atomically Flat Template-Stripped Au Surfaces for Scanning Probe Microscopy. *Surface Science,* 291**,** 39-46.

Hodge, C. D., Rosenberg, D. J., Grob, P., Wilamowski, M., Joachimiak, A., Hura, G. L. & Hammel, M. 2021. Rigid Monoclonal Antibodies Improve Detection of Sars-Cov-2 Nucleocapsid Protein. *mAbs,* 13**,** 1905978-1905978.

Huang, J. C., Chang, Y.-F., Chen, K.-H., Su, L.-C., Lee, C.-W., Chen, C.-C., Chen, Y.-M. A. & Chou, C. 2009. Detection of Severe Acute Respiratory Syndrome (Sars) Coronavirus Nucleocapsid Protein in Human Serum Using a Localized Surface Plasmon Coupled Fluorescence Fiber-Optic Biosensor. *Biosensors and Bioelectronics,* 25**,** 320-325.

Ihling, C., Tänzler, D., Hagemann, S., Kehlen, A., Hüttelmaier, S., Arlt, C. & Sinz, A. 2020. Mass Spectrometric Identification of Sars-Cov-2 Proteins from Gargle Solution Samples of Covid-19 Patients. *Journal of Proteome Research,* 19**,** 4389-4392.

Im, H., Lee, S. H., Wittenberg, N. J., Johnson, T. W., Lindquist, N. C., Nagpal, P., Norris, D. J. & Oh, S.-H. 2011. Template-Stripped Smooth Ag Nanohole Arrays with Silica Shells for Surface Plasmon Resonance Biosensing. *ACS Nano,* 5**,** 6244-6253.

Im, H., Lesuffleur, A., Lindquist, N. C. & Oh, S.-H. 2009. Plasmonic Nanoholes in a Multi-Channel Microarray Format for Parallel Kinetic Assays and Differential Sensing. *Analytical chemistry,* 81**,** 2854-2859.

Im, H., Lindquist, N. C., Lesuffleur, A. & Oh, S.-H. 2010. Atomic Layer Deposition of Dielectric Overlayers for Enhancing the Optical Properties and Chemical Stability of Plasmonic Nanoholes. *ACS Nano,* 4**,** 947-954.

Im, H., Sutherland, J. N., Maynard, J. A. & Oh, S.-H. 2012. Nanohole-Based Spr Instruments with Improved Spectral Resolution Quantify a Broad Range of Antibody-Ligand Binding Kinetics. *Analytical Chemistry,* 84**,** 1941-1947.

Jackman, J. A., Linardy, E., Yoo, D., Seo, J., Ng, W. B., Klemme, D. J., Wittenberg, N. J., Oh, S.-H. & Cho, N.-J. 2016. Plasmonic Nanohole Sensor for Capturing Single Virus-Like Particles toward Virucidal Drug Evaluation. *Small,* 12**,** 1159-1166.

Jackman, J. A., Rahim Ferhan, A. & Cho, N.-J. 2017. Nanoplasmonic Sensors for Biointerfacial Science. *Chemical Society Reviews,* 46**,** 3615-3660.

Jenzsch, M., Bell, C., Buziol, S., Kepert, F., Wegele, H. & Hakemeyer, C. 2018. Trends in Process Analytical Technology: Present State in Bioprocessing. *Adv Biochem Eng Biotechnol,* 165**,** 211-252.

Jeong, H.-H., Erdene, N., Park, J.-H., Jeong, D.-H., Lee, H.-Y. & Lee, S.-K. 2013. Real-Time Label-Free Immunoassay of Interferon-Gamma and Prostate-Specific Antigen Using a Fiber-Optic Localized Surface Plasmon Resonance Sensor. *Biosensors and Bioelectronics,* 39**,** 346-351.

Ji, T., Liu, Z., Wang, G., Guo, X., Akbar Khan, S., Lai, C., Chen, H., Huang, S., Xia, S., Chen, B., Jia, H., Chen, Y. & Zhou, Q. 2020. Detection of Covid-19: A Review of the Current Literature and Future Perspectives. *Biosensors & bioelectronics,* 166**,** 112455-112455.

Jia, P., Jiang, H., Sabarinathan & Yang, J. 2013. Plasmonic Nanohole Array Sensors Fabricated by Template Transfer with Improved Optical Performance. *Nanotechnology,* 24**,** 195501.

Jia, P. & Yang, J. 2013. Integration of Large-Area Metallic Nanohole Arrays with Multimode Optical Fibers for Surface Plasmon Resonance Sensing. *Applied Physics Letters,* 102**,** 243107.

Jia, P. & Yang, J. 2014. A Plasmonic Optical Fiber Patterned by Template Transfer as a High-Performance Flexible Nanoprobe for Real-Time Biosensing. *Nanoscale,* 6.

Jia, P., Yang, Z., Yang, J. & Ebendorff-Heidepriem, H. 2016. Quasiperiodic Nanohole Arrays on Optical Fibers as Plasmonic Sensors: Fabrication and Sensitivity Determination. *ACS Sensors,* 1**,** 1078-1083.

Junesch, J., Emilsson, G., Xiong, K., Kumar, S., Sannomiya, T., Pace, H., Voros, J., Oh, S.-H., Bally, M. & Dahlin, A. B. 2015. Location-Specific Nanoplasmonic Sensing of Biomolecular Binding to Lipid Membranes with Negative Curvature. *Nanoscale,* 7**,** 15080-15085.

Kabir, M. D. A., Ahmed, R., Iqbal, S. M. A., Chowdhury, R., Paulmurugan, R., Demirci, U. & Asghar, W. 2021. Diagnosis for Covid-19: Current Status and Future Prospects. *Expert Review of Molecular Diagnostics***,** 1-20.

Kadhim, R. A., Abdul, A. K. K. & Yuan, L. 2020. Advances in Surface Plasmon Resonance-Based Plastic Optical Fiber Sensors. *IETE Technical Review***,** 1-18.

Kasani, S., Curtin, K. & Wu, N. 2019. A Review of 2d and 3d Plasmonic Nanostructure Array Patterns: Fabrication, Light Management and Sensing Applications. *Nanophotonics,* 8**,** 2065-2089.

Kee, J. S., Lim, S. Y., Perera, A. P., Zhang, Y. & Park, M. K. 2013. Plasmonic Nanohole Arrays for Monitoring Growth of Bacteria and Antibiotic Susceptibility Test. *Sensors and Actuators B: Chemical,* 182**,** 576-583.

Kilic, T., Soler, M., Fahimi-Kashani, N., Altug, H. & Carrara, S. 2018. Mining the Potential of Label-Free Biosensors for in Vitro Antipsychotic Drug Screening. *Biosensors (Basel),* 8**,** 6.

Kim, H.-M., Park, J.-H. & Lee, S.-K. 2019. Fiber Optic Sensor Based on Zno Nanowires Decorated by Au Nanoparticles for Improved Plasmonic Biosensor. *Scientific Reports,* 9**,** 15605.

Krishna, A. & Chopra, T. 2020. Introduction. *In:* CHOPRA, T. (ed.) *Clostridium Difficile Infection in Long-Term Care Facilities: A Clinician's Guide.* Cham: Springer International Publishing.

Lan, X., Cheng, B., Yang, Q., Huang, J., Wang, H., Ma, Y., Shi, H. & Xiao, H. 2014. Reflection Based Extraordinary Optical Transmission Fiber Optic Probe for Refractive Index Sensing. *Sensors and Actuators B: Chemical,* 193**,** 95-99.

Land, K. J., Boeras, D. I., Chen, X.-S., Ramsay, A. R. & Peeling, R. W. 2019. Reassured Diagnostics to Inform Disease Control Strategies, Strengthen Health Systems and Improve Patient Outcomes. *Nature Microbiology,* 4**,** 46-54.

Lau, S. K. P., Woo, P. C. Y., Wong, B. H. L., Tsoi, H.-W., Woo, G. K. S., Poon, R. W. S., Chan, K.-H., Wei, W. I., Peiris, J. S. M. & Yuen, K.-Y. 2004. Detection of Severe Acute Respiratory Syndrome (Sars) Coronavirus Nucleocapsid Protein in Sars Patients by Enzyme-Linked Immunosorbent Assay. *Journal of Clinical Microbiology,* 42**,** 2884-2889.

Lee, B., Park, J.-H., Byun, J.-Y., Kim, J. H. & Kim, M.-G. 2018a. An Optical Fiber-Based Lspr Aptasensor for Simple and Rapid in-Situ Detection of Ochratoxin A. *Biosensors and Bioelectronics,* 102**,** 504-509.

Lee, J., Yang, S., Lee, J., Choi, J.-H., Lee, Y.-H., Shin, J. H. & Seo, M.-K. 2020. Extraordinary Optical Transmission and Second Harmonic Generation in Sub–10-Nm Plasmonic Coaxial Aperture. *Nanophotonics,* 9**,** 3295-3302.

Lee, S., Song, H., Ahn, H., Kim, S., Choi, J.-r. & Kim, K. 2021. Fiber-Optic Localized Surface Plasmon Resonance Sensors Based on Nanomaterials. *Sensors,* 21**,** 819.

Lee, S. H., Lindquist, N. C., Wittenberg, N. J., Jordan, L. R. & Oh, S.-H. 2012. Real-Time Full-Spectral Imaging and Affinity Measurements from 50 Microfluidic Channels Using Nanohole Surface Plasmon Resonance. *Lab on a chip,* 12**,** 3882-3890.

Lee, Y., Song, H., Ahn, H., Choi, J.-r. & Kim, K. 2018b. Rapid and Real-Time Diagnosis of Hypoalbuminemia Using an Extraordinary Optical Transmission Biosensor. *Sensors and Actuators B: Chemical,* 274**,** 595-600.

Lei, C., Man, Z. & Tang, S. 2020. Extraordinary Optical Transmission and Enhanced Magneto-Optical Faraday Effect in the Cascaded Double-Fishnet Structure with Periodic Rectangular Apertures. *Current Optics and Photonics,* 4**,** 134-140.

Leonard, P., Hearty, S., Brennan, J., Dunne, L., Quinn, J., Chakraborty, T. & O'Kennedy, R. 2003. Advances in Biosensors for Detection of Pathogens in Food and Water. *Enzyme and Microbial Technology,* 32**,** 3-13.

Lertvachirapaiboon, C., Pothipor, C., Baba, A., Shinbo, K. & Kato, K. 2018. Transmission Surface Plasmon Resonance Image Detection by a Smartphone Camera. *MRS communications,* 8**,** 1279-1284.

Li, M., Jin, R., Peng, Y., Wang, C., Ren, W., Lv, F., Gong, S., Fang, F., Wang, Q., Li, J., Shen, T., Sun, H., Zhou, L., Cui, Y., Song, H. & Sun, L. 2020a. Generation of

Antibodies against Covid-19 Virus for Development of Diagnostic Tools. *medRxiv***,** 2020.02.20.20025999.

Li, W., Zhang, L., Zhou, J. & Wu, H. 2015. Well-Designed Metal Nanostructured Arrays for Label-Free Plasmonic Biosensing. *Journal of Materials Chemistry C,* 3**,** 6479-6492.

Li, X., Soler, M., Szydzik, C., Khoshmanesh, K., Schmidt, J., Coukos, G., Mitchell, A. & Altug, H. 2018. Label-Free Optofluidic Nanobiosensor Enables Real-Time Analysis of Single-Cell Cytokine Secretion. *Small (Weinheim an der Bergstrasse, Germany),* 14**,** e1800698-n/a.

Li, Y.-H., Li, J., Liu, X.-E., Wang, L., Li, T., Zhou, Y.-H. & Zhuang, H. 2005. Detection of the Nucleocapsid Protein of Severe Acute Respiratory Syndrome Coronavirus in Serum: Comparison with Results of Other Viral Markers. *Journal of virological methods,* 130**,** 45-50.

Li, Z., Yi, Y., Luo, X., Xiong, N., Liu, Y., Li, S., Sun, R., Wang, Y., Hu, B., Chen, W., Zhang, Y., Wang, J., Huang, B., Lin, Y., Yang, J., Cai, W., Wang, X., Cheng, J., Chen, Z., Sun, K., Pan, W., Zhan, Z., Chen, L. & Ye, F. 2020b. Development and Clinical Application of a Rapid Igm-Igg Combined Antibody Test for Sars-Cov-2 Infection Diagnosis. *Journal of medical virology,* 92**,** 1518-1524.

Liang, Y., Ruan, N., Zhang, S., Yu, Z. & Xu, T. 2018. Experimental Investigation of Extraordinary Optical Behaviors in a Freestanding Plasmonic Cascade Grating at Visible Frequency. *Optics Express,* 26**,** 3271-3276.

Liang, Y., Yu, Z., Li, L. & Xu, T. 2019. A Self-Assembled Plasmonic Optical Fiber Nanoprobe for Label-Free Biosensing. *Scientific reports,* 9**,** 7379.

Lin, Y., Zou, Y. & Lindquist, R. G. 2011. A Reflection-Based Localized Surface Plasmon Resonance Fiber-Optic Probe for Biochemical Sensing. *Biomedical Optics Express,* 2**,** 478-484.

Liu, L., Monshat, H., Wu, H.-Y. & Lu, M. 2020. Imprint and Transfer Fabrication of Freestanding Plasmonic Membranes. *Nanotechnology,* 31**,** 375302-375302.

Liu, X., Liu, W. & Yang, B. 2019. Deep-Elliptical-Silver-Nanowell Arrays (D-Eagnwas) Fabricated by Stretchable Imprinting Combining Colloidal Lithography: A Highly Sensitive Plasmonic Sensing Platform. *Nano research,* 12**,** 845-853.

Lübbert, C., John, E. & von Müller, L. 2014. Clostridium Difficile Infection: Guideline-Based Diagnosis and Treatment. *Dtsch Arztebl Int,* 111**,** 723-31.

Luo, P. & Liu, Y. 2020. Detection of Toxin B of Clostridium Difficile Based on Immunomagnetic Separation and Aptamer-Mediated Colorimetric Assay. *Lett Appl Microbiol,* 71**,** 596-604.

Mak, G. C. K., Cheng, P. K. C., Lau, S. S. Y., Wong, K. K. Y., Lau, C. S., Lam, E. T. K., Chan, R. C. W. & Tsang, D. N. C. 2020. Evaluation of Rapid Antigen Test for Detection of Sars-Cov-2 Virus. *Journal of Clinical Virology,* 129**,** 104500.

Mayer, K. M. & Hafner, J. H. 2011. Localized Surface Plasmon Resonance Sensors. *Chemical Reviews,* 111**,** 3828-3857.

Metkar, S. K. & Girigoswami, K. 2019. Diagnostic Biosensors in Medicine – a Review. *Biocatalysis and Agricultural Biotechnology,* 17**,** 271-283.

Mittal, S., Sharma, T. & Tiwari, M. 2021. Surface Plasmon Resonance Based Photonic Crystal Fiber Biosensors: A Review. *Materials Today: Proceedings,* 43**,** 3071-3074.

Mizusawa, M. & Carroll, K. C. 2021. Advances and Required Improvements in Methods to Diagnosing Clostridioides Difficile Infections in the Healthcare Setting. *Expert Review of Molecular Diagnostics,* 21**,** 311-321.

Monteiro, J. P., de Oliveira, J. H., Radovanovic, E., Brolo, A. G. & Girotto, E. M. 2016. Microfluidic Plasmonic Biosensor for Breast Cancer Antigen Detection. *Plasmonics,* 11**,** 45-51.

Nagpal, P., Lindquist, N. C., Oh, S.-H. & Norris, D. J. 2009. Ultrasmooth Patterned Metals for Plasmonics and Metamaterials. *Science,* 325**,** 594.

Nam, K., Kimura, T. & Kishida, A. 2008. Controlling Coupling Reaction of Edc and Nhs for Preparation of Collagen Gels Using Ethanol/Water Co-Solvents. *Macromolecular Bioscience,* 8**,** 32-37.

Nan, J., Zhu, S., Ye, S., Sun, W., Yue, Y., Tang, X., Shi, J., Xu, X., Zhang, J. & Yang, B. 2020. Ultrahigh-Sensitivity Sandwiched Plasmon Ruler for Label-Free Clinical Diagnosis. *Advanced materials (Weinheim),* 32**,** e1905927-n/a.

Nangare, S. & Patil, P. 2021. Black Phosphorus Nanostructure Based Highly Sensitive and Selective Surface Plasmon Resonance Sensor for Biological and Chemical Sensing: A Review. *Critical Reviews in Analytical Chemistry***,** 1-26.

Noh, J., Konno, K., Ito, E. & Hara, M. 2005. Growth Processes and Control of Two-Dimensional Structure of Carboxylic Acid-Terminated Self-Assembled Monolayers on Au(111). *Japanese Journal of Applied Physics,* 44**,** 1052-1054.

Nurrohman, D. T. & Chiu, N.-F. 2021. A Review of Graphene-Based Surface Plasmon Resonance and Surface-Enhanced Raman Scattering Biosensors: Current Status and Future Prospects. *Nanomaterials,* 11**,** 216.

Patra, A., Ding, T., Hong, M., Richards, A. M., Wong, T. I., Zhou, X. & Drum, C. L. 2017. Using Extraordinary Optical Transmission to Quantify Cardiac Biomarkers in Human Serum. *Journal of visualized experiments : JoVE***,** 55597.

Pavlov, D., Porfirev, A., Khonina, S., Pan, L., Kudryashov, S. I. & Kuchmizhak, A. A. 2021. Coaxial Hole Array Fabricated by Ultrafast Femtosecond-Laser Processing with Spatially Multiplexed Vortex Beams for Surface Enhanced Infrared Absorption. *Applied Surface Science,* 541**,** 148602.

Pisano, F., Balena, A., Kashif, M. F., Pisanello, M., de Marzo, G., Algieri, L., Qualtieri, A., Sileo, L., Stomeo, T., D'Orazio, A., De Vittorio, M., Pisanello, F. & Grande, M. 2020. High Transmission from 2d Periodic Plasmonic Finite Arrays with Sub-20 Nm Gaps Realized with Ga Focused Ion Beam Milling. *Nanotechnology,* 31**,** 435301.

Planche, T. D., Davies, K. A., Coen, P. G., Finney, J. M., Monahan, I. M., Morris, K. A., O'Connor, L., Oakley, S. J., Pope, C. F., Wren, M. W., Shetty, N. P., Crook, D. W. & Wilcox, M. H. 2013. Differences in Outcome According to Clostridium Difficile Testing Method: A Prospective Multicentre Diagnostic Validation Study of C Difficile Infection. *The Lancet. Infectious diseases,* 13**,** 936-945.

Polley, N., Basak, S., Hass, R. & Pacholski, C. 2019. Fiber Optic Plasmonic Sensors: Providing Sensitive Biosensor Platforms with Minimal Lab Equipment. *Biosensors and Bioelectronics,* 132**,** 368-374.

Pollock, N. R., Banz, A., Chen, X., Williams, D., Xu, H., Cuddemi, C. A., Cui, A. X., Perrotta, M., Alhassan, E., Riou, B., Lantz, A., Miller, M. A. & Kelly, C. P. 2019. Comparison of Clostridioides Difficile Stool Toxin Concentrations in Adults with Symptomatic Infection and Asymptomatic Carriage Using an Ultrasensitive Quantitative Immunoassay. *Clinical infectious diseases : an official publication of the Infectious Diseases Society of America,* 68**,** 78-86.

Porte, L., Legarraga, P., Vollrath, V., Aguilera, X., Munita, J. M., Araos, R., Pizarro, G., Vial, P., Iruretagoyena, M., Dittrich, S. & Weitzel, T. 2020. Evaluation of a Novel Antigen-Based Rapid Detection Test for the Diagnosis of Sars-Cov-2 in Respiratory Samples. *International journal of infectious diseases : IJID : official publication of the International Society for Infectious Diseases,* 99**,** 328-333.

Prakash, G., Srivastava, R. K., Gupta, S. N. & Sood, A. K. 2019. Plasmon-Induced Efficient Hot Carrier Generation in Graphene on Gold Ultrathin Film with Periodic Array of Holes: Ultrafast Pump-Probe Spectroscopy. *The Journal of chemical physics,* 151**,** 234712.

Prasad, A., Choi, J., Jia, Z., Park, S. & Gartia, M. R. 2019. Nanohole Array Plasmonic Biosensors: Emerging Point-of-Care Applications. *Biosensors and Bioelectronics,* 130**,** 185-203.

Qian, Y., Zeng, X., Gao, Y., Li, H., Kumar, S., Gan, Q., Cheng, X. & Bartoli, F. J. 2019. Intensity-Modulated Nanoplasmonic Interferometric Sensor for Mmp-9 Detection. 19**,** 1267-1276.

Ravindran, N., Kumar, S., M, Y., S, R., C A, M., Thirunavookarasu S, N. & C K, S. 2021. Recent Advances in Surface Plasmon Resonance (Spr) Biosensors for Food Analysis: A Review. *Critical Reviews in Food Science and Nutrition***,** 1-23.

Renuse, S., Vanderboom, P. M., Maus, A. D., Kemp, J. V., Gurtner, K. M., Madugundu, A. K., Chavan, S., Peterson, J. A., Madden, B. J., Mangalaparthi, K. K., Mun, D.-G., Singh, S., Kipp, B. R., Dasari, S., Singh, R. J., Grebe, S. K. & Pandey, A. 2021. A Mass Spectrometry-Based Targeted Assay for Detection of Sars-Cov-2 Antigen from Clinical Specimens. *EBioMedicine,* 69**,** 103465-103465.

Ricciardi, A., Crescitelli, A., Vaiano, P., Quero, G., Consales, M., Pisco, M., Esposito, E. & Cusano, A. 2015. Lab-on-Fiber Technology: A New Vision for Chemical and Biological Sensing. *Analyst,* 140**,** 8068-8079.

Rissin, D. M., Kan, C. W., Campbell, T. G., Howes, S. C., Fournier, D. R., Song, L., Piech, T., Patel, P. P., Chang, L., Rivnak, A. J., Ferrell, E. P., Randall, J. D., Provuncher, G. K., Walt, D. R. & Duffy, D. C. 2010. Single-Molecule Enzyme-Linked Immunosorbent Assay Detects Serum Proteins at Subfemtomolar Concentrations. *Nature Biotechnology,* 28**,** 595-599.

Robinson, C., Justice, J., Petäjä, J., Karppinen, M., Corbett, B., O'Riordan, A. & Lovera, P. 2019. Nanoimprint Lithography–Based Fabrication of Plasmonic Array of Elliptical Nanoholes for Dual-Wavelength, Dual-Polarisation Refractive Index Sensing. *Plasmonics (Norwell, Mass.),* 14**,** 951-959.

Rodrigo, S. G., León-Pérez, F. d. & Martín-Moreno, L. 2016. Extraordinary Optical Transmission: Fundamentals and Applications. *Proceedings of the IEEE,* 104**,** 2288-2306.

Roether, J., Chu, K.-Y., Willenbacher, N., Shen, A. Q. & Bhalla, N. 2019. Real-Time Monitoring of DNA Immobilization and Detection of DNA Polymerase Activity by a Microfluidic Nanoplasmonic Platform. *Biosensors and Bioelectronics,* 142**,** 111528.

Roh, C. & Jo, S. K. 2011. Quantitative and Sensitive Detection of Sars Coronavirus Nucleocapsid Protein Using Quantum Dots-Conjugated Rna Aptamer on Chip. *Journal of Chemical Technology & Biotechnology,* 86**,** 1475-1479.

Rong, X. M., Yang, L., Chu, H. D. & Fan, M. 2020. Effect of Delay in Diagnosis on Transmission of Covid-19. *Math Biosci Eng,* 17**,** 2725-2740.

Sadri-Moshkenani, P., Khan, M. W., Shafiqul Islam, M., Montoya, E., Krivorotov, I., Bagherzadeh, N. & Boyraz, O. 2020. Effect of Magnesium Oxide Adhesion Layer on Resonance Behavior of Plasmonic Nanostructures. *Applied physics letters,* 116**,** 241601.

Sandlund, J., Bartolome, A., Almazan, A., Tam, S., Biscocho, S., Abusali, S., Bishop, J. J., Nolan, N., Estis, J., Todd, J., Young, S., Senchyna, F. & Banaei, N. 2018. Ultrasensitive Detection of Clostridioides Difficile Toxins a and B by Use of Automated Single-Molecule Counting Technology. *Journal of clinical microbiology,* 56**,** e00908-18.

Sandlund, J., Davies, K., Wilcox, M. H. & Kraft, C. S. 2020. Ultrasensitive Clostridioides Difficile Toxin Testing for Higher Diagnostic Accuracy. *Journal of Clinical Microbiology,* 58**,** e01913-19.

Scherino, L., Giaquinto, M., Micco, A., Aliberti, A., Bobeico, E., La Ferrara, V., Ruvo, M., Ricciardi, A. & Cusano, A. 2018. A Time-Efficient Dip Coating Technique for the Deposition of Microgels onto the Optical Fiber Tip. *Fibers,* 6**,** 72.

Shan, D., Johnson, J. M., Fernandes, S. C., Suib, H., Hwang, S., Wuelfing, D., Mendes, M., Holdridge, M., Burke, E. M., Beauregard, K., Zhang, Y., Cleary, M., Xu, S., Yao, X., Patel, P. P., Plavina, T., Wilson, D. H., Chang, L., Kaiser, K. M., Nattermann, J., Schmidt, S. V., Latz, E., Hrusovsky, K., Mattoon, D. & Ball, A. J. 2021. N-Protein Presents Early in Blood, Dried Blood and Saliva During Asymptomatic and Symptomatic Sars-Cov-2 Infection. *Nature communications,* 12**,** 1931-1931.

Shen, E., Zhu, K., Li, D., Pan, Z., Luo, Y., Bian, Q., He, L., Song, X., Zhen, Y., Jin, D. & Tao, L. 2020. Subtyping Analysis Reveals New Variants and Accelerated Evolution of Clostridioides Difficile Toxin B. *Communications Biology,* 3**,** 347.

Shin, S.-H., Shin, S.-H., Choi, J.-H., Lee, J., Choi, D.-G., Jeong, J.-H., Ju, B.-K. & Jung, J.-Y. 2019. Dual Nanotransfer Printing for Complementary Plasmonic Biosensors. *Nanotechnology,* 30**,** 385302.

Shrivastav, A. M., Cvelbar, U. & Abdulhalim, I. 2021. A Comprehensive Review on Plasmonic-Based Biosensors Used in Viral Diagnostics. *Communications Biology,* 4**,** 70.

Singh, M., Kaur, N. & Comini, E. 2020. The Role of Self-Assembled Monolayers in Electronic Devices. *Journal of Materials Chemistry C,* 8**,** 3938-3955.

Soler, M., Belushkin, A., Cavallini, A., Kebbi-Beghdadi, C., Greub, G. & Altug, H. 2017. Multiplexed Nanoplasmonic Biosensor for One-Step Simultaneous Detection of Chlamydia Trachomatis and Neisseria Gonorrhoeae in Urine. *Biosensors and Bioelectronics*, 94**,** 560-567.

Song, C., Jiang, X., Yang, Y., Zhang, J., Larson, S., Zhao, Y. & Wang, L. 2020. High-Sensitive Assay of Nucleic Acid Using Tetrahedral DNA Probes and DNA Concatamers with a Surface-Enhanced Raman Scattering/Surface Plasmon Resonance Dual-Mode Biosensor Based on a Silver Nanorod-Covered Silver Nanohole Array. *ACS Applied Materials & Interfaces,* 12**,** 31242-31254.

Song, L., Zhao, M., Duffy, D. C., Hansen, J., Shields, K., Wungjiranirun, M., Chen, X., Xu, H., Leffler, D. A., Sambol, S. P., Gerding, D. N., Kelly, C. P. & Pollock, N. R. 2015. Development and Validation of Digital Enzyme-Linked Immunosorbent Assays for Ultrasensitive Detection and Quantification of Clostridium Difficile Toxins in Stool. *Journal of clinical microbiology,* 53**,** 3204-3212.

Surjit, M. & Lal, S. K. 2008. The Sars-Cov Nucleocapsid Protein: A Protein with Multifarious Activities. *Infection, genetics and evolution : journal of molecular epidemiology and evolutionary genetics in infectious diseases,* 8**,** 397-405.

Taleghani, N. & Taghipour, F. 2021. Diagnosis of Covid-19 for Controlling the Pandemic: A Review of the State-of-the-Art. *Biosensors and Bioelectronics,* 174**,** 112830.

Terry, J. S., Anderson, L. B., Scherman, M. S., McAlister, C. E., Perera, R., Schountz, T. & Geiss, B. J. 2021. Development of a Sars-Cov-2 Nucleocapsid Specific Monoclonal Antibody. *Virology,* 558**,** 28-37.

Thermo Fisher Scientific. 2021. *Carbodiimide Crosslinker Chemistry* [Online]. Available: https://www.thermofisher.com/au/en/home/life-science/protein-biology/protein-biology-learning-center/protein-biology-resource-library/pierce-protein-methods/carbodiimide-crosslinker-chemistry.html [Accessed].

Thio, T., Lezec, H. J. & Ebbesen, T. W. 2000. Strongly Enhanced Optical Transmission through Subwavelength Holes in Metal Films. *Physica B: Condensed Matter*, 279**,** 90-93.

Tokel, O., Yildiz, U. H., Inci, F., Durmus, N. G., Ekiz, O. O., Turker, B., Cetin, C., Rao, S., Sridhar, K., Natarajan, N., Shafiee, H., Dana, A. & Demirci, U. 2015. Portable Microfluidic Integrated Plasmonic Platform for Pathogen Detection. *Scientific Reports,* 5**,** 9152.

Tu, L., Huang, L. & Wang, W. 2019. A Novel Micromachined Fabry-Perot Interferometer Integrating Nano-Holes and Dielectrophoresis for Enhanced Biochemical Sensing. *Biosensors and Bioelectronics,* 127**,** 19-24.

U.S. Food and Drug Administration 2021. *In Vitro Diagnostics Euas - Antigen Diagnostic Tests for Sars-Cov-2* [Online]. Available: https://www.fda.gov/medical-devices/coronavirus-disease-2019-covid-19-emergency-use-authorizations-medical-devices/in-vitro-diagnostics-euas-antigen-diagnostic-tests-sars-cov-2#iaft1 [Accessed].

Vaisocherová-Lísalová, H., Víšová, I., Ermini, M. L., Špringer, T., Song, X. C., Mrázek, J., Lamačová, J., Scott Lynn, N., Šedivák, P. & Homola, J. 2016. Low-Fouling Surface Plasmon Resonance Biosensor for Multi-Step Detection of Foodborne Bacterial Pathogens in Complex Food Samples. *Biosensors and Bioelectronics,* 80**,** 84-90.

Vala, M., Ertsgaard, C. T., Wittenberg, N. J. & Oh, S.-H. 2019. Plasmonic Sensing on Symmetric Nanohole Arrays Supporting High-Q Hybrid Modes and Reflection Geometry. *ACS sensors,* 4**,** 3265-3274.

Valsecchi, C., Gomez Armas, L. E. & Weber de Menezes, J. 2019. Large Area Nanohole Arrays for Sensing Fabricated by Interference Lithography. *Sensors (Basel, Switzerland),* 19**,** 2182.

Vaskova, H. & Křesálek, V. 2011. Raman Spectroscopy of Epoxy Resin Crosslinking. *13th WSEAS International Conference on AUTOMATIC CONTROL, MODELLING & SIMULATION*. Lanzarote, Canary Islands, Spain: World Scientific and Engineering Academy and Society Press.

Velusamy, V., Arshak, K., Korostynska, O., Oliwa, K. & Adley, C. 2010. An Overview of Foodborne Pathogen Detection: In the Perspective of Biosensors. *Biotechnology Advances,* 28**,** 232-254.

Wang, Y., Dostálek, J. & Knoll, W. 2009. Long Range Surface Plasmon-Enhanced Fluorescence Spectroscopy for the Detection of Aflatoxin M1 in Milk. *Biosensors and Bioelectronics,* 24**,** 2264-2267.

Wehrhahn, M. C., Keighley, C., Kurtovic, J., Knight, D. R., Hong, S., Hutton, M. L., Lyras, D., Wang, Q., Leong, R., Borody, T., Edye, M. & Riley, T. V. 2019. A Series of Three Cases of Severe Clostridium Difficile Infection in Australia Associated with a Binary Toxin Producing Clade 2 Ribotype 251 Strain. *Anaerobe,* 55**,** 117-123.

Wei, J., Singhal, S., Kofke, M. & Waldeck, D. H. Transmission Spr of Gold Nanoslit Array and Ultrasensitive Detection of a Retinol Binding Protein. 2010 4th International Conference on Bioinformatics and Biomedical Engineering, 18-20 June 2010 2010. 1-4.

Xiong, K., Emilsson, G. & Dahlin, A. B. 2016. Biosensing Using Plasmonic Nanohole Arrays with Small, Homogenous and Tunable Aperture Diameters. *Analyst,* 141**,** 3803-3810.

Xue, Y., Li, X., Li, H. & Zhang, W. 2014. Quantifying Thiol–Gold Interactions Towards the Efficient Strength Control. *Nature Communications,* 5**,** 4348.

Yang, J.-C., Ji, J., Hogle, J. M. & Larson, D. N. 2008. Metallic Nanohole Arrays on Fluoropolymer Substrates as Small Label-Free Real-Time Bioprobes. *Nano Letters,* 8**,** 2718-2724.

Yang, L., Biswas, M. E. & Chen, P. 2003. Study of Binding between Protein a and Immunoglobulin G Using a Surface Tension Probe. *Biophysical journal,* 84**,** 509-522.

Yesudasu, V., Pradhan, H. S. & Pandya, R. J. 2021. Recent Progress in Surface Plasmon Resonance Based Sensors: A Comprehensive Review. *Heliyon,* 7**,** e06321.

Yoo, D., Barik, A., de León-Pérez, F., Mohr, D. A., Pelton, M., Martín-Moreno, L. & Oh, S.-H. 2021. Plasmonic Split-Trench Resonator for Trapping and Sensing. *ACS Nano,* 15**,** 6669-6677.

Yu, L., Liang, Y., Chu, S., Gao, H., Wang, Q. & Peng, W. 2021. Freestanding Bilayer Plasmonic Waveguide Coupling Mechanism for Ultranarrow Electromagnetic-Induced Transparency Band Generation. *Scientific reports,* 11**,** 1437-8.

Yuan, X., Yang, C., He, Q., Chen, J., Yu, D., Li, J., Zhai, S., Qin, Z., Du, K., Chu, Z. & Qin, P. 2020. Current and Perspective Diagnostic Techniques for Covid-19. *ACS Infectious Diseases,* 6**,** 1998-2016.

Yue, W., Wang, Z., Yang, Y., Li, J., Wu, Y., Chen, L., Ooi, B., Wang, X. & Zhang, X.-x. 2014. Enhanced Extraordinary Optical Transmission (Eot) through Arrays of Bridged Nanohole Pairs and Their Sensing Applications. *Nanoscale,* 6 14**,** 7917-23.

Zentgraf, T., Zhang, S., Oulton, R. F. & Zhang, X. 2009. Ultranarrow Coupling-Induced Transparency Bands in Hybrid Plasmonic Systems. *Physical Review B,* 80**,** 195415.

Zhang, B., Yu, J., Liu, C., Wang, J., Han, H., Zhang, P. & Shi, D. 2016a. Improving Detection Sensitivity by Oriented Bioconjugation of Antibodies to Quantum Dots with a Flexible Spacer Arm for Immunoassay. *RSC Advances,* 6**,** 50119-50127.

Zhang, J., Irannejad, M., Yavuz, M. & Cui, B. 2015a. Gold Nanohole Array with Sub-1 nm Roughness by Annealing for Sensitivity Enhancement of Extraordinary Optical Transmission Biosensor. *Nanoscale research letters,* 10**,** 944-944.

Zhang, L., Fang, X., Liu, X., Ou, H., Zhang, H., Wang, J., Li, Q., Cheng, H., Zhang, W. & Luo, Z. 2020a. Discovery of Sandwich Type Covid-19 Nucleocapsid Protein DNA Aptamers. *Chemical Communications,* 56**,** 10235-10238.

Zhang, L., Zheng, B., Gao, X., Zhang, L., Pan, H., Qiao, Y., Suo, G. & Zhu, F. 2020b. Development of Patient-Derived Human Monoclonal Antibodies against Nucleocapsid Protein of Severe Acute Respiratory Syndrome Coronavirus 2 for Coronavirus Disease 2019 Diagnosis. *Frontiers in immunology,* 11**,** 595970-595970.

Zhang, S., Palazuelos-Munoz, S., Balsells, E. M., Nair, H., Chit, A. & Kyaw, M. H. 2016b. Cost of Hospital Management of Clostridium Difficile Infection in United States-a Meta-Analysis and Modelling Study. *BMC Infect Dis,* 16**,** 447.

Zhang, Z., Chen, Y., Liu, H., Bae, H., Olson, D. A., Gupta, A. K. & Yu, M. 2015b. On-Fiber Plasmonic Interferometer for Multi-Parameter Sensing. *Optics Express,* 23**,** 10732-10740.

Zhao, E., Jia, P., Ebendorff-Heidepriem, H., Li, H., Huang, P., Liu, D., Li, H., Yang, X., Liu, L. & Guan, C. 2017. Localized Surface Plasmon Resonance Sensing Structure Based on Gold Nanohole Array on Beveled Fiber Edge. *Nanotechnology,* 28**,** 435504.

Zhu, X., Cicek, A., Li, Y. & Yanik, A. A. 2019. Plasmofluidic Microlenses for Label-Free Optical Sorting of Exosomes. *Scientific reports,* 9**,** 8593-10.